Enhancement of the Intestinal Epithelial Permeability of Peripherally Acting Opioid Analgesics by Chitosan

Dissertation

zur Erlangung des akademischen Grades

doctor rerum naturalium

(Dr. rer. nat.)

im Fach Biologie

eingereicht an der

Mathematisch-Naturwissenschaftlichen Fakultät I

der Humboldt-Universität zu Berlin

von

Diplom Biologin

Miriam Stephanie Rubelt (geb. Heydt)

Präsident der Humboldt-Universität zu Berlin

Prof. Dr. Jan-Hendrik Olbertz

Dekan der Mathematisch-Naturwissenschaftlichen Fakultät I

Prof. Stefan Hecht, Ph.D.

Gutachter/innen: 1. Prof. Dr. Hans-Dieter Volk

2. Prof. Dr. Salah Amasheh

3. Prof. Dr. Matthew Larkum

Tag der mündlichen Prüfung: 15.10.2013

“Der Beginn aller Wissenschaften ist das Erstaunen, daß die Dinge so sind, wie sie sind.”

Aristoteles (384 - 322 v. Chr.)

1 Table of contents

1 TABLE OF CONTENTS

1 Table of contents

1 Table of contents

1 Table of contents

2 Abstract

2 ABSTRACT

Analgesic effects of opioids are mediated by opioid receptors that are widely distributed in the central and peripheral nervous systems (CNS and PNS, respectively). Although opioids are the most powerful analgesics, severe side effects restrict their use and affect patient convalescence. These side effects, for example respiratory depression, sedation or dependence, are mediated by the activation of central opioid receptors. This suggests an advantage of new analgesic opioids which selectively bind to opioid receptors in the PNS with no access to opioid receptors in the CNS due to a restricted ability to permeate the blood brain barrier. In clinical practice, oral administration of analgesic drugs is preferred to avoid discomfort to the patient. After oral administration however, peripherally restricted opioids first have to cross the intestinal epithelial barrier before absorption into the circulation and distribution to opioid receptors in peripheral tissues. Here, the transport across intestinal epithelia of two opioid ligands that selectively activate peripheral opioid receptors without entering the CNS, the hydrophilic morphinan AS006 and the lipophilic piperidine derivative loperamide were investigated. To increase the intestinal passage of these drugs, the absorption enhancer chitosan was used.

In vitro transport studies were performed using confluent monolayers of two human intestinal epithelial colon cell lines, HT29/B6 and Caco-2, in Ussing chambers. AS006 and loperamide that passed epithelial monolayers were determined using a liquid chromatography coupled with tandem mass spectrometry method established in the first part of this study. Chitosan significantly decreased the transepithelial resistance of both cell lines after 30 min *in vitro*. The permeability values for AS006 increased from $< 0.3 \times 10^{-6}$ cm/s up to 10×10^{-6} cm/s in the presence of chitosan. In contrast, HT29/B6 monolayers showed moderate loperamide permeability in the presence of chitosan, and chitosan had no effect on the permeability of loperamide using Caco-2 monolayers.

In vivo studies focused on antinociceptive effects of loperamide alone or in combination with chitosan. These effects were analyzed using the paw pressure test in a model of inflammatory pain in rats. Oral administration of loperamide induced a dose-depended elevation of paw pressure thresholds in inflamed paws that lasted for 60 min. This effect was comparable to that of intravenously applied loperamide. Oral administration of loperamide combined with chitosan slightly but nonsignificantly enhanced the antinociceptive effect of loperamide.

2 Abstract

In conclusion, chitosan is a suitable absorption enhancer for *in vitro* intestinal permeability studies. Epithelial permeability enhancement by chitosan appears to be more effective for hydrophilic opioids (AS006) than for lipophilic ones (loperamide). Future *in vivo* experiments might investigate different formulations and application schedules, and further address the effects of chitosan on the antinociceptive efficacy of hydrophilic opioids.

3 Zusammenfassung

3 ZUSAMMENFASSUNG

Die schmerzstillende Wirkung von Opiaten wird über Opioidrezeptoren im zentralen und peripheren Nervensystem (ZNS und PNS) vermittelt. Die Schmerzlinderung kann jedoch mit sehr starken Nebenwirkungen einhergehen, die das Patientenwohlbefinden beeinträchtigen. Nebenwirkungen wie Atemdepression, Sedierung oder Abhängigkeit werden durch die Aktivierung von zentralen Opioidrezeptoren vermittelt. Dies legt die Bedeutung von neuen Opioidanalgetika nahe, die ihre schmerzstillende Wirkung ausschließlich über Opioidrezeptoren im PNS entfalten, ohne unerwünschte zentrale Nebenwirkungen zu induzieren. Die orale Gabe von Medikamenten minimiert Unannehmlichkeiten für den Patienten, jedoch müssen die Substanzen die intestinale Barriere passieren können, um in die Blutzirkulation eintreten zu können.

Die intestinale Permeabilität von zwei peripher wirksamen Opiaten, dem hydrophilen Morphinderivat AS006 und dem lipophilen Piperidinderivat Loperamid, wurde in Ussing-Kammer Experimenten untersucht. Für diese *in vitro* Studien wurden zwei humane Darmzelllinien (HT29/B6 und Caco-2 Zellen) genutzt. Um die Darmepithelpermeabilität für beide Opiate zu erhöhen, wurde der Absorptionsverstärker Chitosan verwendet. Im Rahmen dieser Studie wurden für die Bestimmung der Konzentration von AS006 und Loperamid zwei neue LC-MS/MS Methoden entwickelt, validiert und angewendet.

Chitosan bewirkte nach 30 Minuten bei beiden Zelllinien eine Abnahme des epithelialen Widerstands *in vitro*. Die Permeabilität für AS006 war bei beiden Zelllinien erhöht, für Loperamid nur bei HT29/B6, jedoch nicht bei Caco-2 Zellmonolayern.

Verhaltensexperimente zur Messung des antinozizeptiven Effektes von oral appliziertem Loperamid auf Entzündungsschmerz wurden an Ratten durchgeführt. Die orale Gabe von Loperamid induzierte eine Dosis-abhängige antinozizeptive Wirkung in der entzündeten Hinterpfote, die vergleichbar mit der Wirkung von Loperamid nach intravenöser Gabe ausfiel. Bei oraler Gabe von Loperamid in Kombination mit Chitosan wurde keine signifikante Verstärkung des maximalen antinozizeptiven Effekts von Loperamid beobachtet.

Zusammenfassend ist Chitosan ein geeigneter Absorptionsverstärker für intestinale Permeabilitätsstudien von peripher wirksamen Opioidanalgetika *in vitro*. Die *in vitro* Ergebnisse haben gezeigt, dass der Effekt von Chitosan auf lipophile Opiate (Loperamid) möglicherweise schwächer ist als auf hydrophile (AS006). Dementsprechend fiel die Wirkung

des Absorptionsverstärkers auf Loperamid-induzierte Analgesie im Verhaltensversuch eher gering aus. Die *in vitro* Wirkung von Chitosan auf den Transport von hydrophilen peripher wirkenden Opioiden (AS006) war jedoch signifikant und sollte in weiteren Studien untersucht werden.

4 INTRODUCTION

4.1 Pain and opioids

Pain is defined by the International Association for the Study of Pain (IASP) as “an unpleasant sensory and emotional experience associated with actual or potential tissue damage, or described in terms of such damage” (IASP, 1979). Pain perception is always subjective and is influenced by individual experiences related to injuries in previous phases of life. In most cases, pain is accompanied by suffering of the individual. Nevertheless, acute pain perception prevents additional tissue damage and can be lifesaving. In 1983, Dennis and Melzack (Dennis and Melzack, 1983) postulated three purposes of pain:

1) Short-lasting pain causes us to withdraw from the source, often reflexively, thus preventing further damage.
2) Long-lasting pain promotes behaviors such as sleep, inactivity, grooming, feeding, and drinking that promote recuperation.
3) The expression of pain serves as a social signal to other animals. For example, screeching after a painful stimulus signals the potential harm to genetically related individuals, and elicits caregiving behavior from them, such as grooming, defending, and feeding.

Pain perception is mediated via nociceptors which are high-threshold neurons of the peripheral somatosensory nervous system. They are able to transduce and encode noxious stimuli (IASP, 1979) and send information first to the dorsal root ganglion and further onto the spinal cord and, via the ascending pathways to the brain (thalamus, somatosensory cortex and other parts of the cortex) for interpretation and response (Dobrila-Dintinjana and Nacinović-Duletić, 2011), as shown in Fig. 1. Nociceptors are found in skin, tendons, joints, muscles, and other organs and consist of A-delta and C fibers (Messlinger, 1997). For the induction of pain the noxious stimulus has to reach a certain threshold. Pain can be categorized into two classes; acute and chronic pain. Acute pain fulfills a warning role whereas chronic pain, which includes inflammatory, cancer and neuropathic pain, has no biological function (Millan, 1999).

Opioids are powerful drugs to treat severe pain (IASP, 1979; Ripamonti et al., 2011). Opioids are classified by the World Health Organization (WHO) according to their ability to control mild to moderate pain (e.g. codeine, dihydrocodeine, tramadol) or moderate to severe pain

(e.g. morphine, methadone, oxycodone, fentanyl) (WHO, 1996). In addition, non-opioid analgesics like paracetamol or non-steroidal anti-inflammatory drugs (NSAIDs) like aspirin and ibuprofen are used (McNicol et al., 2005). The long-term usage of NSAIDs has to be monitored due to their side effects like gastrointestinal bleeding and renal insufficiency (Ripamonti, 2012).

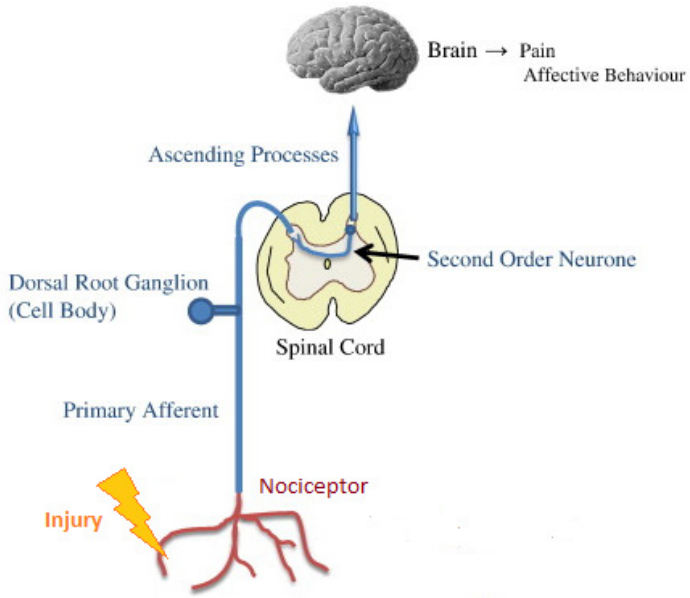

Figure 1: Pain transmission pathway from the periphery to the central nervous system. A nociceptive stimulus (injury) activates peripheral nociceptors leading to the sensation of pain (modified after McDougall, 2011).

For the classification of pain in humans, standardized scales such as the visual analogue scales, verbal rating scale, and the numerical rating scale are used (Caraceni et al., 2002). For pain studies in animals different pain detection models have been established, due to the lack of verbal communication. Nociceptive tests use electrical, thermal, mechanical, or chemical stimuli for analysis of pain behavior (Le Bars et al., 2001). Nociceptive tests in rodents are summarized by Barrot (Barrot, 2012). The most common are the formalin test (Ko et al., 2012), von Frey test (Chaplan et al., 1994), hot plate test (de Sá et al., 2012), tail flick test (Aydin et al., 2012), hargreaves test (Saika et al., 2012) and the paw pressure test (Brack et al., 2004a).

The treatment of pain with opioids has a long history. The first written records describing the production and usage of morphine as a pharmaceutical compound go back to 4000 BC. These days morphine, codeine, fentanyl and oxycodone are the most powerful drugs to relieve severe pain (Spetea et al., 2004) by activation of opioid receptors in the CNS and PNS,

respectively (Ossipov et al., 2004; Yaksh and Rudy, 1978). Pain relief is mediated via the three classical opioid receptors: μ, δ and κ, which belong to the family of seven-transmembrane G-protein-coupled receptors (van Rijn et al., 2010). The signal pathways activated after agonist binding to opioid receptors are well characterized. First, the opioid binds to a binding pocket within the receptor. After binding, conformational changes allow intracellular coupling of heterotrimeric Gi/o proteins to the C terminus of the receptor. GTP replaces GDP in the Gα subunit which results in dissociation of the trimeric G protein complex into Gα and Gβγ subunits. Hereafter the Gα subunit inhibits the synthesis of cyclic adenosine monophosphate (cAMP). Gβγ subunits interact directly with Ca^{2+} channels, the transient receptor potential vanilloid type 1 or other ion channels in the membrane (Endres-Becker et al., 2007; Stein and Zöllner, 2009), as shown in Fig. 2. As a consequence, opioid agonists reduce the excitability of nociceptive neurons and the release of the pronociceptive neuropeptides (e.g. substance P and calcitonin gene-related peptide) from central and peripheral neuronal terminals.

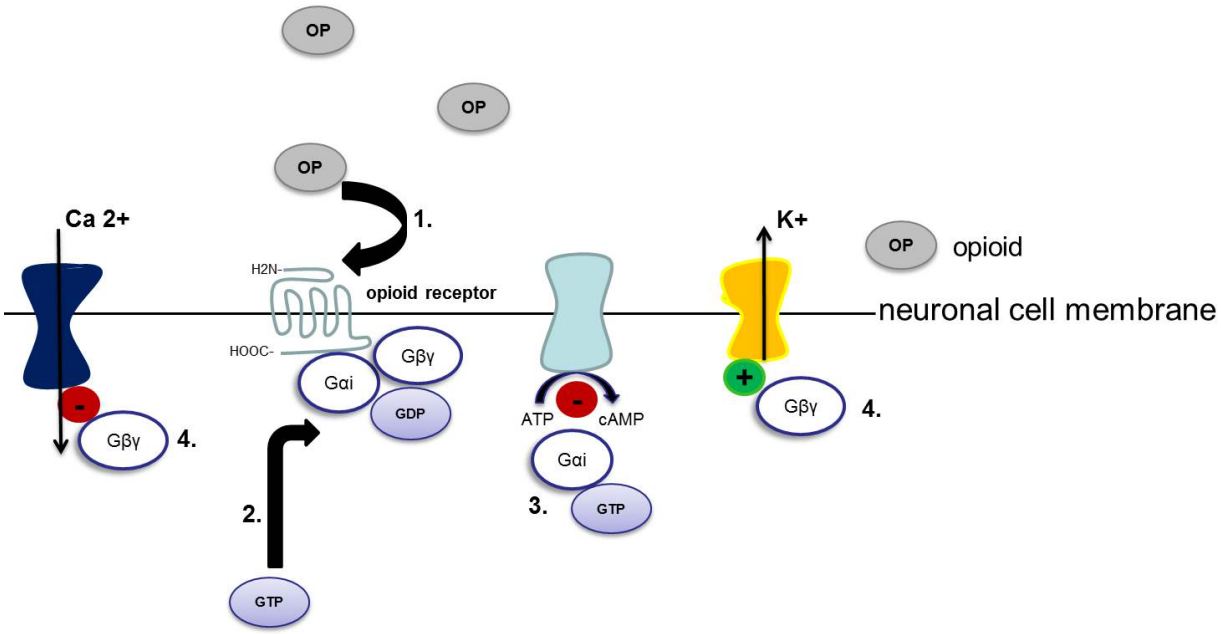

Figure 2: Intracellular signaling pathways of the μ-opioid receptor.

1. Agonist binds to opioid receptor. 2. Agonist binding to the receptor induces an exchange of GDP by GTP on the trimeric G protein complex which then dissociates from the receptor; the α subunit also dissociates from the β/γ subunits. 3. The GTP-bound α subunit inhibits the enzyme adenylyl cyclase leading to a decrease in intracellular cAMP concentrations. 4. The β/γ subunits activate potassium channels and inhibit voltage-sensitive calcium channels. As a result, the neuronal excitability and neurotransmitter release is attenuated.

Usage of centrally active drugs like morphine can come along with undesirable side effects such as respiratory depression, nausea, mental clouding, addiction, and tolerance (MacPherson, 2002; Nicholson, 2003; Zöllner and Stein, 2007). These side effects are mediated through opioid receptor binding in the CNS. Opioid receptors are expressed in the CNS (Pert and Snyder, 1973) and PNS (Stein, 1993; Stein et al., 1988a), as well as in non-neuronal cells such as immune and ectodermal cells (Zöllner and Stein, 2007). Under inflammatory conditions, peripheral opioid receptors on sensory neurons are upregulated (Stein et al., 2001). Activation of such peripheral opioid receptors can reduce pain both in humans (analgesia) (Khoury et al., 1990; Meiser and Laubenthal, 1997) and in animals (antinociception) (Rittner and Brack, 2007; Stein and Zöllner, 2009; Stein et al., 2003).

In contrast to the parenteral route, which bears the risk of infection and needs to be conducted by specialized staff, oral drug administration is simple and minimize discomfort to the patient (Hans, 2007; Hurst et al., 2007; Thomas et al., 2006).

Thus, there is a need for opioids which selectively activate peripheral opioid receptors and can be administered orally.

To synthesize peripherally acting opioids, the chemical structure of conventional opiates has been modified, for example to increase hydrophilicity which blocks passage into the CNS (DeHaven-Hudkins and Dolle, 2004). In addition, lipophilic compounds can be substrates of efflux membrane transporters like P-glycoprotein (P-gp), which is located in endothelial cells of the blood-brain barrier and in epithelial cells of the intestinal barrier (Crowe and Wong, 2003). The combined introduction of hydrophilic and hydrophobic chemical characteristics has been shown to result in analgesic compounds (e.g. the κ agonist asimadoline, EMD 61753) with restricted access to the CNS (Machelska et al., 1999). In a rat model of short-lasting inflammation EMD 61753 produced dose-dependent, naloxone-reversible antinociception after systemic administration (Barber et al., 1994). Additionally, an antiarthritic action of EMD 61753 has been shown in polyarthritic rats after oral administration (Binder and Walker, 1998), but in humans undergoing, knee surgery, orally given EMD 61753 had no effect on postoperative pain (Machelska et al., 1999).

However, increased hydrophilicity not only inhibits the transport across endothelial cell membranes of the blood-brain barrier, it would also restrict absorption through the intestinal epithelial barrier into the circulation (Matsuhisa et al., 2009). Thus, modulation of drug passage through the intestinal epithelial barrier is required to improve oral delivery of such compounds. This may be achieved by absorption enhancers which are exclusively acting on intestinal epithelial cells.

4.2 Intestinal barrier and tight junctions

Tight junctions (TJs) represent the main component of the barrier formed by the intestinal epithelium. This barrier determines the paracellular movement of solutes between the functionally external compartments, including the intestinal lumen, and the internal compartments of the intestinal wall, including the blood vessels. TJs are localized in the apicolateral membrane of epithelial cells and organized in strands. Within these strands, four types of transmembrane proteins have been identified: occludin (Furuse et al., 1993), claudins (González-Mariscal et al., 2003), tricellulin (Ikenouchi et al., 2005) and junctional adhesion molecules (JAM) (Martìn-Padura et al., 1998). Occludin, claudins and tricellulin bear four transmembrane domains, two extracellular domains, and their amino and carboxyl terminal ends are oriented towards the intracellular region (González-Mariscal et al., 2003). They are known to determine paracellular barrier properties (Furuse et al., 1993, 1998; Ikenouchi et al., 2005). In contrast, JAM have just one transmembrane region and are not only localized in TJ of epithelial and endothelial cells, but also expressed in leukocytes (Martìn-Padura et al., 1998). Tricellulin is localized in tricellular TJs, the meeting points of three epithelial cells (Ikenouchi et al., 2005). Trans-interaction between the extracellular domains of those proteins closes the cleft between neighbouring cells. On the intracellular side, the transmembrane proteins are connected to the actin cytoskeleton via adaptor proteins such as zona occludens (ZO) 1, 2, and 3 (Aktories and Barbieri, 2005) as shown in Fig. 3. The expression of TJ proteins influences the local barrier properties and differs between organs and tissues (Amasheh et al., 2011; Markov et al., 2010).

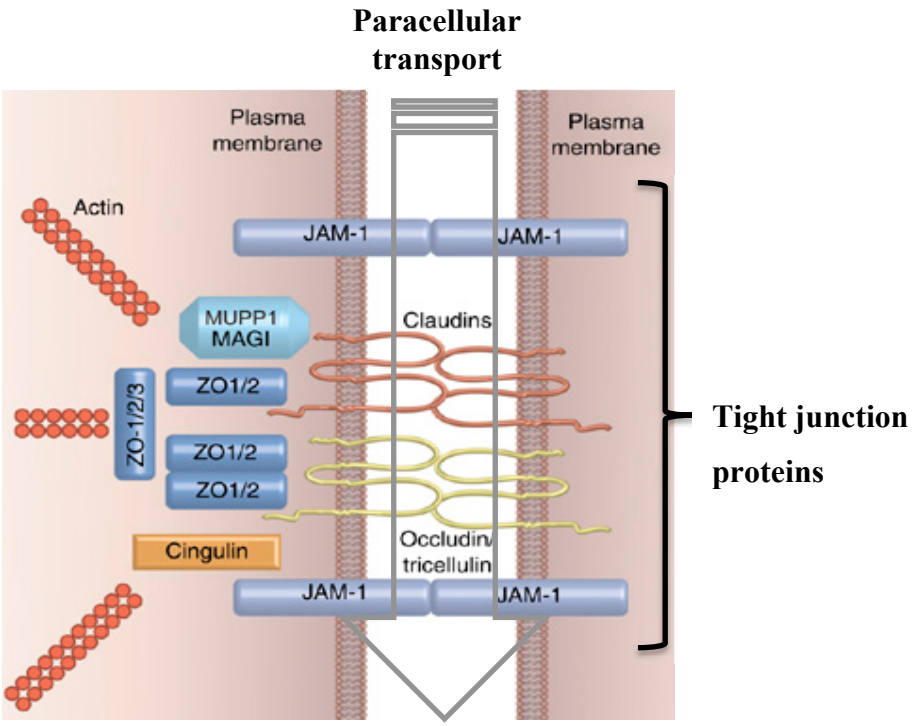

Figure 3: TJ protein distribution in intestinal epithelial cells.

TJs represent the main barrier of the intestinal epithelium by closing the paracellular cleft between two adjacent epithelial cells. Components of the cytoplasmic region underlying the TJ ("cytosolic plaque") are built by transmembrane (occludin, claudins and junctional adhesion molecules, JAMs), and scaffolding proteins (ZO1, ZO2, ZO3, MUPP1, and MAGI). ZO proteins directly interact with occludins and claudins; via their C-terminus they are connected with the actin cytoskeleton. MUPP1 and MAGI can directly interact with one or more of the transmembrane components (modified after Aktories and Barbieri, 2005; Niessen, 2007).

In addition to the paracellular pathway, the intestinal barrier can be crossed via the transcellular route and through leaky areas caused by apoptosis, as summarized in Fig. 4. For transcellular passage, hydrophobic substances can be delivered passively by diffusion into the cell membrane (Watts and Fasano, 2000). Active transcellular passage is energy dependent and substrate specific, involving transporters like the intestinal oligopeptide transporter (PepT1) or P-gp in the cell membrane (Majumdar et al., 2004; Mizuno et al., 2003; Rosenthal et al., 2012a). PepT1 catalyzes electrogenic peptide transport by coupling of substrate translocation to the cotransport of H^+ with the transmembrane electrochemical proton gradient providing the driving force (Döring et al., 1998). PepT1 recognizes therapeutics such as beta-lactam antibiotics and 5-aminolevulinic as substrates (Amasheh et al., 1997; Döring et al., 1998). P-gp is an adenosine triphosphate (ATP)-dependent transporter. Its activation leads to an active efflux of substrates from the cells. Opioids like morphine (King et al., 2001;

Schinkel et al., 1996a; Thomas et al., 2006), asimadoline (Jonker et al., 1999), and loperamide (Callaghan and Riordan, 1993; Huwyler et al., 1998), as well as a broad variety of peptides (Ganapathy and Miyauchi, 2005) are substrates of P-gp.

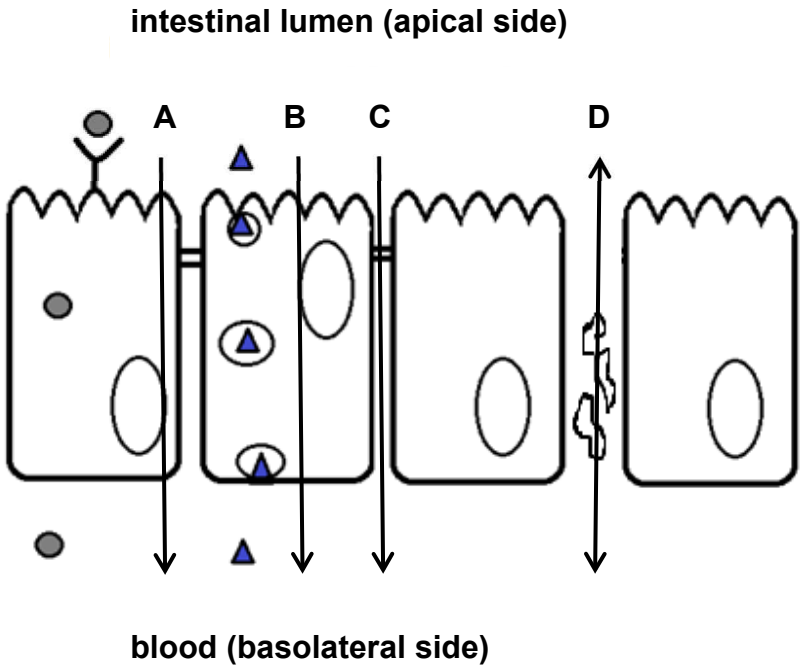

Figure 4: The four intestinal transepithelial pathways: A: transcellular passive transport (limited to small molecules like amino acids and sugars), B: transcellular active transport (hydrophobic compounds), C: paracellular transport (drugs and vaccines), D: local leaks caused by apoptosis (modified after Rosenthal et al., 2012a; Watts and Fasano, 2000).

To increase the paracellular passage of macromolecules, TJs have to be modified. *In vitro* studies on intestinal permeability were mostly conducted with the epithelial human colon cell lines Caco-2 and HT29/B6 (Amasheh et al., 2012; Kowalik et al., 2004; Kreusel et al., 1991; Merzlikine et al., 2009; Moran et al., 2012; Press and Di Grandi, 2008). They form polarized, confluent monolayers, and develop microvilli and TJs between adjacent cells. HT29/B6 cells are Cl^--secreting and mucus producing cells while Caco-2 cells have minor Cl^--secreting and mucus producing properties (Hayslett et al., 1987; Hidalgo et al., 1989; Kreusel et al., 1991; Sun et al., 2008). They also differ in TJ protein expression patterns. HT29/B6 express claudin-5 in colocalization with occludin, whereas Caco-2 cells show a marginal or no expression of claudin-2 and -5 (Amasheh et al., 2005; Escaffit et al., 2005).

4.3 Absorption enhancers

The first attempts to increase drug passage via the paracellular pathway using absorption enhancers date back to the 1980s. Absorption enhancers can directly act on TJs and open the paracellular pathway for orally administered pharmaceutical compounds. The opening of TJs results in a drop of the transepithelial electrical resistance (TER), which is due to a higher passage of ions through the paracellular space. The TER is an indicator of how tightly adjacent epithelial cells are connected and thereby affect paracellular transport.

A variety of molecules has been tested with respect to their properties to increase the permeability of intestinal epithelia. These molecules include surfactants, calcium chelating agents, fatty acids, medium chain glycerides, chitosans, steroidal detergents and, cyclodextrin (Aungst, 2000). Only sodium caprate is currently used as an absorption enhancer in pharmacological therapy as a component of a rectal ampicillin suppository (Kondoh et al., 2005; Lindmark et al., 1997). Sodium caprate induces a remarkable drop in TER, which is reversible and associated with the transient dissociation of tricellulin from TJs (Krug et al., 2013).

Another well described enhancer is chitosan, which is produced by deacetylation of the second most abundant natural polymer chitin (Fig. 5).

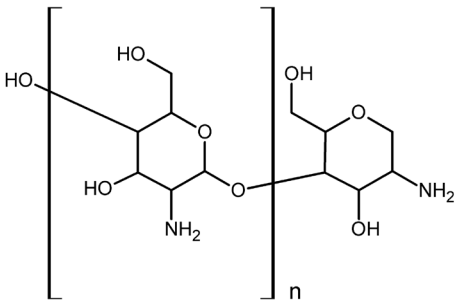

Figure 5: Basic chemical structure of low molecular weight chitosan. Molecular weight 50 – 190 kDa.

Due to its pKa of 5.5 - 7.0 it is most efficient in solvents with a pH lower than 7 (Kotzé et al., 1998, 1999; Rosenthal et al., 2012b). Chitosan is a biocompatible, antibacterial and environmentally friendly polyelectrolyte lending itself to a variety of applications (Kobayashi et al., 1996) including water treatment, chromatography, additives for cosmetics, textile treatment for antimicrobial activity (Shin et al., 1999), novel fibers for textiles, photographic

papers, biodegradable films (Hirano, 1996), decorporation of radioactive substances (Levitskaia et al., 2009), scaffolds for bone marrow mesenchymal stem cells (Cho et al., 2008), biomedical devices, and microcapsule implants for controlled release in drug delivery (Bartkowiak and Hunkeler, 1999; Sezer and Akbuğa, 1999; Sonaje et al., 2009; Suzuki et al., 1999). It affects different kinds of barriers including dermal (Valenta and Auner, 2004), nasal (Casettari et al., 2010; Luppi et al., 2010; Valenta and Auner, 2004), ocular (Alonso and Sánchez, 2003; Paolicelli et al., 2009; Wadhwa et al., 2009), pulmonary (Davis, 1999), and gastrointestinal epithelia (Chopra et al., 2006; Masuda et al., 2012; Thanou et al., 2001a).

Chitosan induces a decrease in the paracellular resistance of intestinal epithelial cells by opening the TJs via interaction between the positively charged amino groups of the chitosan molecule with the negatively charged surface proteins of the TJ (Aungst, 2000; Borchard et al., 1996). In HT29/B6 cells, chitosan affects both transcellular (R^{trans}) and paracellular (R^{para}) resistance parameters via its positive charge. The decrease in R^{trans} can be explained by activation of a chloride-bicarbonate exchanger involved in intracellular pH regulation, while no effects on expression and subcellular distribution of HT29/B6 TJ proteins or the actin cytoskeleton were found (Rosenthal et al., 2012b).

In addition, chitosan can activate the protein kinase C α (PKC α) signaling pathway which catalyzes the phosphorylation of target protein(s) followed by the reorganization of the actin cytoskeleton. This leads to the polymerization of soluble G-actin into F-actin and causes a rearrangement of actin filaments followed by the displacement of proteins (including ZO1 and ZO2) from the junctional complex. The delocalization of the junctional complex opens the paracellular space between adjacent intestinal epithelial cells (Fasano, 1999, 2001; Smith et al., 2004). It has been shown that chitosan is involved in dissociation of claudin 4 and claudin 1 in the Caco-2 junctional complex, thus reducing TJ integrity and decreasing intestinal epithelial resistance (Dorkoosh et al., 2004; Yeh et al., 2011).

Low molecular weight chitosan has a molecular weight of 50 - 190 kDa which prevents it from crossing the epithelium even after opening of the paracellular path. Several derivatives have been developed. The most recent are chitosan nanoparticles, which interact directly with the cell membrane via endocytosis and transcytosis and enhance the transport of drug molecules through the blood-brain barrier or the intestinal barrier (Lalatsa et al., 2012a, 2012b; Sandri et al., 2010; Vllasaliu et al., 2010). Thus, this new generation of enhancer is able to modulate transcellular transport in addition to the paracellular pathway.

4.4 Peripheral opioid receptor agonists

AS006 (Fig. 6 A) is a morphinan derivative which selectively activates μ-opioid receptors. Its structure is similar to the morphine molecule (Fig. 6 B) and is the equivalent to 2-(4,5α-epoxy-3-hydroxy-14β-methoxy-17-methyl-morphinan-6β-yl)aminoacetic acid (HS-731). It is a zwitterionic molecule with increased hydrophilicity (log P = 0.27) and a molecular weight of 374.4 Da. The hydrophilicity is enhanced by the presence of an amino acid residue (glycine) at C-6 of the morphinan. This restricts the opioid from crossing the blood–brain barrier (Schütz et al., 2003). Bileviciute-Ljungar and colleagues have shown that subcutaneous (s.c.) administration of AS006 reduces nociceptive responses as manifested by increased paw withdrawal latencies to mechanical and thermal stimulation in a rat model of inflammatory pain. Oral administration of AS006 significantly reduced hyperalgesia ("pain sensitivity") in inflamed paws. This effect was reversible by naloxone methiodide (NLXM), an opioid receptor antagonist that does not cross the blood-brain barrier (Bileviciute-Ljungar et al., 2006). In a mouse model of visceral pain preemptive s.c. administration of AS006 produced potent peripherally mediated antinociception (Al-Khrasani et al., 2007). In summary, AS006 has demonstrated analgesic efficacy in several models for acute and chronic inflammatory pain (Bileviciute-Ljungar et al., 2006; Al-Khrasani et al., 2007).

Loperamide, another selective μ-opioid receptor agonist, is a synthetic piperidine derivative with a molecular weight of 477.0 Da (Fig. 6 C). Previous studies have shown that intravenously (i.v.) injected loperamide cannot cross the blood-brain barrier because it is a substrate of P-gp (Mercer and Coop, 2011; Schinkel et al., 1996a). Others have demonstrated that the high lipophilicity of loperamide (log P = 4.26) is underlying its high affinity to P-gp (Wiese and Pajeva, 2001). Studies in humans have shown that inhibition of P-gp with quinidine leads to an increased entry of loperamide into the CNS with resultant respiratory depression (Sadeque et al., 2000). Several experimental studies have shown that loperamide is an effective peripherally acting analgesic administered by mouth wash (in humans) (Nozaki-Taguchi et al., 2008), i.v. (in rats), intraperitoneal (i.p.) (in rats and mice), and intraplantar (i.pl.) injection in different pain models (inflammatory, muscular, neuropathic, cancer, and visceral pain) (DeHaven-Hudkins et al., 1999; Guan et al., 2008; Nozaki-Taguchi and Yaksh, 1999; Sánchez et al., 2010; Sevostianova et al., 2005; Shannon and Lutz, 2002; Shinoda et al., 2007). Clinically, loperamide is currently used to control diarrhea (Baselt, 2004; Niemegeers et al., 1981; Tseong, 1995). In the gastrointestinal tract, μ-opioid receptors are expressed by

myenteric and submucosal neurons, and on immune cells in the lamina propria (Tonini et al., 1992). Loperamide can inhibit acetylcholine release from myenteric motor neurons to attenuate twitch contractions of longitudinal muscles in response to transmural electrical stimulation (Dingledine and Goldstein, 1976). Since P-gp is located on the apical membrane of intestinal epithelial cells and is able to pump loperamide back into the intestinal lumen, only low amounts of loperamide can enter the blood circulation when administered orally (Silverman, 1999; Thiebaut et al., 1987a). Due to its low absorbance from the intestinal tract, loperamide is viewed as a compound with a low oral bioavailability with no side effects on the CNS (Baselt, 2004). Taken together, loperamide represents a peripheral opioid receptor agonist that is readily available and already in clinical use. Therefore, we decided to initially focus our *in vivo* studies on this compound.

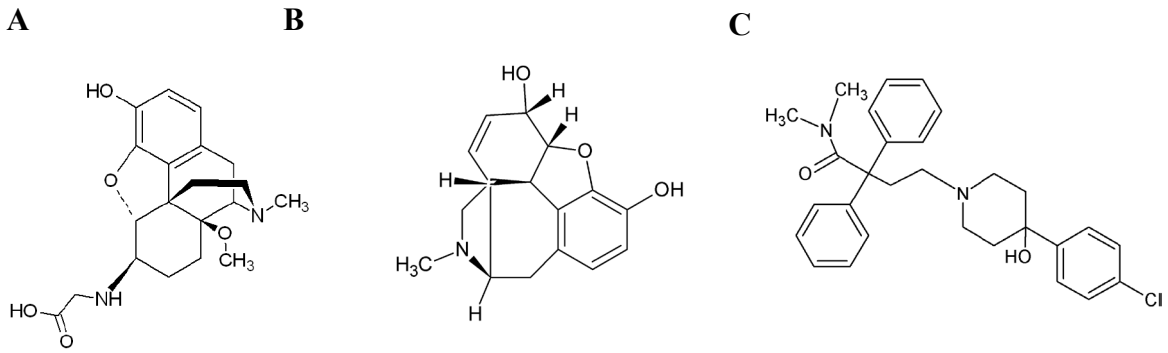

Figure 6: Chemical structures of AS006 (A), morphine (B) and loperamide (C)

5 Objectives

5 OBJECTIVES

The aim of this study was to investigate the intestinal transport of peripherally acting opioids (AS006, loperamide) and their antinociceptive properties after oral administration. To increase intestinal absorption, chitosan was used.

Hypothesis 1: The intestinal permeability for AS006 is low. To test this hypothesis, a detection method for the quantification of AS006 using liquid chromatography coupled with tandem mass spectrometry (LC-MS/MS) had to be developed and validated for the specific *in vitro* conditions applied here. Ussing chamber experiments were performed to analyze the amount of AS006 passing human intestinal colon cell monolayers.

Hypothesis 2: The intestinal permeability for loperamide is low. To test this hypothesis, a detection method for the quantification of loperamide using LC-MS/MS had to be developed and validated for the specific *in vitro* conditions applied here. Ussing chamber experiments were performed to analyze the loperamide passage across human intestinal colon cell monolayers.

Hypothesis 3: Chitosan increases permeability of AS006 across intestinal epithelia. To test this hypothesis, *in vitro* Ussing chamber experiments were performed to analyze the transepithelial flux of AS006 across human intestinal colon cell monolayers in the presence of chitosan. AS006 was quantified using LC-MS/MS.

Hypothesis 4: Chitosan increases the permeability of loperamide across intestinal epithelia. To test this hypothesis, *in vitro* Ussing chamber experiments were performed to analyze loperamide flux across human intestinal colon cell monolayers in the presence of chitosan. Loperamide was quantified using LC-MS/MS.

Hypothesis 5: Chitosan improves the antinociceptive effect of orally administered loperamide in rats with hindpaw inflammation *in vivo*. To test this hypothesis, paw pressure thresholds were assessed in rats receiving oral combinations of loperamide with/without chitosan.

6 MATERIALS AND METHODS

6.1 Materials

6.1.1 Liquid chromatography coupled with tandem mass spectrometry (LC-MS/MS)

Auto sampler SIL-HTA	Shimadzu, Duisburg, Germany
Column thermostat CTO-20A	Shimadzu, Duisburg, Germany
Degasser 2 DGU 20 A	Shimadzu, Duisburg, Germany
HPLC	Shimadzu, Duisburg, Germany
Pumps 2 LC-20AD	Shimadzu, Duisburg, Germany
Switching valves 2 FCV-14 AH	Shimadzu, Duisburg, Germany
Triple-Quadrupol-Massenspektrometer QTrap 3200	AB SCIEX, Darmstadt, Germany

6.1.2 Ussing chamber system

Ohmmeter	Institut für Klinische Physiologie, Charité Universitätsmedizin Berlin, Germany
Ussing-chamber	Institut für Klinische Physiologie, Charité Universitätsmedizin Berlin, Germany

6.1.3 Behavioral experiments

Alsident® system 25 - Cabinet type 1	Alsident System A, Hammel, Denmark
Analgesy-Meter	Ugo Basile, Comerio, Italy
Feeding needle (metal, gauge 15, length 78 mm, ball OD 2.9 mm)	AgnTho's AB Lidingö, Sweden
Glass exsiccator	DURAN Group GmbH, Wertheim/Main, Germany

6.1.4 General appliances

Analytical scale XS 105 with printer RS-P42	Mettler-Toledo, Gießen, Germany
CO_2 incubator CB-150	Binder, Tuttlingen, Germany
Microliter syringes	Hamilton, Bonaduz, Switzerland
Pipettes	Eppendorf, Köln, Germany
sterile bench	Gelaire Flow Laboratories, Meckenheim, Germany
Vortex-Genie 2	Scientifica Industries, Inc., New York, USA

6.1.5 LC-MS/MS

Atlantis dC18 column, 2.1 mm x 20 mm, 3 µm	Waters GmbH, Eschborn, Germany
C18 guard column 4 x 3.0 mm	Phenomenex Aschaffenburg, Germany
Luna PFP column, 150 mm × 3.0 mm, 3 µm	Phenomenex Aschaffenburg, Germany
Luna PFP guard column 4 x 3.0 mm	Phenomenex Aschaffenburg, Germany
Autosampler vials, 2 mL, 12 x 32 mm	Laubscher Labs, Miecourt, Switzerland
screw cap for autosampler vials	CS-Chromatographie Service Langerwehe, Germany
Vial inserts, 200 µL, glass	Kunz & Müller Berlin, Germany

6.1.6 Cell culture

Cell scrapers	Coster, Corning, NY, USA

Dishes	Nunc, Karlsruhe, Germany
Flasks	Nunc, Karlsruhe, Germany
Membrane filter, 0.22 µm, Polyvinyl-denfluorid	Millipore Eschborn, Germany
Tips	Eppendorf, Köln, Germany
Transwell filter, Millicell-HA, Millicell- PCF, 0.6 cm²	Millipore, Schwalbach, Germany
Tubes	Eppendorf, Köln, Germany

6.1.7 Behavioral experiments

BD Microlance 3™ (26 Gx1/2, 0.45mm x 13mm)	Becton Dickinson GmbH Heidelberg, Germany
BD Microlance 3™ (30 Gx1/2, 0.3 mm x 13mm)	Becton Dickinson GmbH Heidelberg, Germany
BD Plastipak 1 mL	Becton Dickinson GmbH Heidelberg, Germany
Health care respirator, FFP3	3M, St. Paul, MN, USA

6.1.8 Chemicals

Acetic acid, 96%	Merck, Darmstadt, Germany
Acetonitrile, Optigrade	LGC Standards, Wesel, Germany
Acetylcysteine	Hexal, Barleben, Germany
Ammonium acetate p.a.	Merck, Darmstadt, Germany
AS006	AlcaSynn GmbH, Austria
Chitosan with low molecular weight (50 - 190 kDa based on viscosity), 75 - 85% deacetylation	Sigma-Aldrich, Steinheim, Germany
Freund's Complete Adjuvant, (10 mL homogenized in the following proportions by weight: 85% Drakeol 5NF, 15% Aracel A (mannide monooleate emulsifier), 0.1% *Mycobacterium butyricum* dry cells)	Merck KGaA, Darmstadt, Germany
ddH_2O	membraPure, Bodenheim, Germany
Dimeticon 350-siliciumdioxid 92,5 : 7,5	Sab Simplex, Pfizer GmbH, Berlin, Germany
DMSO	Sigma-Aldrich, Steinheim, Germany
Fetal bovine serum (FBS)	PAA Laboratories GmbH, Pasching, Austria
Formic acid (>98%)	Fluka, Buchs, Switzerland
Glucose	Sigma-Aldrich, Steinheim, Germany
D-(+)-glucose monohydrate	Sigma-Aldrich, Steinheim, Germany

L-Glutamine	Sigma-Aldrich, Steinheim, Germany
HEPES	Serva, Heidelberg, Germany
Histoacryl® tissue glue	Aesculap AG, Tuttlingen, Germany
3-Hydroxybutyric acid	Sigma-Aldrich, Steinheim, Germany
Isoflurane	Abbott, Wiesbaden-Delkenheim, Germany
Loperamide hydrochloride	Sigma-Aldrich, Steinheim, Germany
Magnesium chloride	Merck, Berlin, Germany
D-(+)-mannose	Sigma-Aldrich, Steinheim, Germany
Methadone-d_3, 100 ug/mL	Cerilliant Corporation, Texas, USA
Methanol, LC-MS Chromasolv	Fluka, Buchs, Switzerland
Minimum Essential Medium (MEM) + GlutaMAXTM	Gibco®, Karlsruhe, Germany
Morphine-d_3, 1.0 mg/mL	Cerilliant Corporation, Texas, USA
Morphine sulfate salt pentahydrate (758.83 MW)	Sigma-Aldrich, Steinheim, Germany
Natrium chloride	Serva, Heidelberg, Germany
Penicillin	PAA Laboratories GmbH, Pasching, Austria
Piperacillin	Hexal, Barleben, Germany

RPMI 1640-Medium	PAA, Pasching, Austria
Sab Simplex	Pfizer GmbH, Berlin, Germany
Streptomycin	PAA Laboratories GmbH, Pasching, Austria
Trypsin-EDTA	Sigma-Aldrich, Steinheim, Germany
Zienam	Msd Sharp & Dohme GmbH, Haar, Germany

6.1.9 Solutions

HEPES-buffered Ringer's solution:

140 mM NaCl, 5.4 mM KCl, 1 mM $MgSO_4$, 1.2 mM, $CaCl_2$, 10 mM HEPES, 10 mM glucose, adjusted to pH 7.4 with NaOH (1M)

Substrate solution for rat duodenum experiments:

3-Hydroxybutyric acid 1.26 g, L-glutamine 7.3 g, D-(+)-mannose 36.04 g, D-(+)-glucose monohydrate 39.6 g, piperacillin 1.0 g, Zienam 0.2 g for 20 L HEPES

6.1.10 Software

ACD/ChemSketch (freeware version)	Advanced Chemistry Development (ACD/Labs), Frankfurt, Germany
Adobe Photoshop CS5 Extended	Adobe Systems Inc., San Jose, California, USA
Analyst™ software version 1.5.1	AB SCIEX, Darmstadt, Germany
B.E.N. version 2.03	ARVECON GmbH, Walldorf, Germany
Software program Analogon	D. Sorgenfrei, Institut für Klinische Physiologie, Charité Univeritätsmedizin Berlin, Berlin, Germany
Statistics program GraphPad Prism 5	GraphPad Software Inc., San Diego, California, USA
VALISTAT version 2.0	ARVECON GmbH, Walldorf, Germany

6.2 Methods

6.2.1 Liquid chromatography coupled with tandem mass spectrometry

The LC-MS/MS technique combines high performance liquid chromatography (HPLC) with tandem mass spectrometry (MS/MS). For data recording and analysis the Analyst ™ software (version 1.5.1; AB SCIEX, Darmstadt, Germany) was used.

6.2.1.1 High performance liquid chromatography

HPLC is an analytical method to separate, identify and quantify substances in solution. The mobile phase containing the analyte of interest is injected through a pump into a column made of specific chromatographic packing material (the stationary phase). The analyte interacts with the stationary phase according to its physicochemical properties resulting in a specific retention time for each analyte.

The HPLC system consisted of two DGU 20-A degassers, two LC-20AD pumps, one optionBox and two FCV-14 AH switching valves, a CTO-20A column thermostat and an SIL-HT_A auto sampler (all from Shimadzu, Duisburg, Germany). The liquid chromatograph was coupled to a *triple* quadrupole mass spectrometer (3200 QTRAP®; AB SCIEX, Darmstadt, Germany). The mobile phase was consisted of:

Eluent A: MeOH/H_2O (97/3, v/v) + 10 mM ammonium acetate + 0.1% acetic acid

Eluent B: MeOH/H_2O (10/90, v/v) + 5 mM ammonium acetate + 0.1% formic acid

Eluents were filtered through a Millipore filter (0.22 μm) before being used.

6.2.1.2 Mass spectrometry

Mass spectrometry (MS) is an analytical method to measure the molecular weight (MW) of atoms, molecules and molecule fragments. Mass spectrometry measures the mass-to-charge ratio (m/z) of ionized particles spraying in droplets from the needle with a surface charge of the same polarity as the charge of the needle. This ion source is named electro spray ionization (ESI). Because of the equal charges the droplets are repelled from the needle and directed towards the source sampling cone on the counter electrode. As the droplets cross the space between the needle tip and the orifice, the surface tension can no longer sustain the charge (the Rayleigh limit) at which point a “Coulombic explosion” occurs and the droplets

are dispersed. The molecules of the sample are charged in single or multiple ways (Griffiths et al., 2001). Once the molecules are ionized in the gas phase, their m/z ratio is determined (Griffiths and Wang, 2009).

The ESI ion source is combined with a quadrupole analyzer, with a continuous ion flow. The quadrupole works as a mass filter and consist of four parall metal rods with identical interspaces. The metal rods have an alternate current (ac) voltage and a direct current (dc) voltage, the diagonal partners have the same ac and dc voltage while the other pair is oppositely charged. Only ions with a specific m/z pass all the way through the quadrupole with a specific ac/dc (Chernushevich et al., 2001, Wade, 2002).

A MS/MS was used to provide improved sensitivity and selectivity. Therefore, three quadrupoles were connected in series. The first analyzer isolates the precursor ion, (Q1), the next step is the fragmentation of the ion in the second quadrupole, (Q2). The last analyzer separates the fragments according to their m/z ratio (Q3) (see Fig. 7). The detection occurs via a continuous-dynode electron multiplier. Ions impact on the lead-coated surface of a glass capillary followed by a release of electrons. The resulting cascade increases the amount of electrons which is amplifying the signal intensity (Pavia and Lampman, 2009).

The *triple* quadrupole mass spectrometer with a turbo electrospray ion source (EIS) used here operated in the positive ionization mode (ESI+). The source temperature was 450 °C and the ion source voltage was set to 4500 V. For the analytes (AS006, loperamide) two mass transitions (quantifier and qualifier) were chosen. For each internal standard (IS) a single mass transition was used. Compounds were quantified in the multiple reaction mode (MRM), which allows a screening of several target ions (Kitteringham et al., 2009).

To reduce contamination of the MS system by highly concentrated salts of experimental buffer solution, a switching valve on board 3200 QTRAP® was used, which opened 1.7 min before the initial peak and closed after 3.6 min for the detection of AS006. For loperamide, the valve opened 0.8 min before the initial peak and closed after 2.3 min.

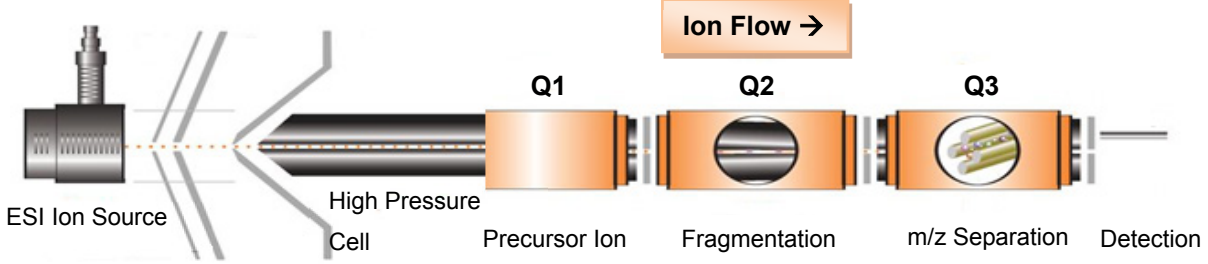

Figure 7: The QTrap 3200 mass spectrometer (modified after Applied Biosystems, 2005.)

6.2.2 Columns

6.2.2.1 Pentafluorophenyl column

For the chromatographic separation of the hydrophilic AS006 (log P = 0.27) a Phenomenex pentafluorophenyl (PFP) column (150 mm × 3. 0 mm, 3 µm particle size) and a Luna PFP 4 x 3 mm guard column was used. This stationary phase is specifically designed for polar compounds and applies a unique dipole retention mechanism to improve selectivity especially for polar analytes. The analytical column contains silica gel functionalized with PFP-groups. Analyte compounds are separated due to π-π-interactions, dipole-dipole interactions as well as hydrogen bonds.

The following gradient was used for elution: 0 - 3 min: 95 - 6% B (linear), 3 - 3.5 min: 6% B, 3.5 - 5.0 min: 5 - 95% B (linear). The flow rate was 0.5 mL/min, and the total run time was 5 min.

6.2.2.2 Atlantis dC18 Column

For the LC-MS/MS analyzes of the hydrophobic loperamide (log P = 4.26) the Atlantis dC18 Column (2.1 mm x 20 mm, 3 µm particle size) was used. C18 columns are highly hydrophobic and used for reversed phase liquid chromatography.

To prevent rapid deterioration of the analytical column, a Phenomenex C18 guard column 4 x 3.0 mm was used.

The following gradient was used for elution: 0 - 1.5 min: 95 - 5% B (linear), 1.5 - 2.5 min: 5% B, 2.5 - 3.0 min: 5 - 95% B (linear). The flow rate was 0.7 mL/min, and the total run time was 3 min.

6.2.3 Validation

The validation of analytical methods is a prerequisite for the quality and comparability of results. The validations of these two methods were performed following the guidelines published by Peters et al. (Peters et al., 2007) and the guidelines of the Society of Toxicological and Forensic Chemistry (GTFCh) (Peters et al., 2009) to fulfill quality requirements for routine analysis of pharmacologically active substances applied in humans. The validation focused on homogeneity of calibrators, homogeneity of controls, specificity, selectivity, ion suppression, definition of measurement range, calibration, lower limit of quantification, and verification of accuracy of measurement. It is a widely performed standard validation procedure employed at the Institute Labor Berlin, Department of Clinical Toxicology and Pharmacology (Köhler et al., 2011) and other clinical toxicology laboratories for novel methods of drug detection. The suitability of each procedure must be demonstrated and documented before sample testing (Peters et al., 2007).

6.2.3.1 Precision and bias

The bias is calculated as a reference for the difference between the actual and a desired value and serves as a tool for the accuracy of quantitative analysis methods:

6.2.4 Validation of LC-MS/MS method for AS006

6.2.4.1 Determination of quantifier and qualifier ion fragments

Two fragments of the analyte were monitored. The fragment yielding the most intense signal was used as the quantifier ion, the less intense fragment served as qualifier ion. Each of them has a specific mass transition as analyzed by MS/MS.

6.2.4.2 Sample preparation protocol for measurements of AS006

50 µL internal standard morphine-d_3 (100 ng/mL) were added to 100 µL of each sample, mixed and then measured with an injection volume of 10 µL. Samples with an AS006 concentration higher than 100 ng/mL were diluted 1:1000 in HEPES-buffered Ringer`s solution to fit the linear range of the standard curve. This way of sample preparation should reveal a standard curve with linear regression coefficients ≥ 0.999. All results are related to the mass transition of the quantifier ion.

6.2.4.3 Quantification of AS006

To determine the analyte concentration, samples with defined amounts of analyte (calibrators, 1, 4, 8, 25, 40, and 100 ng/mL) in HEPES-buffered Ringer's solution were used to create an AS006 standard curve. The standard curve usually showed a linear regression coefficient close to 1 (≥ 0.999). In addition, three quality control samples (QC I, QC II, QCL III: 7.5, 40, and 75 ng/mL) were used. For quantification, the relative peak area of the analyte was compared to the peak area of the IS. Sample peaks were automatically integrated and concentrations in unknown samples were calculated from the resulting calibration curves.

The linearity of the calibration was tested using the software "B.E.N."(version 2.03, Arvecom, Walldorf, Germany). This program plots the relative peak area (y-axis) against the calibrator concentration (x-axis) and the characteristics of the calibration are automatically calculated.

The following settings were used:

Significance level: 99% (homogeneity of variance)

Uncertainty of results: 3 /33% (K-value / percent value)

Number of measurements: 1

Outlier test (F-test):

First, outliers were identified using the outlier test (F-test). If an outlier (significance level 99%) was found, it was excluded and the test was repeated. When the highest calibrator had to be excluded, the linear range was adjusted accordingly.

Linearity of the calibration (F-test for linearity, Mandel test): A 1st order calibration was always performed.

6.2.4.4 Homogeneity of calibrators

Calibrator C (8.00 ng/mL AS006) of the in-house pool was considered representative of all other calibrators. The calibrator was analyzed six times following the analytical procedure described above, to check its homogeneity.

The relative peak area (Q values) was calculated according to the following equation:

$$Q = \frac{AREA(Analyt)}{AREA(IS)}$$

Here, outliers were found and eliminated using the Grubbs test (Microsoft Office Excel). At least five values should remain to provide evidence on the calibrator`s homogeneousness. The relative standard deviation (RSD) should be ≤ 20%.

6.2.4.5 Homogeneity of controls

The controls (QC I and QC III) were analyzed six times according to the analysing protocol to check their homogeneities.

Outliers were identified and eliminated using the Grubbs test (Microsoft Office Excel). At least five values are needed to ascertain the homogeneousness of the calibrators.

The RSD should be lower than ≤ 20%.

6.2.4.6 Specificity

The specificity test verifies the identity of the analyte and reflects interferences caused by other compounds contained in the sample. Therefore, individual solutions of the substances (including IS) with a concentration of 1 µg/mL in mobile phase B (s.a.) were prepared (100 µL standard solution (β = 0.01 mg/mL) + 900 µL mobile phase B) and analyzed.

6.2.4.7 Selectivity

The selectivity test shows that the analyte can be clearly identified without disturbance of other potentially contaminating substances (e.g. metabolites, impurities, and matrix).

Selectivity was tested in a mixture of 100 µL HEPES buffered Ringer`s solution and 50 µL IS morphine-d_3 (100 ng/mL); the injection volume was 10 µL.

6.2.4.8 Selectivity test for chitosan

1. 1 mL HEPES (+ 5 µL ddH_2O)

2. 1 mL HEPES (+ 5 µL Chitosan 1% solution)

100 µL of each solution were mixed with 50 µL internal standard morphine-d_3 (100 ng/mL). The injection volume was 10 µL.

6.2.4.9 Ion suppression test (peak area evaluation)

Co-elution of analytes and matrix components can significantly reduce or enhance the ionization of the analyte. Due to low and/or fluctuating signal intensity quantification can get impossible. To exclude a possible ion suppression/enhancement, the analyte was dissolved and analyzed in eluent B (reconstitution solution, RCS) and in processed blank solution (without IS) (spiked blank sample) as follows:

First, the stock solution of the analyte AS006 (0.1 mg/mL) was diluted 1:100 in MeOH. Then 40 µL of this dilution were dried to remove the MeOH and redissolved in 1 mL HEPES + 0.5 mL ddH_2O.

The analyte peak areas of the spike blank sample were compared to those of the RCS sample. A peak area reduction/increase exceeding 15% was considered to be ion suppression/enhancement.

$$\text{Peak area reduction} = \left(\frac{\text{Area pure solvent - Area spiked blank}}{\text{Area pure solvent}} \right) \times 100\%$$

6.2.4.10 Ion suppression test for chitosan

First, the stock solution of the analyte AS006 (0.1 mg/mL) was 1:100 diluted in MeOH.

Afterwards 40 µL were evaporated and redissolved in 1 mL HEPES + 0.5 mL ddH_2O and in 1 mL HEPES + Chitosan 7.5µL (0.00025%) + 0.5 mL ddH_2O.

The analyte peak areas of the spiked blank sample were compared to those of the RCS. The peak area reduction < -15% was considered as ion suppression.

6.2.4.11 Lower limit of quantification

The calibrator with the lowest analyte concentration (A = 1 ng/mL) was diluted 1:2 and 1:5 in HEPES Ringer`s solution to determine the lower limit of quantification (LLOQ) of the method. The measurement was repeated six times and samples were prepared according to the analysing protocol (see paragraph 6.7.4.2).

6.2.4.12 Definition of measurement range

The range of calibrators corresponds to the concentration range of the analyte in the sample, which allows a quantitative determination of the analyte with defined accuracy. The lower limit corresponds to the LLOQ. The upper limit is the upper limit of linear range (see paragraph 6.7.4.3 on calibration).

6.2.4.13 Verification of accuracy of measurement

On eight consecutive days calibrators and control samples were analyzed following the procedure detailed above.

For testing the linearity of the calibration the software "B.E.N." was used. The program plots the relative peak area (y-axis) against the calibrator concentration (x-axis) and the characteristics of the calibration are automatically calculated.

The following settings were used:

Significance level: 99% (variant homogeneity)

Uncertainty of results: 3 / 33% (K-value / percent-value)

Number of measurements: 8

Outlier test (F-test):

Outliers were identified using the F-test. If an outlier (significance level 99%) was found, it was excluded and the test was repeated. When the highest calibrator had to be excluded, the linear range was adjusted accordingly.

Linearity of the calibration (F-test for linearity, Mandel test): A 1st order calibration was always performed.

6.2.5 Validation of LC-MS/MS method for loperamide

6.2.5.1 Sample preparation protocol

A volume of 50 µL IS methadone-D_3 (50 ng/mL solved in acetonitrile) was added to 100 µL of the sample, briefly vortexed and centrifuged for 5 min at 20,000 x g. Subsequently, 100 µL were carefully transferred into a glass vial and measured with an injection volume of 25 µL. Samples with a concentration higher than 100 ng/mL were diluted in HEPES-buffered Ringer's solution to fit the linear range of the standard curve. This revealed a standard curve with linear regression coefficients > 0.995. All results are related to the mass transition of the quantifier ion.

6.2.5.2 Quantification of loperamide in HEPES-buffered Ringer`s solution

Samples with defined amounts of analyte (calibrators) were used to create a loperamide standard curve in HEPES-buffered Ringer's solution. A linear standard curve based on six different calibrators (1, 5, 10, 25, 50 and 100 ng/mL) and two QC samples (QC I: 7.5 and QC II: 75 ng/mL) was used. For quantification, the relative peak area of the analyte loperamide was compared to the peak area of the IS. Sample peaks were automatically integrated and concentrations in unknown samples were calculated from the resulting calibration curves (Analyst™ software, version 1.5.1, AB Sciex, Darmstadt, Germany).

The linearity of the calibration was tested using the VALISTAT- software for method validation in forensic toxicology (version 2.0, ARVECON GmbH, Germany, Walldorf). This program plots the relative peak area (y-axis) against the calibrator concentration (x-axis) and the characteristics of the calibration are automatically calculated.

The following settings were used:

Significance level: 99% (homogeneity of variance)

Uncertainty of results: 3 /33% (K-value / percent value)

Number of measurements: 1

Outlier test (F-test): as described above (6.2.4.13)

6.2.5.3 Specificity

Solutions of the substances (including IS) with a concentration of 1 µg/mL in the mobile phase B were prepared (100 µl standard solution β = 0.01 mg/mL + 900 µl mobile phase B) and analyzed. Two solutions, one with loperamide and one with the IS methadone-D_3 were measured.

6.2.5.4 Selectivity

The analyte should be clearly identifiable without any disturbances of other potentially contaminating substances (e.g. metabolites, impurities, and matrix) in the HEPES-buffered Ringer's solution. Therefore, HEPES solutions without IS were measured twice and the chromatogram was analyzed.

6.2.5.5 Precision and accuracy

Inter-day precision and accuracy were determined by analysing eight QC samples from both concentrations on eight consecutive days. Both sample levels were processed and analyzed. Intra-day precision and accuracy were determined by analysing eight QC samples of both concentrations on the same day. The measured concentrations were tested for outliers using the Grubbs test. Outliers were eliminated when criteria fulfilled recommendations for relative standard deviation, and bias values.

6.2.5.6 Limits of quantification

The lower limit of quantification (LLOQ) was the lowest concentration yielding a relative standard deviation and bias ≤ 20%. The calibrator with the lowest analyte concentration (A = 1 ng/mL) was diluted 1:2, 1:5 and 1:10 in HEPES Ringer's solution to determine the LLOQ. The measurement was repeated 8 times and samples were prepared according to the protocol for analysis. The upper limit of quantification (ULOQ) was assumed to be equal to

the upper limit of the linear range. To determine the ULOQ a complete series of calibrators was analyzed on 8 consecutive days.

6.2.5.7 Matrix effect

A possible effect of coeluting matrix compounds on the ionization of the analyte was investigated by post-column infusion of a standard solution containing loperamide (10 µg/mL in eluent B) and methadone-D_3 (10 µg/mL in eluent B) via a syringe pump (Harvard Apparatus, Holliston, MA, USA) with a flow rate of 10 µL/min while simultaneously analysing a blank HEPES-buffered Ringer's solution sample.

6.2.5.8 Stability

To investigate freeze/thaw stability, six samples from each QC (QC I: 7.5 ng/mL and QC II: 75 ng/mL) were subjected to three freeze/thaw cycles, each consisting of a 20 h freezing phase and a 20 h thawing phase. Concentrations of these pretreated samples were compared to untreated samples (n = 6). The mean of the pretreated samples had to be within a ±10% interval of the mean of the untreated samples, while the 90% confidence interval was supposed to be within a ±20% interval of the mean of untreated samples.

6.2.6 Epithelial cell culture

Two different colon epithelial cell lines were used. To avoid contamination of the growing cell culture, cells were trypsinated in the presence of EDTA three times for 5 min at 37°C and 5% CO_2. Trypsin helps to detach the cells from the flask surface and EDTA binds Ca^{2+} ions and destabilizes membrane proteins which lead to relaxation of cell structures. To avoid deactivation of trypsin the flask was washed before trypsination with Ca^{2+} and Mg^{2+} free PBS (Boxberger, 2006). For each cell filter (0.6 cm^2) 500 µL of the cell suspension was seeded, which corresponded to approximately 450,000 cells.

6.2.6.1 Caco-2 cell line

The Caco-2 cell is a well-characterized, human colon adenocarcinoma cell line. It is used for high-throughput screening of drug permeability. Caco-2 cells form a confluent epithelial cell monolayer consisting of columnar and polarized cells that expresses microvilli on the apical membrane and forms TJs between adjacent cells (Hidalgo et al., 1989). Caco-2 cells express various transporters, enzymes, and nuclear receptors (Sun et al., 2008).

Caco-2 cells were grown near confluence in monolayer cultures on permeable Millicell HA filters (pore size 0.45µm) at 37°C in an atmosphere of 5% CO_2 in Minimum Essential Medium (MEM) + GlutaMAXTM containing 15% (v/v) fetal bovine serum (FBS) and 1% penicillin/streptomycin. Cell filters with 0.6 cm^2 surface (~ 450,000 cells) were used for the Ussing chamber experiments 14 days after cell monolayers had reached a polarized confluence, giving a TER of ~ 300 Ω·cm².

6.2.6.2 HT29/B6 cell line

The HT29/B6 cell line consists of human colonic adenocarcinoma cells which form polarized and confluent growing monolayers (Kreusel et al., 1991). They have chloride-secreting and mucus producing properties (Hayslett et al., 1987). HT29/B6 were cultivated in RPMI 1640 with 10% FBS and 1% Penicillin/Streptomycin and grown on permeable Millicell PCF filters (pore size 3 µm). After 7 - 8 days, the cell monolayer filters were mounted in Ussing chambers filled with HEPES-buffered Ringer's solution. The TER of HT29/B6 was ~ 500 Ohm*cm² which indicated a tight epithelial cell model.

6.2.7 Ussing chamber technique

This *in vitro* method is used to analyze the electrical resistance of cell monolayers or native tissues as well as transport mechanisms for ions and macromolecules (Sun et al., 2008). TER is calculated from voltage changes (ΔV) induced by short current pulses (50 mA, 0.3 s). The electrical circuitry is used to determine resistance (*R*), current (*I*) and voltage (*V*), as well as impedance and capacitance (Kreusel et al., 1991). The Ussing chamber (Fig. 8 and 9) consists of a U-shaped tube two chamber system, which separates the basolateral and the apical side of a cell monolayer grown on a permeable support. Both chamber sides were filled with 5 mL HEPES-buffered Ringer's solution at a pH of 7.4 and heated up to 37°C. To ensure good circulation and oxygenation of the solution, both chamber sides were permanently gassed with a mixture of 95% O_2 and 5% CO_2. The compound of interest (AS006, loperamide, chitosan) was added to the apical side, respecticely. Samples from both sides were taken at defined time intervals.

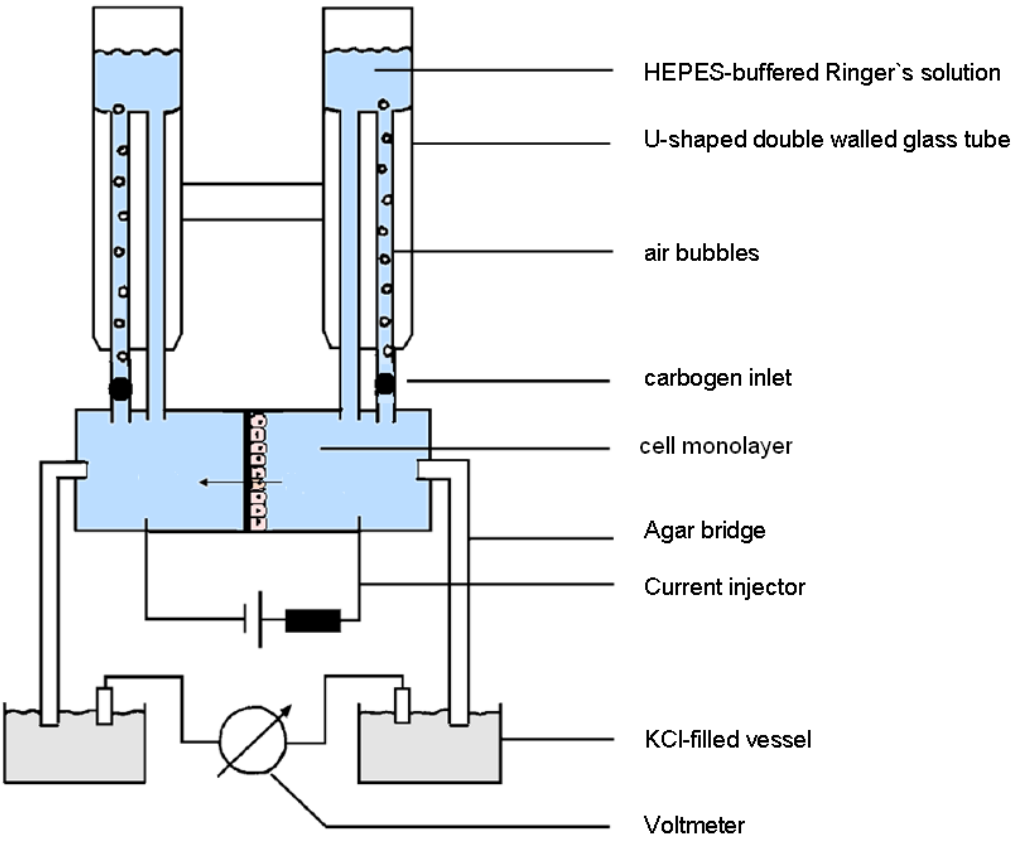

Figure 8: Ussing chamber setup (modified after Li et al., 2004).

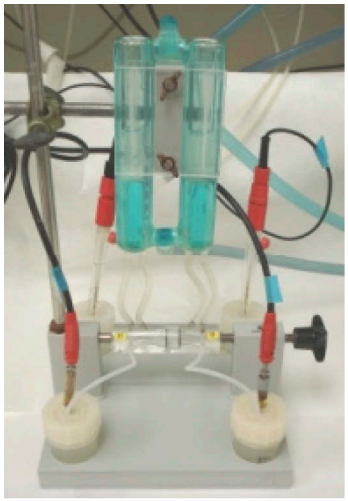

Figure 9: Typical Ussing chamber system.

The Ussing chamber system was checked for noise and offset voltages prior to the experiments. Subsequently, the resistance of the empty chambers, a parameter required for correct calculation of resistance and currents, was determined (Kreusel et al., 1991). For controlling and timing of measurements the software program Analogon (Ing. grad. D. Sorgenfrei) was used.

6.2.8 Transepithelial resistance

Transepithelial resistance was recorded as an indicator for barrier properties of the epithelial cell monolayers grown on permeable supports. The major structural correlate of barrier properties is the tight junction, which determines polarity and paracellular permeability, and therefore integrity of the epithelial tissue (Kreusel et al., 1991). A decrease in electrical resistance can reflect a decrease in tightness of TJs, and therefore an increased paracellular permeability for solutes.

Using the current (I) and the potential difference (U) the electrical resistance (R^t) is calculated using Ohm`s law:

$$R = \left(\frac{\Delta U}{\Delta I} \right)$$

6.2.9 Ussing chamber experiments with cell monolayers

After inserting the cell culture filter, both chamber sides were filled with 5 mL HEPES-buffered Ringer's solution, and TER was measured. After reaching a stable baseline, the transepithelial voltage was clamped to 0 mV. Loperamide was first solved in ≥ 99.7% DMSO and then further diluted in HEPES-buffered Ringer's stock solution to a final concentration of 10 µM. AS006 was used at a final concentration of 27.2 µM (10.2 µg/mL) dissolved in ddH_2O. Chitosan and the vehicle control were added at the same volume (25 µL) to the apical side. First, the substance of interest (AS006 or loperamide) was added to the apical side. After 5 min samples were taken from both chamber sides, representing the time point zero. Each time an equal volume of fresh HEPES-buffered Ringer's solution was replaced. Subsequently, chitosan was added to the apical side. Samples were then taken at defined intervals and stored at -80°C until they were analyzed by LC-MS/MS.

6.2.10 Permeability

The permeability describes the rate of drug transport into the receiver compartment (basolateral side) depending on the drug concentration on the apical side and the area of the cell filter membrane (Hernández-Covarrubias et al., 2012; Kataoka et al., 2011; Yamashita et al., 2002).

The following equation was used to determine the permeability P:

$$P = \left(\frac{\Delta M / \Delta t}{Co} \right) \Big/ AREAfilter\left[cm/\sec\right]$$

$\Delta M/\Delta t$ rate of drug transport into receiver compartment in ng/sec

ΔM amount of drug on the basolateral side in ng

Δt time interval in sec

Co concentration of drug added to the apical side in ng/mL

$AREAfilter$ area of the filter membrane in cm²

Substances with permeability values of $P > 10 \times 10^{-6}$ cm/s, between 0.3×10^{-6} and 10×10^{-6} cm/s, $< 0.3 \times 10^{-6}$ cm/s are termed to be highly, moderate, and poorly permeable compounds, respectively (Fichert et al., 2003).

6.2.11 Ussing chamber experiments with rat duodenum

Male Wistar rats (250 - 300 g) (from Harlan Laboratories, Netherlands) were kept on a constant light-dark cycle with free access to tap water and food in temperature-regulated (23°C) animal rooms. Rats were killed by CO_2 overdosing and the duodenum was removed and washed in gassed HEPES-buffered Ringer`s solution immediately. To avoid mucus secretion the duodenum was additionally washed in HEPES-buffered Ringer`s solution containing dimeticon (Sab Simplex, Pfizer GmbH, Berlin, Germany) and acetylcystein (MW 163.2 g/mol; ACC 300 mg / 3mLHexal AG, Holzkirchen, Germany). Plastic rings were then fixed with tissue glue (Histoacryl® Gewebekleber, Braun, Aesculap AG, Tuttlingen Germany) on the mucosal side of the duodenum (Fig. 10) and vertically mounted in the Ussing chamber. Both chamber sides were filled with 5 mL HEPES solution containing 2.14 g substrate mixture (Hydroxybutyrate 1.26 g, L-glutamin 7.3 g, D+-mannose 36.04 g, glucose monohydrat 39.6 g, piperacillin 1.0 g, Zienam 0.2 g supplemented with HEPES solution to a total amount of 20 L) at a pH of 7.4 and heated up to 37°C. Both chamber sides were permanently gassed with a mixture of 95% O_2 and 5% CO_2.

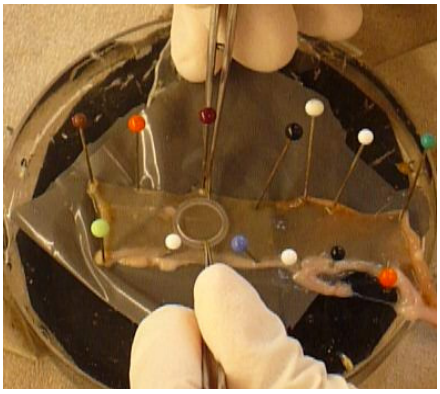

Figure 10: Rat duodenum tissue preparation.

6.3 Behavioral experiments

6.3.1 Animals

Male Wistar rats (200 – 250 g) (Harlan Laboratories, Netherlands) were housed in groups (three rats / cage). The cages were lined with ground corncob bedding. Rats were kept in climate- and light-controlled rooms (22 ± 0.5°C; relative humidity, 60 – 65%; 12 h light / dark cycle) with standard rodent food pellets and water *ad libitum*. Animal protocols were approved by the local animal care committee (Landesamt für Arbeitsschutz, Gesundheitsschutz und Technische Sicherheit, Berlin, Germany; G 0340/10) and were in accordance with the guidelines of the International Association for the Study of Pain (Zimmermann, 1983). All efforts were made to minimize the number of animals used and their suffering.

6.3.2 Complete Freund's adjuvant-induced inflammation

Under brief isoflurane anesthesia rats received unilateral intraplantar (i.pl.) injections of 150 µL complete Freund's adjuvant (CFA) into the right hind paw as described (Stein et al., 1988b) (Fig. 11). Rats were handled daily to get used to the experimenter and to reduce stress. To this end, rats were carefully placed under tissue wadding and held in this position for at least 30 seconds. This procedure was repeated twice per day with each animal. Experiments were conducted four days after inoculation.

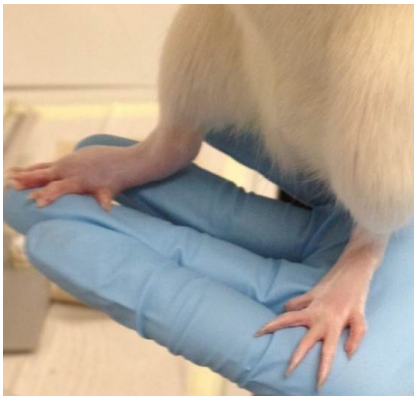

Figure 11: Inflamed (right) and non-inflamed rat paw (left) on day four after CFA injection.

6.3.3 Test compounds

Intravenous (i.v.) injections were administered into the tail vein. Loperamide hydrochloride (1, 5 and 10 mg/kg) was dissolved in 20% DMSO. Morphine sulfate (1, 2.5 and 5 mg/kg), dissolved in 0.9% NaCl, was used as a positive control. Control group received 20% DMSO i.v.. The oral administration of loperamide hydrochloride and morphine sulfate was performed with a metal feeding needle (gauge 15, length 78 mm, ball OD 2.9 mm) into the stomach in volumes of 1 mL per animal. To avoid regurgitation, rats did not receive food the night before the experiments but had free access to water. For oral administration loperamide hydrochloride was dissolved in 10% ethanol and morphine sulfate was solved in saline. Control groups received 1 mL of 10% ethanol solution. Chitosan was solved in a 1:40 solution of acetic acid plus ddH_2O and 500 µL at different concentrations for oral administration 30 min before loperamide hydrochloride or morphine sulfate. Both i.v. and oral administrations were performed under brief isoflurane anesthesia.

6.3.4 Assessment of nociceptive thresholds

Mechanical nociceptive thresholds were assessed using the paw pressure algesiometer (modified Randall-Selitto test; Ugo Basile) as previously described (Brack et al., 2004b; Stein et al., 1988b). Rats were handled for 4 days before testing. Rats were gently restrained under paper wadding, and increasing pressure was applied via a wedge-shaped, blunt piston onto the dorsal surface of the hindpaw by means of an automated gauge (Ugo Basile, Comerio VA, Italy). The pressure required to elicit paw withdrawal was recorded (cutoff at 250 g). The average of three consecutive measurements separated by 10 second intervals was calculated (Machelska et al., 2003; Stein et al., 1990). Ipsi- and contralateral (non-inflamed) paws were tested in alternating sequence. Before drug administrations, baseline thresholds were determined in both hindpaws.

6.4 Statistical analyzes

Statistical analyzes for the AS006 and loperamide method validation are described under 6.7.4.3 and 6.7.5.2.

Statistical analyzes for Ussing chamber and behavioral experiments were performed using GraphPad Prism 5 software. Experiments were repeated at least three times; the numbers of experiments used for statistical analysis are given in the figure legends. One- or two-way ANOVA was used for multiple groups. If animals were tested repeatedly (e.g. after treatment with a different drug), repeated measures (RM) two-way ANOVA were performed. Posthoc comparisons were performed with Bonferroni post test when appropriate. A p-value < 0.05 was considered significant. For non-parametric data Kruskal–Wallis one-way analysis of variance and Dunn`s post-test were used.

To test normality of data distribution the D´Agostino and Pearson omnibus test was used. In experiments with an $n < 9$ it was assumed that data were normally distributed and Two-way ANOVA and Bonferroni posttests were used. The Mann–Whitney or Wilcoxon tests were used for non-parametric data. The statistical analysis was performed in collaboration with André le Blond (INWT Statistics GmbH, Berlin, Germany).

7 RESULTS

7.1 Validation of LC-MS/MS for AS006

7.1.1 Determination of quantifier and qualifier ion fragments

The following transitions were monitored (m/z): AS006: *375.2 → 343.2/227.2*; morphine-d_3: *289.3 → 201.2*. The retention time was 2.18 min for AS006 and 3.08 min for the internal standard (IS) morphine-d_3.

7.1.2 Specificity

An interfering signal was defined by a signal/noise ratio > 10, in a time interval of ± 5% of the expected retention time of the particular analyte. Two solutions, one with AS006 and one with the IS, were measured. With each measurement three mass transitions were chosen, (Fig. 12). In Fig. 13, a representative fragmentation spectrum of AS006 and the IS in HEPES-buffered Ringer's solution is shown.

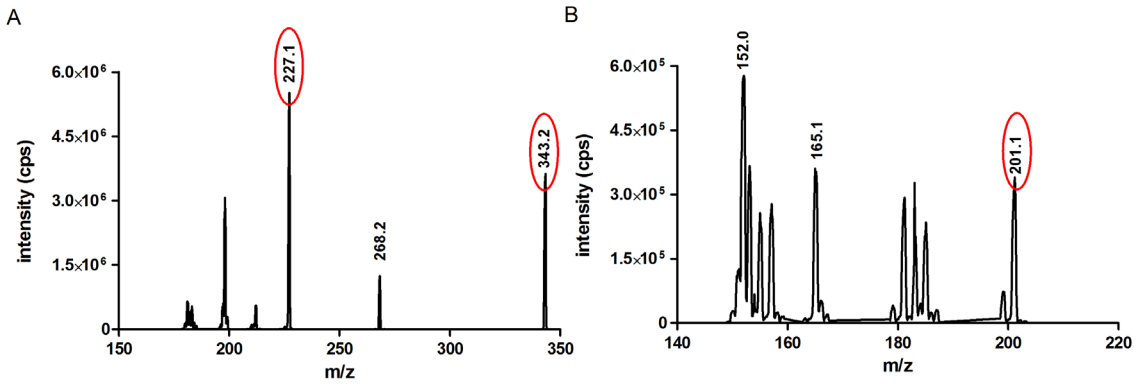

Figure 12: LC-MS/MS fragmentation spectrum of AS006 (A) and morphine-d_3 (B). Red ovals indicate the m/z of quantifier ion.

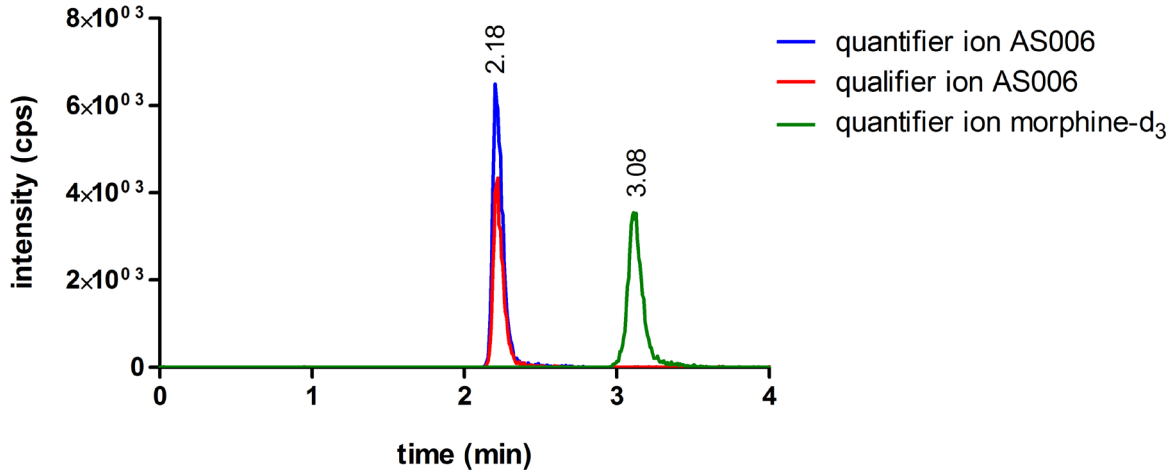

Figure 13: Representative MRM-chromatogram of AS006 and the IS morphine-d_3 in HEPES-buffered Ringer's solution. From left to right: peak intensity of AS006 (40 ng/mL, quantifier in blue and qualifier in red) and morphine-d_3 (quantifier ion in green). The total run time was 5 min.

7.1.3 Selectivity

No interfering signals occurred in the selectivity tests, indicating that chitosan had no effect on the proper identification of AS006 or the IS.

7.1.4 Ion suppression test

Chitosan produced a 33.6% increase of peak area (table 1), indicating that it interfered with the analytical method. The AS006 concentration in the sample with chitosan taken from the apical side was too high for the calibration curve. Dilution of the samples with HEPES-buffered Ringer`s solution decreased chitosan concentration as well as interference.

Table 1: Ion suppression induced by chitosan

	quantifier (Q1) (peak area)	qualifier (Q2) (peak area)
HEPES plus H_2O	1.07×10^4	6.39×10^3
HEPES plus chitosan	1.43×10^4	9.38×10^3

7.1.5 Homogeneity of calibrators

The standard deviation of relative peak areas was 2.4% for the quantifier ion of AS006 and 3.5% for the qualifier ion. These deviations fulfill the requirements of the validation protocol (RSD ≤ 20%).

7.1.6 Homogeneity of controls

The RSD for QC I was not higher than 2.4%, for QC II not higher than 6.1% and for QC III 8%. Six values for inter-day measurements remained for calculation after the Grubbs test. The condition of a bias ≤ 20% and a RSD ≤ 20% was fulfilled for all three QCs.

7.1.7 Lower limit of quantification

The detection limit of AS006 in HEPES-buffered Ringer's solution was 0.5 ng/mL, with a bias of ± 20%, precision of ≤ 20% and a significance level of 99%.

7.1.8 Definition of measurement range

The measurement range corresponds to the lower limit of quantification (LLOQ) of 0.5 ng/mL and the upper limit of linear range of 100 ng/mL. (R ≥ 0.999)

7.1.9 Accuracy of measurements

Inter-day bias for QC I was not greater than 1.43%, for QC II not greater than -1.56% and for QC III 1.76%. Eight values for inter-day measurements remained for calculation after the Grubbs test. The condition of a bias ≤ 20% and a precision ≤ 20% was fulfilled for all three QCs.

7.2 Validation of LC-MS/MS for loperamide

7.2.1 Determination of quantifier and qualifier ion fragments

The following transitions were monitored (m/z): loperamide: 477.3 → 266.3/210.2; IS (methadone-d_3): 313.3 → 268.3 (Fig. 14). The retention time was 1.81 min for loperamide and 1.72 min for methadone-d_3.

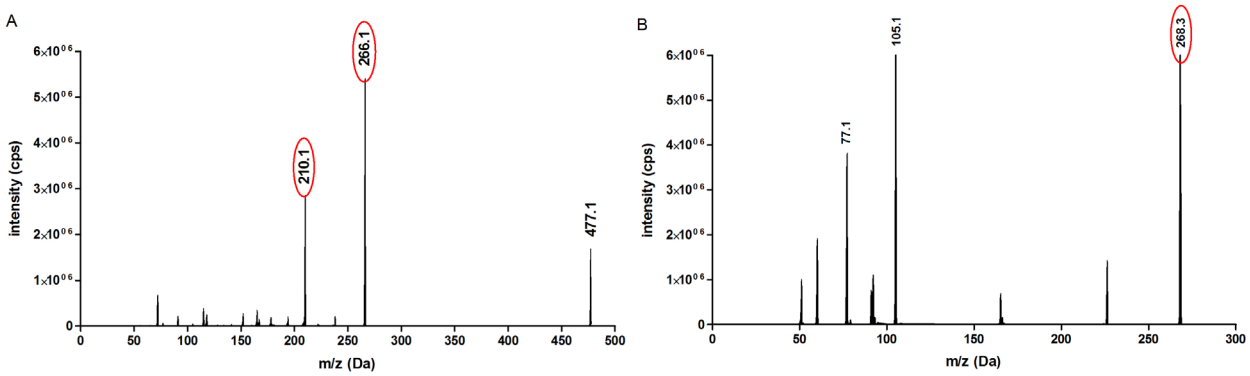

Figure 14: LC-MS/MS fragmentation spectrum of loperamide (A) and methadone-d_3 (B). Red ovals indicate the m/z of quantifier and qualifier ion.

7.2.2 Specificity

An interfering signal was defined by a signal/noise ratio > 10 in a time interval of ± 5% of the expected retention time of the particular analyte. No interfering signals occurred. In Fig. 15, a representative MRM-chromatogram of loperamide and the IS methadone-d_3 in HEPES-buffered Ringer's solution is shown.

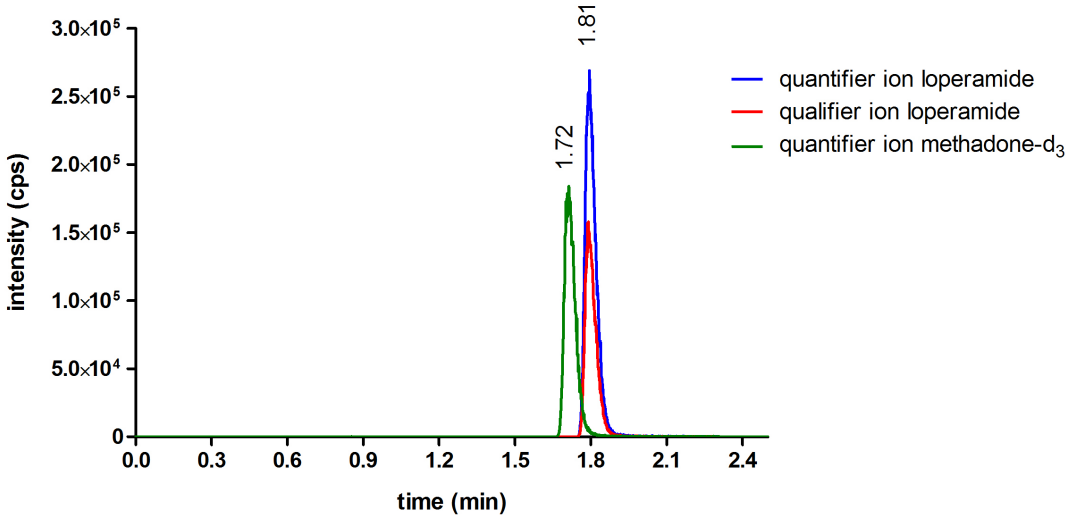

Figure 15: Representative MRM-chromatogram of loperamide (50 ng/mL) and the IS methadone-d_3 in HEPES-buffered Ringer's solution. The quantifier ion of loperamide is shown in blue, the qualifier ion of loperamide is shown in red and the quantifier of the IS methadone-d_3 is shown in green.

7.2.3 Selectivity

Both chromatograms showed no interfering signals. This indicates that the HEPES-buffered Ringer's solution had no effect on the identification of the analyte loperamide.

7.2.4 Precision and accuracy

Inter-day bias for QC I was not higher than 13.2% and for QC II not higher than 7.4%. Intra-day bias for QCI did not exceed 7.4% within a precision of 6.6%, and 14.6% for QCII within a precision of 8.2%. Eight values for inter-day and intra-day measurements remained for calculation after the Grubbs test. The conditions of precision and bias < 15% were fulfilled for both QCs.

7.2.5 Measurement range

The LLOQ of loperamide in HEPES Ringer's solution was 0.2 ng/mL within a bias $\pm$ 20% (-5.7%), precision of $\leq$ 20% (9.8%) and a significance level of 99%. All data points were tested for potential outliers using the F-test (significance level 99%). The goodness of fit was tested according to Mandel (Neitzel, 2002). The coefficient of correlation (R) was determined as well. The detection limit of loperamide in HEPES-buffered Ringer's solution was 0.1 ng/mL, within a bias $\pm$ 50% (-48.5%), precision of $\leq$ 50% (17.7%) and a significance level of 95%.

7.2.6 Matrix effect

During post column infusion the signal intensity for loperamide and methadone-d_3 did not change indicating that no ion suppression or enhancement occurred (Fig. 16).

7 Results

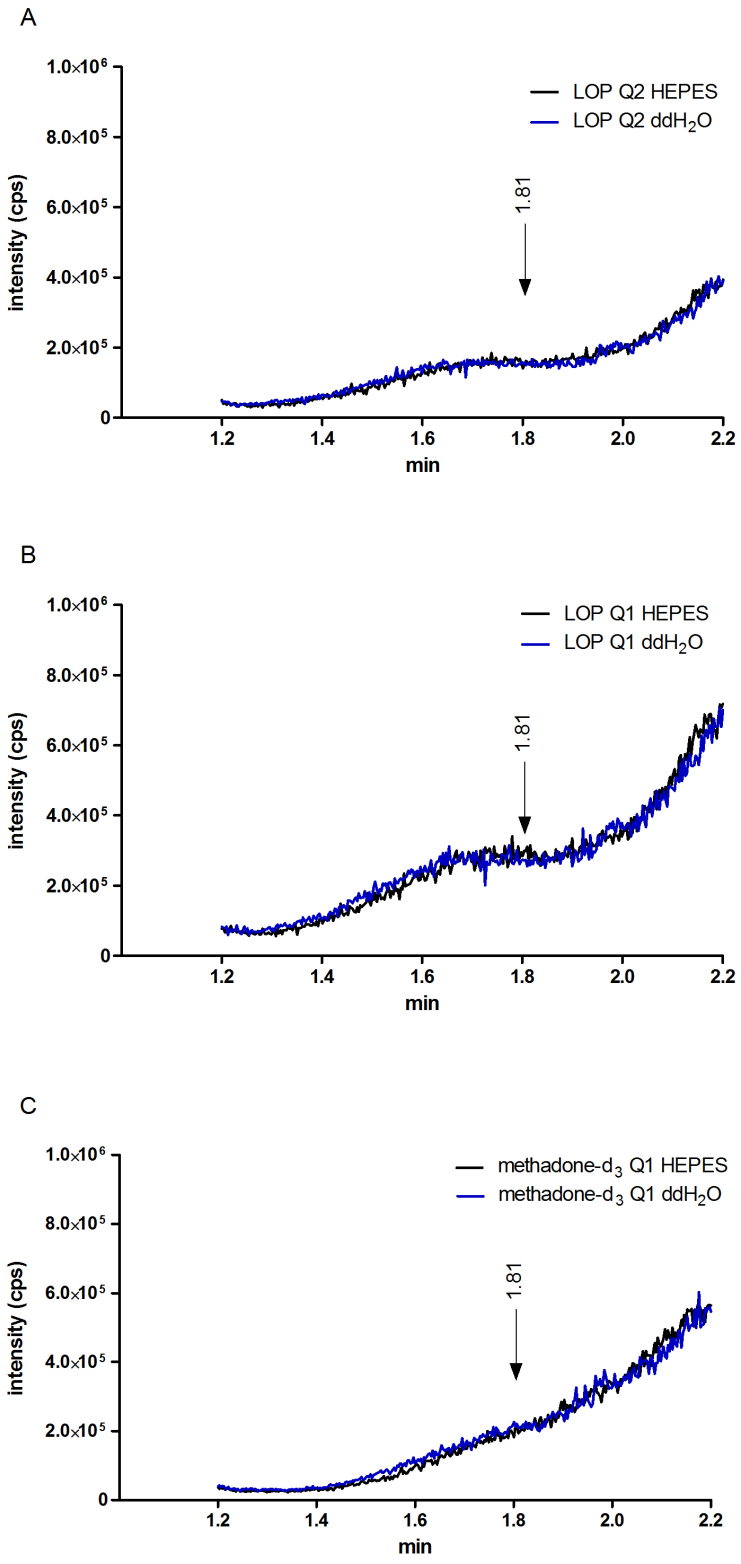

Figure 16: Ion-suppression profiles. Ion chromatograms for qualifier (A) and quantifier (B) of loperamide (LOP) and quantifier of methadone-d_3 (C), comparison between HEPES-buffered Ringer`s solution and blank solution of ddH_2O. The arrow indicatesthe expected loperamide peak on the x-axis (retention time).

7.2.7 Stability

The peak area values of the two untreated QC samples and those subjected to three freeze/thaw cycles did not differ over at least 6 h. The means of the pretreated samples (QCI 7.7 and QCII 92.7 ng/mL) were within a ± 10% interval of the mean of the untreated samples (QC I 7.4 and QC II 89 ng/mL). The 90% confidence interval was within a ± 20% interval of the mean of untreated samples.

7.3 Ussing chamber experiments with AS006

Monolayer filters of HT29/B6 and Caco-2 cells were used and AS006 and loperamide concentrations were determined in samples collected from the basolateral and apical side.

7.3.1 Effect of chitosan on permeability of HT29/B6 cell monolayers

The TER of HT29/B6 cell monolayers was determined continuously over a time period of 120 min. Four representative time points including time point zero (baseline) are shown in Fig. 17. After TER reached a stable baseline value, chitosan or vehicle (acetic acid) were added. After 30 min, the TER decreased significantly and to similar degrees at doses of 0.3 µM, 1 µM and 3 µM chitosan compared to vehicle (two-way RM ANOVA, $p < 0.001$). In cell monolayers treated with 1 µM and 3 µM chitosan the resistance showed a time-dependent decrease that was not observed at lower chitosan doses. At 0.30, 1.00 and 3.00 µM chitosan significantly drecreased the TER at 120 min compared to time point zero (one-way ANOVA, $p < 0.05$ and $p < 0.001$). In vehicle treated cells, the TER did not differ between the time points investigated (one-way ANOVA, $p > 0.05$).

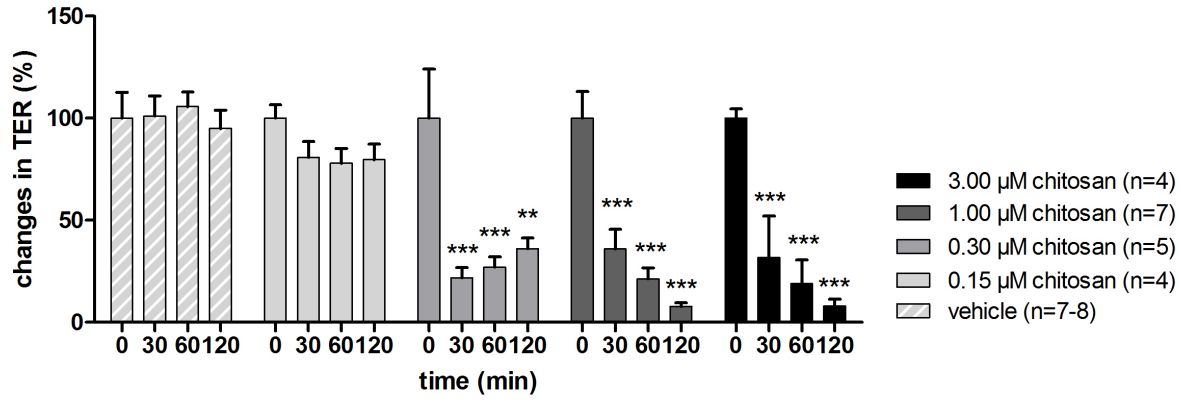

Figure 17: Effect of chitosan on the TER of HT29/B6 cell monolayers. Data represent means ± SEM, baseline TER was set to 100%. Statistical analysis was performed with two-way RM ANOVA, t-test and Bonferroni correction for multiple comparisons, ***$p < 0.001$ and **$p < 0.01$, compared to vehicle.

7 Results

Next, the effect of chitosan on intestinal transport of AS006 was analyzed.

The AS006 concentration on the basolateral side increased with time in all five chambers (Fig. 18). A marked increase of AS006 concentrations was observed after 60 and 120 min incubation with 1 µM and 3 µM chitosan ($p < 0.001$, respectively). The strongest increase was found for 3 µM chitosan after 120 min representing a 0.6% permeation rate of AS006 applied to the apical side. At 120 min chitosan-induced permeation was dose dependent (linear regression coefficient 0.95). On the apical side the AS006 concentration (mean 12.23 ± 0.64 µg/mL) did not change significantly during the experiments.

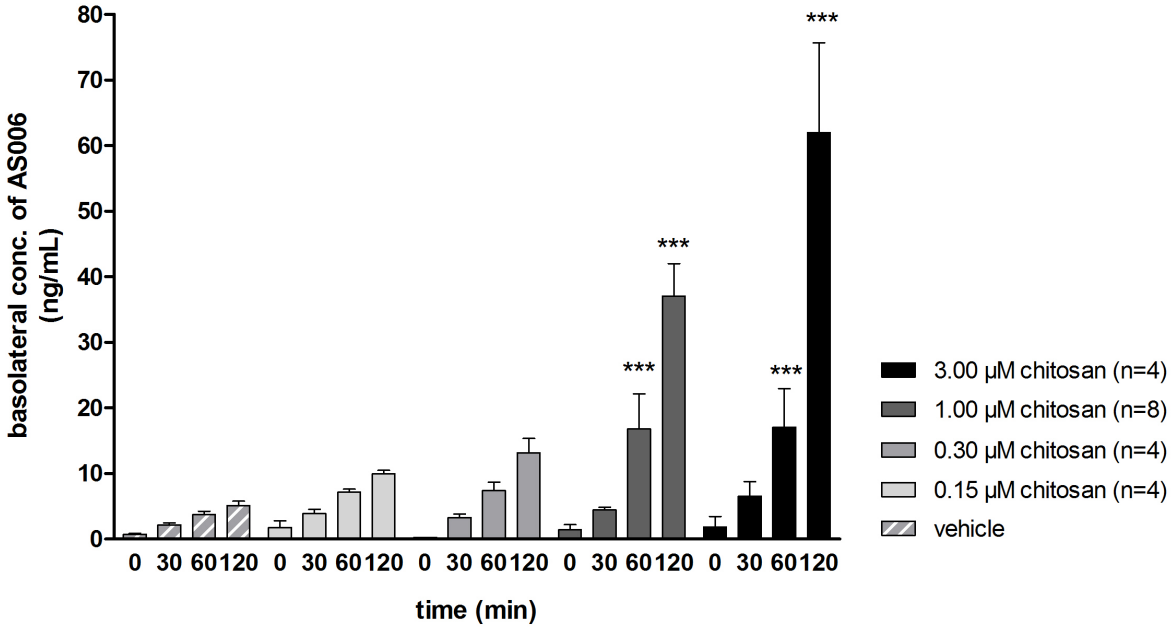

Figure 18: Time- and dose-dependent effect of chitosan on the basolateral concentration of AS006. Data represent mean AS006 concentrations ± SEM in ng/mL. Statistical analysis was performed with two-way RM ANOVA, t-test and Bonferroni correction for multiple comparisons, ***$p < 0.001$, compared to vehicle.

7 Results

Permeability P was determined using basolateral and apical AS006 concentrations (see chapter 6.2.10). The permeability of AS006 was significantly increased by 1 µM and 3 µM chitosan compared to vehicle ($p < 0.05$, $p < 0.01$, $p < 0.001$, respectively), but not by 0.15 µM or 0.3 µM chitosan (Fig. 19).

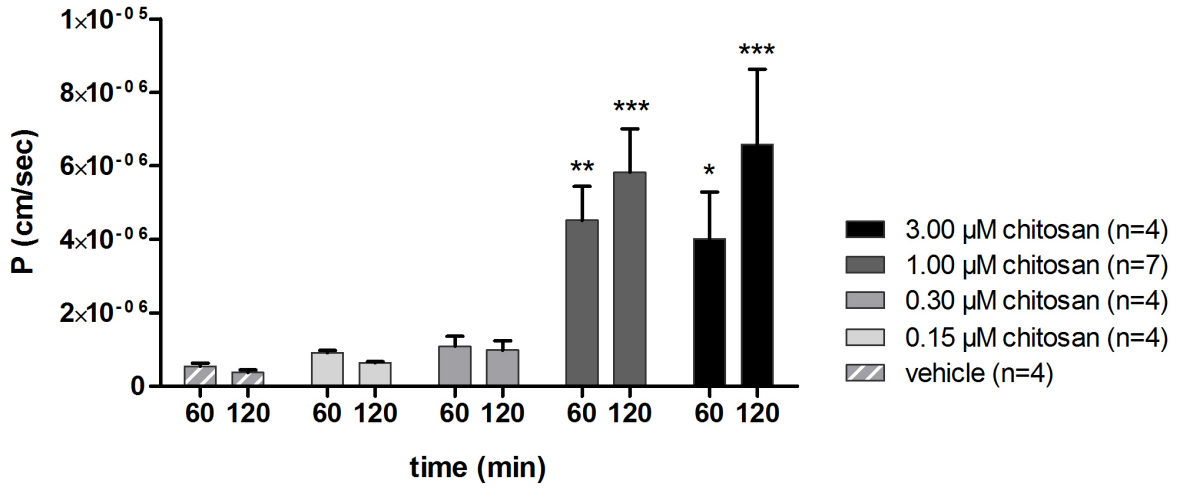

Figure 19: Effect of chitosan on AS006 permeability of HT29/B6 cell monolayers. Data represent the mean permeability P of AS006 ± SEM in cm/sec. Statistical analysis was performed with two-way RM ANOVA, t-test and Bonferroni correction for multiple comparisons, *p < 0.05, **p < 0.01, ***p < 0.001, compared to vehicle.

7.3.2 Effect of chitosan on permeability of Caco-2 cell monolayers

First, TER was measured over 120 min (Fig. 20). The TER decreased over time at all four chitosan concentrations, whereas the TER of controls (acetic acid) did not change over 120 min. 1 µM and 3 µM chitosan induced the strongest decrease in TER after 60 and 120 min ($p < 0.05$, $p < 0.01$, $p < 0.001$) compared to vehicle. 0.15 µM and 0.3 µM chitosan did not induce significant changes compared to vehicle. 0.3, 1 and 3 µM chitosan significantly decreased the TER from time point zero to 120 min (one-way ANOVA, $p < 0.05$ and $p < 0.001$).

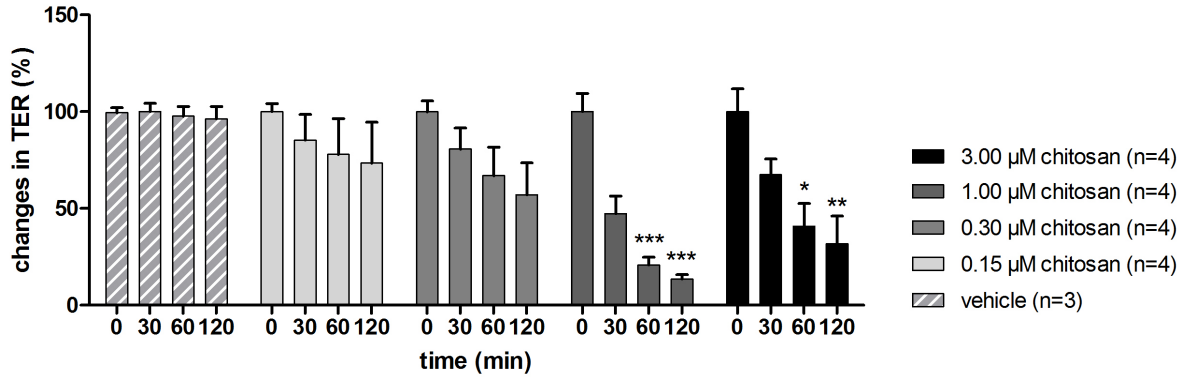

Figure 20: Time- and dose-dependent effect of chitosan on TER of Caco-2 cell monolayers. Data represent means ± SEM. Statistical analysis was performed with two-way RM ANOVA, t-test and Bonferroni correction for multiple comparisons, ***$p < 0.001$, **$p < 0.01$ and *$p < 0.05$, compared to vehicle.

7 Results

AS006 concentrations in the basolateral compartment increased over 120 min at all chitosan doses (Fig. 21). At 120 min 1 µM and 3 µM chitosan induced a marked increase of AS006 concentration compared to vehicle (acetic acid) ($p < 0.001$, respecively). 1 µM and 3 µM chitosan induced a similar increase of AS006 permeation after 120 min.

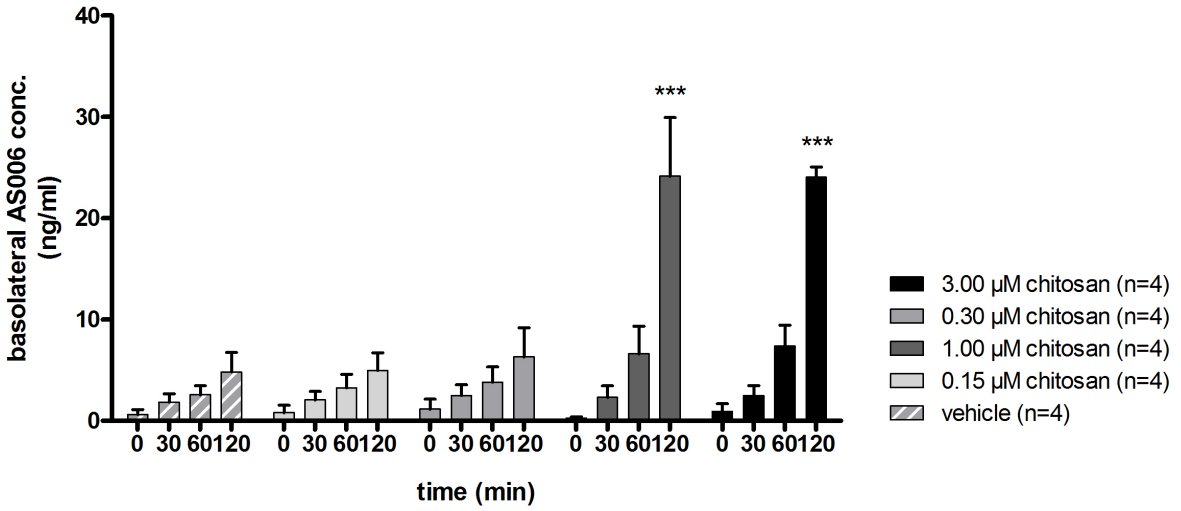

Figure 21: Time- and dose-dependent effect of chitosan on the basolateral concentration of AS006. Data represent mean AS006 concentrations ± SEM in ng/mL. Statistical analysis was performed with two-way RM ANOVA, t-test and Bonferroni correction for multiple comparisons, ***$p < 0.001$, compared to vehicle.

On the apical side AS006 concentrations remained stable over 120 min (mean $\pm$ SEM: 13.39 µg/mL $\pm$ 1.56 µg/mL).

For the calculation of AS006 permeability, the apical and basolateral concentrations were used as described in chapter 6.2.10.

7 Results

Incubation with 0.15 µM and 0.3 µM chitosan did not significantly increase permeability. After 120 min, 1 µM and 3 µM chitosan induced a marked increase in AS006 permeability ($p < 0.01$, respectively; Fig. 22).

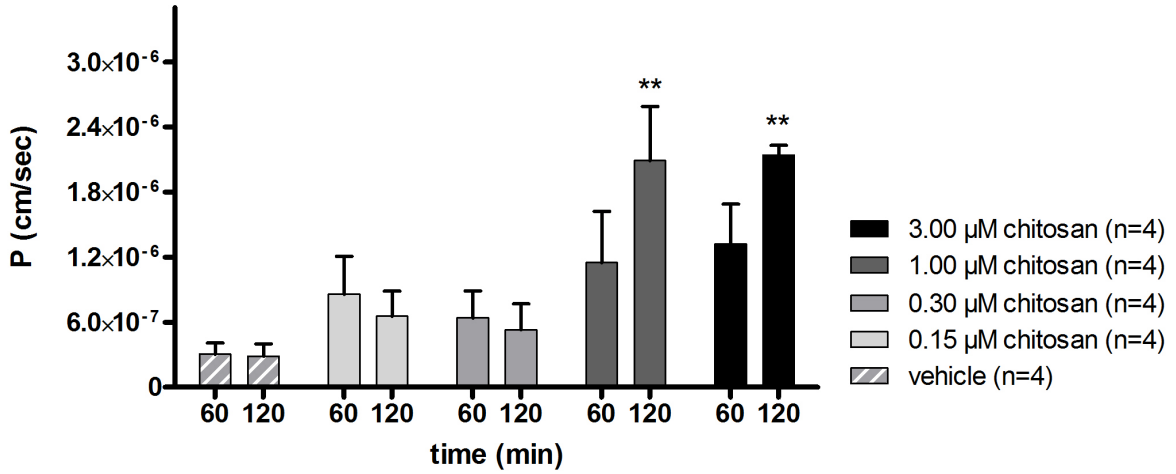

Figure 22: Effect of chitosan on the AS006 permeability of Caco-2 cell monolayers. Data represent the mean permeability P of AS006 ± SEM in cm/sec. Statistical analysis was performed with two-way RM ANOVA, t-test and Bonferroni correction for multiple comparisons, **$p < 0.01$, compared to vehicle.

7.4 Ussing chamber experiments with loperamide

7.4.1 Effect of chitosan on the permeability of HT29/B6 cell monolayers

Chitosan induced the same decrease in TER as already shown in Fig. 17. For the loperamide transport studies, one additional chitosan concentration (0.075 µM) was tested (Fig. 23). This did not affect TER. The loperamide concentration increased after 120 min in all chambers. A significant increase compared to the vehicle (acetic acid) was found with 1 µM and 3 µM chitosan ($p < 0.01$ and $p < 0.05$), no dose-dependency was observed.

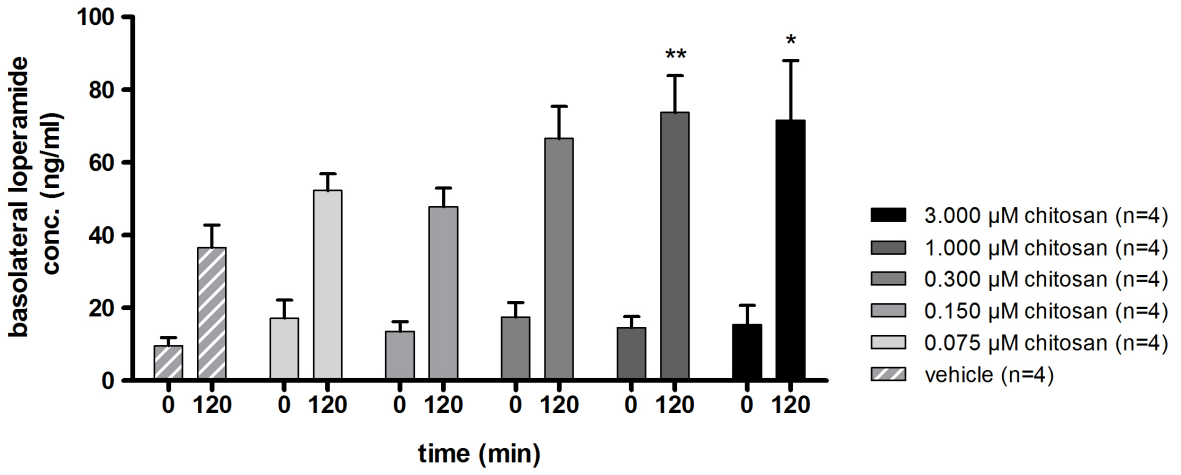

Figure 23: Time- and dose-dependent effect of chitosan on the basolateral concentration of loperamide. Data represent the mean loperamide concentration ± SEM in ng/mL. Statistical analysis was performed with two-way RM ANOVA, t-test and Bonferroni correction for multiple comparisons, *$p < 0.05$, **$p < 0.01$, compared to vehicle.

On the apical side the loperamide concentrations remained stable (mean ± SEM: 20.79 µg/mL ± 4.29 µg/mL) in all groups over 120 min. To calculate permeability, loperamide concentrations on the apical side before treatment with chitosan and the basolateral loperamide concentrations after 120 min were used as described in chapter 6.2.10.

7 Results

Permeability of cell monolayers treated with 1 µM and 3 µM chitosan showed a slight (nonsignificant) increase, otherwise loperamide permeability was unchanged compared to vehicle (Fig. 24).

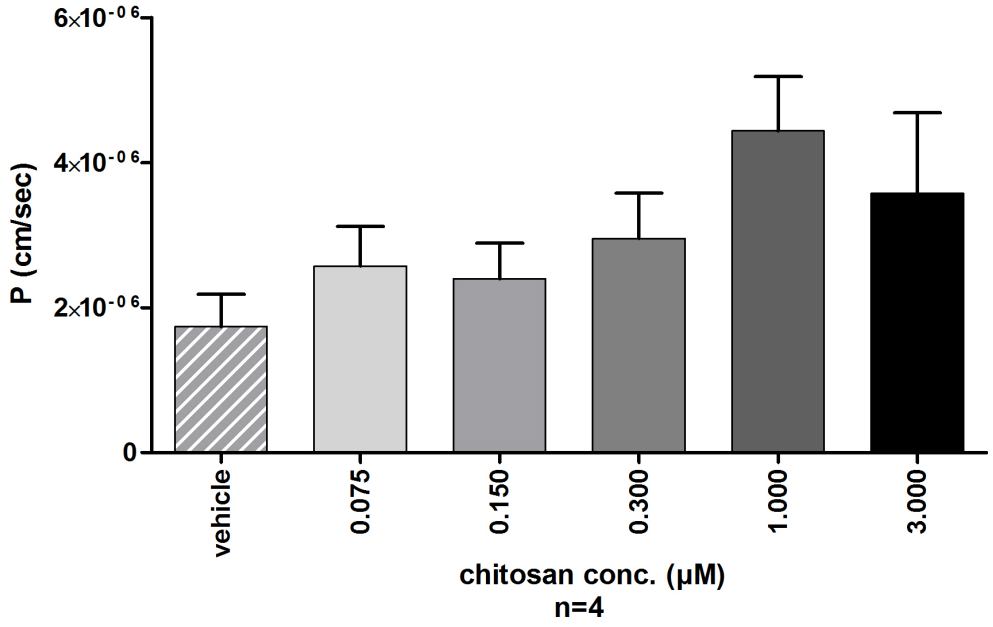

Figure 24: Effect of chitosan on loperamide permeability of HT29/B6 cell monolayers after 120 min. Data represent the mean permeability P of loperamide ± SEM in cm/sec (n = 4 per chitosan concentration (conc.). Statistical analysis was performed with one-way ANOVA.

7.4.2 Effect of chitosan on permeability of Caco-2 cell monolayers

Chitosan influenced TER in the same way as shown in Fig. 20. One additional chitosan concentration (0.075 µM) was tested, which had no effect on the TER. No chitosan concentration had significant effects on loperamide permeability (Fig. 25). A small (nonsignificant) increase in basolateral loperamide concentration (compared to vehicle) was observed using 3 µM chitosan.

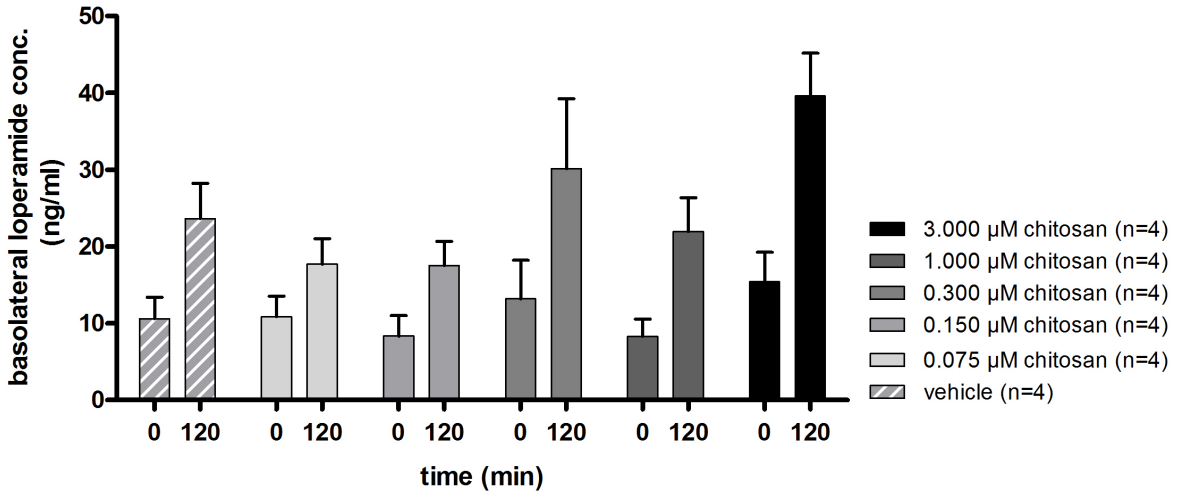

Figure 25: Time- and dose-dependent effect of chitosan on the basolateral concentration of loperamide. Data represent the mean loperamide concentration ± SEM in ng/mL. Statistical analysis was performed with two-way RM ANOVA, t-test and Bonferroni correction for multiple comparisons of values at 120 min to vehicle at 120 min.

7 Results

On the apical side loperamide concentrations remained unchanged (mean ± SEM: 19.17 µg/mL ± 8.47 µg/mL) in all groups over 120 min. To calculate permeability, the loperamide concentration on the apical side before treatment with chitosan and the basolateral loperamide concentrations were used as described in chapter 6.2.10.

Permeability P for loperamide did not significantly change at any chitosan concentration (Fig. 26).

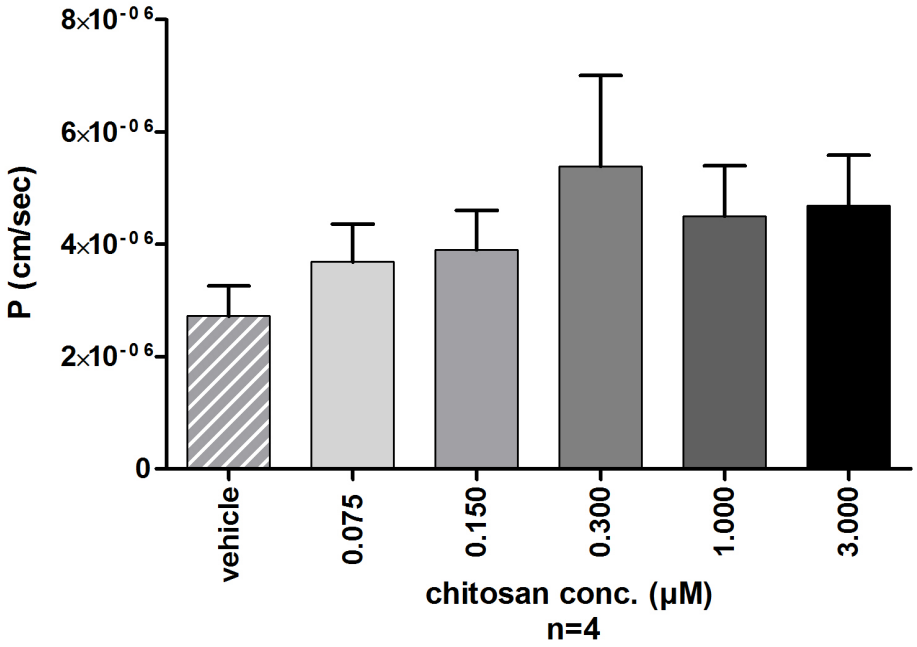

Figure 26: Effect of chitosan on loperamide permeability coefficiets of Caco-2 cell monolayers after 120 min. Data represent the permeability P of loperamide ± SEM in cm/sec (n = 4 per chitosan concentration (conc.). Statistical analysis was performed with one-way ANOVA.

7.5 Effect of chitosan on the permeability of rat duodenum

The duodenum was divided into four consecutive sections with section 1 representing the most proximal region. After TER reached stable baselines (set as 100%), chitosan (sections 1 and 3) or vehicle (sections 2 and 4) were added to the apical side and TER was measured over 180 min (Fig. 27).

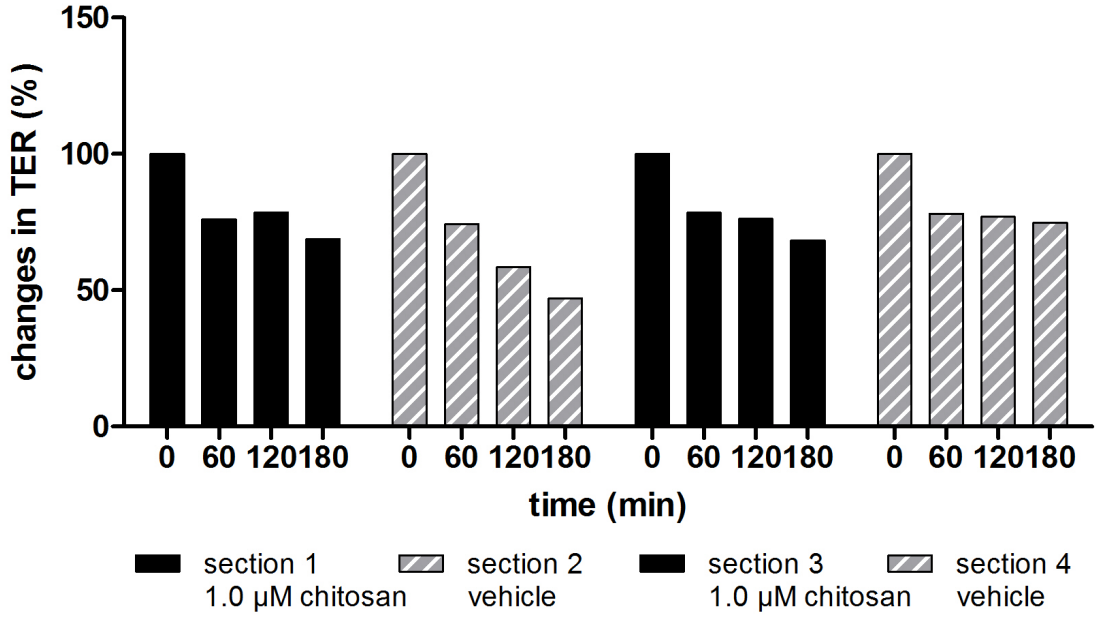

Figure 27: Effect of chitosan on TER of rat duodenum. Data represent the results of one experiment, baseline values were set as 100%.

The resistance in all four sections decreased over time. Section two, treated with vehicle, showed the strongest decrease (53%) in TER. Chitosan reduced the TER in section 1 by 31% and in section four by 26%. In section three, treated with vehicle, the TER decreased by 32%. Subsequently, two higher chitosan concentrations were tested (3.0 µM and 6.0 µM) but none of these affected TER. The application of chitosan to both chamber sides did not affect the TER either. The addition of acetylcysteine and dimeticon to decrease mucus and frothing formation on the apical side of the tissue did not result in significant improvement. In summary, chitosan did not significantly decrease TER of duodenum compared to vehicle.

7 Results

7.6 Behavioral experiments

7.6.1 Intravenous injection of morphine sulfate and loperamide

The antinociceptive effects of several different doses of intravenously (i.v.) injected morphine sulfate and loperamide were evaluated in preliminary pilot experiments using the paw pressure test. The experiments were conducted in small groups (n = 2 - 6) four days after CFA injection into the right hindpaw. Before drug injections (time zero), the baseline paw pressure thresholds (PPT) were determined and were measured repeatedly over 120 min thereafter.

In the non-inflamed hindpaws (Fig. 28 A) i.v. morphine sulfate (5 mg/kg) induced significant PPT elevations ($p < 0.01$) lasting for 60 min, whereas 10 mg/kg loperamide and 20% DMSO were ineffective. In the inflamed hindpaws (Fig. 28 B), both 5 mg/kg morphine sulfate and 10 mg/kg loperamide induced significant ($p < 0.01$ and $p < 0.001$) increases in PPT. The effect of morphine sulfate lasted for 60 min, the effect of loperamide for about 30 min.

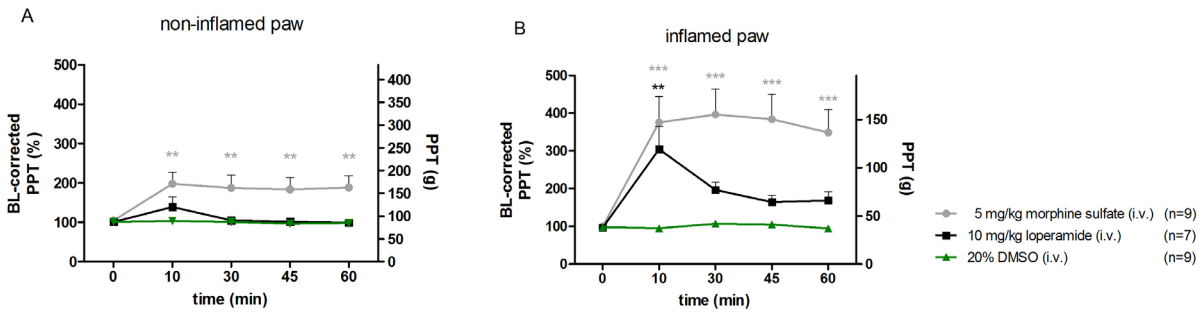

Figure 28: Effects of i.v. loperamide, morphine sulfate and vehicle (20% DMSO) on paw pressure thresholds (PPT) in non-inflamed (A) and inflamed (B) hindpaws. Data represent % of baseline (BL) (means ± SEM**, left y-axis**) and their corresponding PPT in gram (g**, right y-axis**). The BL was calculated as mean of all vehicle data (A: 87 g, B: 39 g). Statistical analysis was performed on raw PPT values with two-way RM ANOVA, t-test and Bonferroni correction for multiple comparisons. **p < 0.01, ***p < 0.001, compared to vehicle.

7.6.2 Oral administration of morphine sulfate and loperamide

Orally administered morphine sulfate induced dose-dependent PPT elevations (Fig. 29 C: $R^2 = 0.72$; Fig. 29 D: $R^2 = 0.97$, determined by linear regression ANOVA on areas under the curve (AUC) of raw PPT values) in both paws. As shown by PPT elevations in % of baseline (BL), the effects were significantly higher in inflamed than in noninflamed paws and lasted for about 120 min (Fig.29).

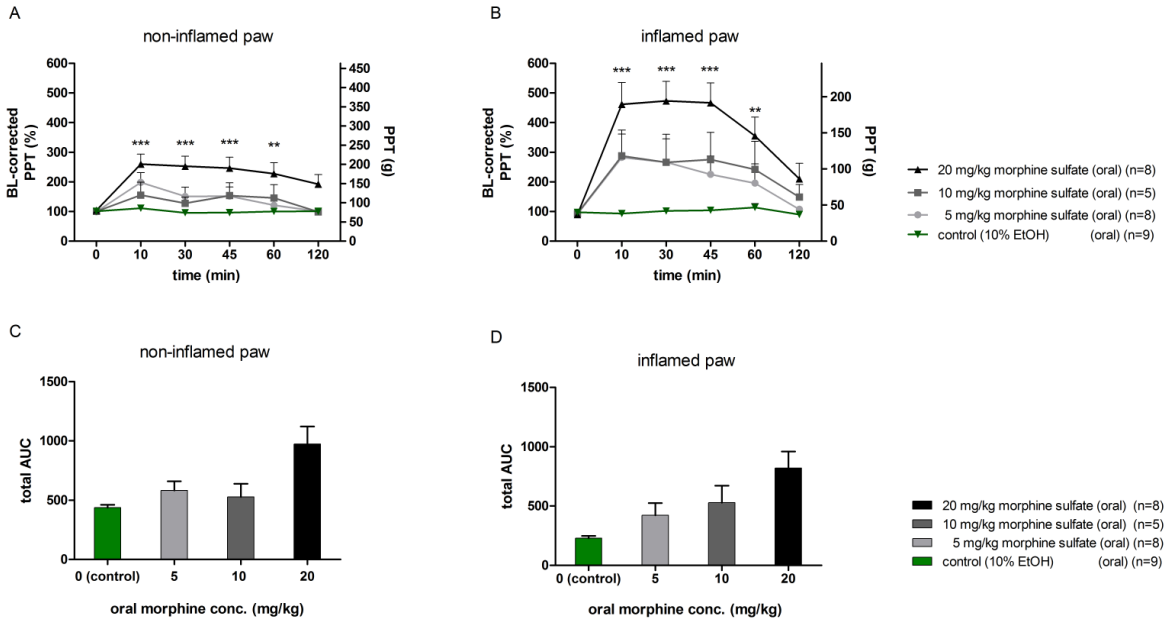

Figure 29: Effect of oral morphine sulfate and control (10% EtOH) on PPT in non-inflamed (A, C) and inflamed (B, D) hindpaws. Data represent % BL (means ± SEM**, left y-axis**) and their corresponding PPT in gram (g**, right y-axis**). The BL was calculated as mean of all vehicle data (A: **77** g, B: 41 g). Statistical analysis was performed on raw PPT values with two-way RM ANOVA, t-test and Bonferroni correction for multiple comparisons. **p < 0.01, ***p < 0.001, compared to control. Bar graphs show the total AUC of PPT values (g) shown in (A) and (B). Data in C and D represent mean total AUC ± SEM over the time period of 120 min. Statistical analysis was performed with linear regression ANOVA (C: $R^2 = 0.72$; D: $R^2 = 0.97$).

7 Results

Orally administered loperamide induced dose-dependent PPT elevations (Fig. 30 C: $R^2 = 0.70$; Fig. 30 D: $R^2 = 0.93$, determined by linear regression ANOVA on AUC of raw PPT values) in inflamed paws and a much smaller effect (only at the highest dose) in noninflamed paws. The effects lasted for about 30 min (Fig. 30).

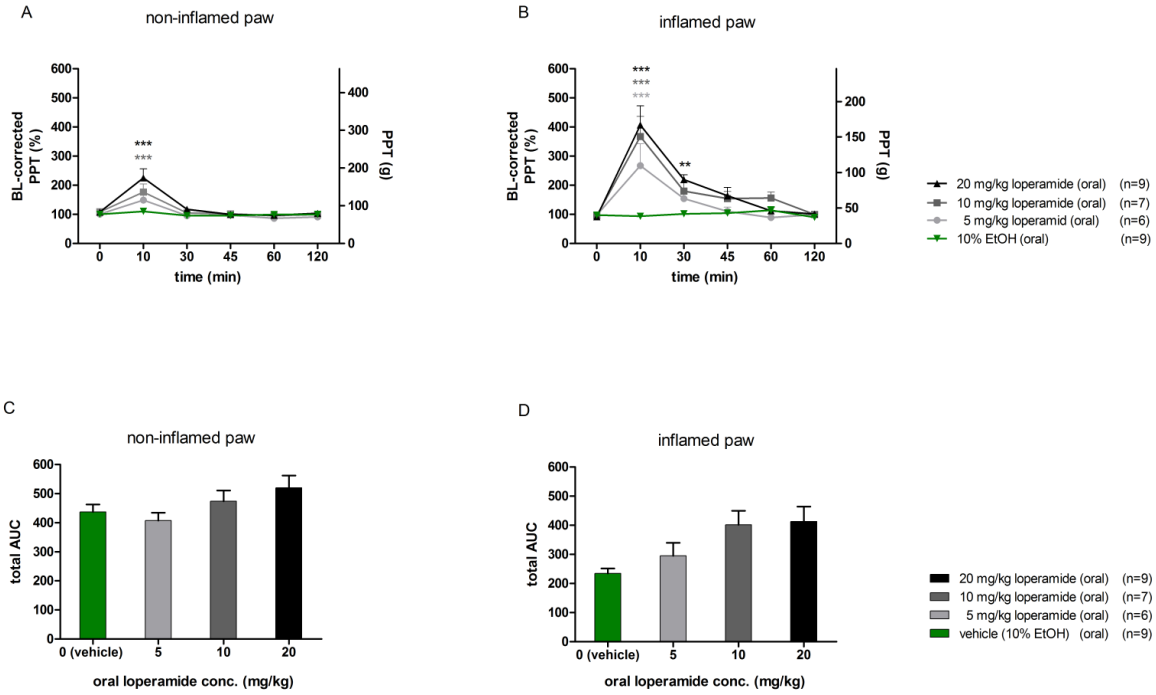

Figure 30: Effects of oral loperamide and vehicle (10% EtOH) on PPT in non-inflamed (A, C) and inflamed (B, D) hindpaws. Data represent % BL (means ± SEM**, left y-axis**) and their corresponding PPT in gram (g**, right y-axis**). The BL was calculated as mean of all vehicle data (A: **77** g, B: 41 g). Statistical analysis was performed on raw PPT values with two-way RM ANOVA, t-test and Bonferroni correction for multiple comparisons. **p < 0.01, ***p < 0.001, compared to vehicle. Bar graphs show the total AUC of PPT values (g) shown in (A) and (B). Data in C and D represent mean total AUC ± SEM over the time period of 120 min. Statistical analysis was performed with linear regression ANOVA (C: $R^2 = 0.70$; D: $R^2 = 0.93$).

7.6.3 μ-opioid receptor antagonist (NLXM) in combination with orally administered loperamide

To following experiments were performed to identify the site of action of loperamide (Fig. 31). The μ-opioid receptor antagonist NLXM was injected subcutaneously (s.c.) 10 min before oral adminstration of loperamide. When applied systemically, NLXM does not cross the blood-brain barrier, which helps to distinguish between centrally and peripherally mediated analgesic effects. In the non-inflamed paw neither loperamide nor combinations with NLXM induced significant changes on PPT. In the inflamed paw loperamide produced significant PPT elevations which were reduced by 2.5 and 5 mg/kg (but not by 10 mg/kg) of NLXM (Fig. 31).

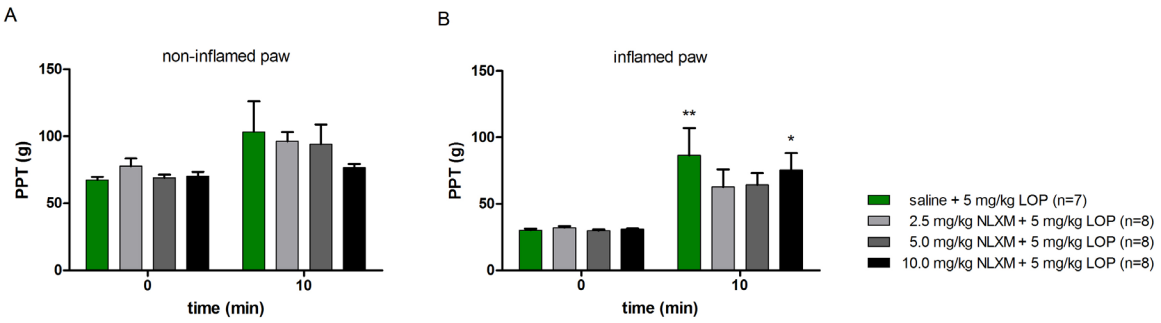

Figure 31: Effects of NLXM on PPT elevations induced by loperamide (LOP) in the non-inflamed (A) and inflamed (B) hind paw. Data represent mean PPT ± SEM. Statistical analysis was performed with one-way ANOVA, t-test and Bonferroni correction for multiple comparisons. Loperamide-induced PPT elevations compared to BL were similar in groups receiving vehicle (saline) and 10 mg/kg NLXM (*$p < 0.05$; **$p < 0.01$). PPT after 2.5 and 5 mg/kg NLXM were not significantly different from BL ($p > 0.05$).

7.6.4 Oral administration of loperamide in combination with chitosan

Following a number of pilot experiments to determine optimal dosage and time intervals, chitosan (or its vehicle acetic acid) was given orally 30 min before oral loperamide (5 mg/kg) administration and PPT were measured repeatedly thereafter.

In the non-inflamed hindpaws (Fig. 32 A), small but significant elevations of PPT were observed for vehicle ($p < 0.05$) and 3% chitosan ($p < 0.001$) compared to control (3.0% chitosan plus 10% EtOH) (Fig. 32 A, C). Compared to vehicle (acetic acid), none of the chitosan concentrations increased the effect of loperamide (Fig. 32 A, C). In the inflamed hindpaws (Fig. 32 B, D) the loperamide-induced PPT elevations were significantly increased in animals treated with 0.5% and 3.0% chitosan compared to the control group (3.0% chitosan plus 10% EtOH) at 10 min ($p < 0.01$). Compared to vehicle (acetic acid), none of the chitosan concentrations increased the overall effect of loperamide (Fig. 32 B, D). Only at 10 min the effect of loperamide was slightly but insignificant increased by 0.5 % and 3.0 % chitosan compared to vehicle (aa) plus loperamide.

7 Results

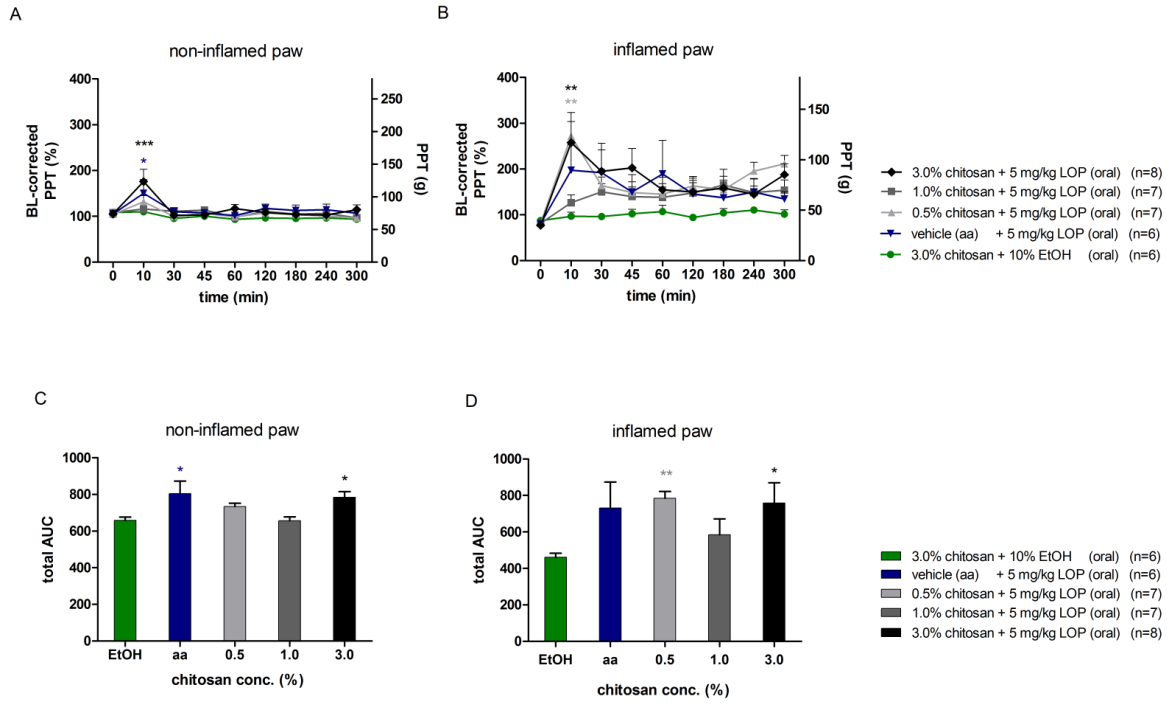

Figure 32: Effects of oral chitosan or its vehicle (aa = acetic acid) in combination with oral loperamide (LOP) or its vehicle (10% EtOH) on the PPT in non-inflamed (A, C) and inflamed (B, D) hindpaws. Data represent % BL (means ± SEM**, left y-axis**) and their corresponding PPT in gram (g**, right y-axis**). The BL was calculated as mean of all vehicle data (A: 70 g and B: 45 g). Statistical analysis was performed on raw PPT values with two-way RM ANOVA, t-test and Bonferroni correction for multiple comparisons. **p < 0.01, ***p < 0.001, compared to control (10% EtOH). Bar graphs show the total AUC of PPT values (g) shown in (A) and (B). Data in C and D represent mean total AUC ± SEM over the time period of 300 min. Statistical analysis was performed with Kruskal-Wallis test, t-test and Dunn´s multiple comparsion test. *p < 0.05 and **p < 0.01 compared to control (10% EtOH).

8 DISCUSSION

Peripheral opioid receptors can mediate pain relief without unwanted CNS side effects (Stein et al., 1988a; Stein et al. 2003). Thus, several opioid analgesics with restricted ability to cross the blood brain barrier have been designed (Stein and Machelska, 2011). However, intestinal epithelial permeability limits the effective oral administration of such compounds. The objective of this work was to evaluate the intestinal epithelial permeability of peripherally acting μ-opioid receptor agonists (AS006, loperamide) in combination with the absorption enhancer chitosan, and to investigate the impact of chitosan on the analgesic effect of these opioids when applied orally.

The major findings are: I) Chitosan increased the permeability of AS006 in HT29/B6 and Caco-2 cell monolayers *in vitro*. II) Loperamide showed moderate ability to cross HT29/B6 monolayers that slightly increased in the presence of chitosan *in vitro*. Chitosan had no effect on the permeability of loperamide in Caco-2 cell monolayers. III) *In vivo*, both i.v. and oral morphine sulfate and loperamide produced antinociceptive effects that were stronger in inflamed compared to noninflamed tissue. The effects of orally administered morphine sulfate and loperamide were dose-dependent and those of loperamide were reduced by the peripherally restricted opioid receptor antagonist NLXM. IV) The addition of oral chitosan slightly (but nonsignificantly) enhanced the peak antinociceptive effect of oral loperamide *in vivo*.

8.1 Validation of LC-MS/MS method

For the distinctive detection of AS006 and loperamide, two new LC-MS/MS methods were developed and validated (Rubelt et al., 2012). A HPLC combined with a MS/MS was used to achieve detection within a high sensitivity and selectivity. This relatively new analytical technology provides high accuracy and specificity, and helps to achieve high-throughput of sample measurements with increased data quality (Chen et al., 2000; Jian et al., 2010; Rubelt et al., 2012; Youdim and Saunders, 2010). In comparison to immune-assay techniques like enzyme linked immunosorbent assay and radioimmunoassay (Michiels et al., 1977; Killinger et al., 1979), the LC-MS/MS technique is much faster, samples can be quantified within minutes instead of hours or days. In addition, it has higher intraclass correlation coefficients, lower coefficients of variation (Faupel-Badger et al., 2010), and less cross reactivity regarding metabolites.

8 Discussion

LC-MS/MS does have limitations. For example, complex matrix solutions like the organic 4-(2-hydroxyethyl)-1-piperazineethanesulfonic acid (HEPES)-buffered Ringer's solution, which was used during *in vitro* studies present here, have high salt concentrations, which can interfere with a proper detection of the analyte of interest. Interferences such as ion suppression can occur due to the sample matrix, coelution of compounds, and cross-talk. Previous studies have shown that one of the major causes of ion suppression is a change in the spray droplet solution properties caused by the presence of nonvolatile (e.g., salts, ionpairing agents, endogenous compounds, drugs/metabolites) or low volatile solutes (King et al., 2000). To analyze if ion suppression was provoked using a physiological concentration of salts in the buffer solution (HEPES) and would affect the analyte quantification, post column analyzes were conducted. The post column infusion applied directly to the MS did not change the signal intensity of the target analytes, which indicated that no ion suppression or enhancement occurred.

The newly developed detection method for AS006 was designed to detect even low (ng/mL) AS006 concentrations in HEPES-buffered Ringer`s solution with a high reproducibility. For a distinctive detection of AS006, the mass spectrometer was set to scan a specific mass range regarding the molecular weight of AS006. For scanning and acquiring MS data, the well-established MRM scanning mode was used (Ding et al., 2013; Wang, 2009; Yang et al., 2012). MRM is an appropriate method for monitoring single fragment ions in complex matrix solutions. For specific detection of the target analyte, the fragment ions with the highest peak mass were chosen. As an internal positive control the IS morphine-d_3 was found to be suitable. Morphine-d_3 was chosen because of its high chemical similarity to the target analyte AS006. The lower limit of quantification was 0.5 ng/mL AS006. Lower concentrations of AS006 were not detectable with a clear signal from the MS. The efficiency of this method was enhanced by a switching valve, which was introduced to minimize the column contamination and to reduce its high abrasion. A simple sample preparation protocol by just adding the internal standard morphine-d_3, combined with a short mixing time proved to be sufficiently fast and easy and revealed a standard curve with a linear regression coefficient close to 1 ($R \geq 0.999$).

Previously, LC-MS/MS methods were only available for the detection of loperamide in mouse serum and brain tissue and human plasma (He et al., 2000; Kalvass et al., 2007) but not in HEPES-buffered Ringer's solution. Therefore it was necessary to develop a new method. No interfering signals occurred, ensuring a specific detection of the analyte. The validation data

revealed reliable and reproducible results according LC-MS/MS guideline requirements (Peters et al., 2009, 2007), covering a loperamide concentration range from 0.2 to 100 ng/mL. The use of two mass transitions as well as specific retention time as criteria for quantification and identification reduces the risk of interferences and enhances specificity. Sample preparation is convenient and cost effective because of the short run time and suitable for high throughput. Sample workup by just adding the IS methadone-d_3 with a short mixing time and centrifugation time of 5 min proved to be sufficiently fast and easy. No interfering signals and no matrix effects occurred during the analyzes using methadone-d_3, which indicates that it is a suitable internal standard. Sample preparation with acetonitrile followed by centrifugation of the samples insured a clear solution (due to the precipitation of proteins and salt). This way of sample preparation revealed a standard curve with linear regression coefficients close to 1 ($R \geq 0.995$). In summary, this assay achieved a high specificity and sensitivity even for small amounts of loperamide. The short run time of 3 min compares favorably to other assays (He et al., 2000), and it uses a fast and easy sample preparation protocol.

The detection of loperamide and AS006 in HEPES buffered Ringer´s solution is useful for several *in vitro* studies, for example cell culture experiments within the same matrix. Furthermore, *in vivo* approaches can benefit from this LC-MS/MS detection protocol. Variations of single parameters are marginal compared to the effort of the development of a full detection protocol.

8.2 Ussing chamber experiments

Ussing chamber experiments were conducted to test intestinal permeability of AS006 and loperamide, and the influence of chitosan *in vitro*, in line with the "3R" ("Refine, Reduce, Replace") concept to decrease the number of *in vivo* animal experiments (Go3R, 2012; Grune et al., 2004; Russell WMS and Burch RL., 1959). Two epithelial human colon cell lines, Caco2- and HT29/B6, which are frequently used for intestinal permeability studies (Amasheh et al., 2012; Kowalik et al., 2004; Kreusel et al., 1991; Merzlikine et al., 2009; Moran et al., 2012; Press and Di Grandi, 2008) were investigated.

8.2.1 Stability of AS006 and loperamide in Ussing chambers

LC-MS/MS assays established that the AS006 and loperamide concentrations added to the apical side of the Ussing chamber were generally stable over a time period of 120 min in all experiments. This indicated that these substances were not degraded by ultraviolet light or enzymatic cleavage and were not affected by the Ussing chamber system. Absorbance by the cell monolayers and interaction with the HEPES Ringer`s solution was also excluded for this time frame. The pH drop induced by addition of chitosan and vehicle (acetic acid) solution had no effect on the apical AS006 and loperamide concentrations either. Freeze/thaw stability for both substances was checked during the LC-MS/MS method validation and no disintegrations were observed. Only the intact molecule can bind to the stationary phase and is afterwards forwarded to the MS, where it is fragmented and detected. Consequently, no degraded molecules can be detected by the LC-MS/MS method. In conclusion, the Ussing chamber system in combination with the HEPES Ringer`s solution provides a suitable system for permeability studies of AS006 and loperamide. Only minor variations in the concentrations might be explained by the distribution system of the Ussing chambers.

8.2.2 Chitosan effect on epithelial resistance

A decrease in TER usually indicates a higher permeability for ions and larger molecules, as shown in previous studies using the same cell systems (Amasheh et al., 2008; Rosenthal et al., 2012b). In the presence of chitosan, the TER decreased significantly over time, which is likely induced by the enhanced transport of ions through the paracellular gap and indicates an opening of the TJs. The maximal effect of chitosan on the TER occurred after 30 min for both cell monolayers. The underlying mechanism involves the adhesion of chitosan to the TJs of

neighboring epithelial cells. As previously shown by others, chitosan is positively charged and has the ability to bind to negatively charged groups of TJ proteins (Aungst, 2000). This interaction results in a structural modification of the TJs that increases space between neighboring epithelial cells. Rosenthal and colleagues found that this decrease in resistance can be blocked by the addition of heparin, which is negatively charged and thus competes with the negatively charged groups of the TJ proteins (Rosenthal et al., 2012b). Similar to those findings, in pilot experiments heparin reversed the chitosan effect on TER (data not shown). Taken together, chitosan decreased the TER of HT29/B6 and Caco-2 cell monolayers in Ussing chambers indicating that the epithelial barrier was opened in agreement with previous studies (Borchard et al., 1996; Merzlikine et al., 2009; Rosenthal et al., 2012b; Yeh et al., 2011).

8.2.3 AS006 permeability of epithelial cell monolayers is augmented by chitosan

The μ-opioid receptor agonist AS006 has a strong polar structure due to its zwitterionic character and the presence of a glycine residue at C-6 of the morphinan scaffold. This polar structure restricts permeation across the blood-brain barrier (Schütz et al., 2003) and intestinal barriers (Gad, 2008). This was reflected by the marginal permeation of AS006 from the apical to the basolateral side of HT29/B6 and Caco-2 cell monolayers (< 5 ng/mL) determined here in vehicle treated Ussing chambers. However, AS006 permeated when the TER dropped after adding 1 - 3 μM chitosan to both cell monolayers. Lower chitosan concentrations (0.15 and 0.3 μM) also decreased the TER but the permeability values of AS006 were indistinguishable from vehicle controls. Apparently, the enhanced passage of ions, reflected by the decrease in TER, does not directly correlate with permeation of AS006. In accordance with the present findings, low chitosan concentrations have previously been found ineffective while 1 - 3 μM chitosan also enhanced the transport of other hydrophilic compounds such as [^{3}H]-mannitol and FITC-dextran (Rosenthal et al., 2012b). These authors also demonstrated that the maximum size of polar molecules passing via the paracellular path after addition of chitosan was 10 kDa (Rosenthal et al., 2012b). As AS006 has a molecular weight of only 374.4 Da, it should easily pass paracellularly if size was the only restriction.

By use of 3 μM and 1 μM of chitosan, the AS006 concentrations on the basolateral side of HT29/B6 cell monolayers were significantly increased after 60 min and 120 min. Using Caco-2 cell monolayers, the basolateral AS006 concentration was significantly increased after 120 min. Higher chitosan concentrations damaged the epithelial cell monolayer irreversibly.

8 Discussion

Rosenthal and co-workers (2012b) performed most of their experiments using 1 µM (0.005%) chitosan, since they found enhanced lactate dehydrogenase activity at higher concentrations. This cytosolic enzyme is released into the medium when cells are injured and therefore acts as a marker of cytotoxicity. Cells exposed to a 3 µM (0.015%) chitosan solution, however, were able to recover within 24 h. Taken together, 3 µM appears to be the maximum dose recommendable *in vitro*. Chitosan derivatives seem to be of lower toxicity. For example, Merzlikine and colleagues found that 3.0% chitosan glutamate enhanced paracellular passage of acyclovir (log P = −1.59) *in vitro* using Caco-2 cells (Merzlikine et al., 2009). Kudsiova and Lawrence showed that chitosan-coated phospholipid vesicles caused a decrease in TER and increased the permeability of FITC-dextran to a similar degree as seen using chitosan solution. In this study, the chitosan-coated phospholipid vesicles and the chitosan solution were both tolerated well by Caco-2 cells but the vesicles had a lower toxic effect on 16HBE14o-cell monolayers (Kudsiova and Lawrence, 2008). Chitosan nanoparticles, however, were of similar toxicity for Calu-3 cells as chitosan solution and did not enhance the passage of FITC-dextrans (Vllasaliu et al., 2010). Together these findings demonstrate that chitosan is a potent absorption enhancer of AS006 and other polar compounds, but at high doses it can lead to cell damage.

A parameter to describe the passage of a drug across an epithelial barrier is the permeability value. The permeability reflects the rate of drug movement into the receiver compartment (basolateral side) depending on the drug concentration on the apical side and the area of the cell filter membrane (Hernández-Covarrubias et al., 2012; Kataoka et al., 2011; Yamashita et al., 2002). According to previous studies (Fichert et al., 2003; Kaldas et al., 2003), compounds with permeability values $< 0.3 \times 10^{-6}$ cm/s, between 0.3×10^{-6} and 10×10^{-6} cm/s, and $> 10 \times 10^{-6}$ cm/s are defined as poorly, moderately, and highly permeable, respectively. Using HT29/B6 cell monolayers, AS006 permeability values were significantly increased from a poor (0.5×10^{-6} cm/s) up to a moderate permeability (7×10^{-6}cm/s) using 1 µM and 3 µM chitosan. These findings are comparable to those of Rosenthal et al., 2012b, who studied the transport of mannitol (5×10^{-6} cm/s) and dextrane (0.9×10^{-6} cm/s) in combination with chitosan. In Caco-2 cells the permeability values for AS006 increased only from 0.3×10^{-6} cm/s to 2.4×10^{-6} cm/s using 3 µM chitosan. Thus, HT29/B6 cell monolayers showed a better permeability for AS006. This difference may be explained by structural or functional differences between these cell types. For example, HT29/B6 cells secrete more Cl^- than Caco-2 cells (Kreusel et al., 1991). In addition, chloride-bicarbonate exchangers may be involved in chitosan-induced opening the paracellular pathway (Rosenthal et al., 2012b). In

conclusion, chitosan is an efficient enhancer of the intestinal paracellular passage of hydrophilic molecules including AS006 *in vitro*.

8.2.4 Permeability of loperamide across the intestinal barrier augmented by chitosan

In contrast to AS006, loperamide is a highly hydrophobic molecule (log P 4.26) and sequestered in lipid membranes. Unlike AS006, loperamide is a substrate of the efflux membrane transporter P-gp (Ooms et al., 1984; Thiebaut et al., 1987b). These two features keep loperamide from passing the blood-brain barrier (Schinkel et al., 1996b) despite its hydrophobic character.

Without chitosan treatment, the basolateral amount of loperamide increased 2- and 4-fold within 120 min using HT29/B6 and Caco-2 cell monolayers, respectively. These data indicate that hydrophobicity and P-gp active transport do not completely prevent the passage of loperamide across intestinal cell monolayers. In the present study pilot experiments addressed the effect of quinidine, another P-gp substrate that competes with loperamide, but no effect was found (data not shown). This is in accordance with previous findings in humans (Vandenbossche et al., 2010) and suggests that additional mechanisms are involved in the intestinal membrane transport of loperamide, as in MDCKII-hMDR1 cell monolayers (Acharya et al., 2008). Examples may be passive diffusion or basolateral transporters, as suggested by observations in a human kidney cell line (Agnani et al., 2011).

Using 0.3, 1 and 3.0 µM chitosan, the loperamide passage through HT29/B6 cell monolayers was significantly elevated after 120 min, similar to AS006. However, in Caco-2 cells, the loperamide passage was lower and showed an increase only at 3 µM chitosan, although TER was already reduced by 1 µM chitosan. As mentioned above, additional mechanisms such as chloride-bicarbonate exchangers may contribute to the opening of the paracellular pathway in HT29/B6 cell monolayers (Rosenthal et al., 2012b) and may render this cell type more permeable for the opioids analyzed here.

1 µM chitosan increased loperamide permeability in HT29/B6 cells in comparison to loperamide alone ($4.4 \pm 0.15 \times 10^{-6}$ vs. $1.7 \pm 0.9 \times 10^{-6}$ cm/s) but both values were in the range of moderate permeability and Caco-2 cell monolayers showed only a slight (nonsignificant) increase in permeability in the presence of chitosan. Thus, HT29/B6 cells showed a better permeability for loperamide both in the presence and absence of chitosan as compared to Caco-2 cell monolayers.

8.2.5 Chitosan effect on AS006 permeability in rat duodenum

In rat duodenum the TER decreased over time. This is a common phenomenon (Petersen et al., 2012) and most likely reflects the loss of integrity of native tissue after its removal from the animal. Chitosan had no additional effect on TER. It is possible that the thick mucus layer on the apical surface of the tissue may have hindered chitosan to reach the cell surface, as was previously observed by Schippers and colleagues. These authors found that mucus prevents the actions of chitosan in rat ileum, which can be overcome by increased drug and chitosan concentrations (Schipper et al., 1999). To reduce the amount of mucus, acetylcystein plus dimeticon were applied to the apical side but chitosan still had no effect on TER. Chitosan may have been bound to mucin proteins (Silva et al., 2012; Sogias et al., 2008). The mucoadhesive properties of chitosan have been interpreted as beneficial since these interactions increase gastrointestinal residence time and promote the absorption of orally administered drugs (Bernkop-Schnürch and Walker, 2001; Gu et al., 1988; Keely et al., 2005). It is therefore reasonable to assume that the duration of experiments were not long enough to observe the chitosan effect.

Another factor is pH. It has been shown that chitosan loses its effects in a pH environment higher than 7.0 (Aungst, 2000). Chitosan has a pK_a of 5.5 – 7.0, thus it is deprotonated at a pH higher than 7.0. Deprotonated chitosan likely does not act on TJs in rat duodenum (Kotzé et al., 1999), where the pH is around 7.8 (Hurst et al., 2007; Martinez et al., 2002). During the present study, the pH in the Ussing chamber was reduced by acetic acid (vehicle) or chitosan solution. However, since the experimental set-up and buffer was similar to the HT29/B6 and Caco-2 cell monolayers, the pH did not seem to interfere in those experiments. In future investigations modified chitosan compounds with enhanced mucus adhesion properties like chitosan glutamate, trimethyl chitosan or mono-N-carboxymethyl chitosan (Merzlikine et al., 2009; Thanou et al., 2001a, 2001b) should be tested. Those compounds have been shown to affect TER and TJs *in vivo* and *in vitro*.

8.3 Behavioral experiments

Based on the *in vitro* results, *in vivo* experiments using an animal model of inflammatory pain were performed. Since AS006 production had been discontinued and loperamide is already in clinical use, the experiments focused on loperamide. Initially, the analgesic effects of i.v. loperamide were compared to i.v. morphine sulfate as a positive control (Cho et al., 2013; Khalefa et al., 2012; Vann et al., 2009; Wang et al., 1994). In accordance with previous reports, morphine sulfate induced higher PPT elevations in inflamed than in noninflamed hindpaws. This has been attributed to the functional recruitment of peripheral opioid receptors in inflamed tissue (Stein, 1993; Stein et al., 1988a, 2003). Loperamide induced PPT evaluations in inflamed but not in noninflamed hindpaws. During the experiments no sedation or respiratory depression was observed. The absence of such centrally mediated side effects is an indication for the predominant involvement of peripheral opioid receptors at the doses tested here. Peripherally mediated antinociceptive effects of i.v. loperamide were also observed by others within the same dosage range (Khalefa et al., 2012) but in other animal models (Guan et al., 2008; Shinoda et al., 2007). Mortality, sedation or respiratory depression, as described with higher doses of i.v. loperamide (10 mg/kg) (Khalefa et al., 2012; Niemegeers et al., 1979) were not observed during the present experiments. Loperamide is a preferred P-gp substrate (Elkiweri et al., 2009; Shin et al., 2011; Thiebaut et al., 1987b) in contrast to morphine (Dagenais et al., 2004; Wandel et al., 2002). This has been proposed to underlay the relatively low penetration of loperamide into the CNS.

Orally administered morphine sulfate and loperamide also induced dose-dependent PPT evaluations. Similar to i.v. injections, both compounds produced stronger effects in inflamed tissue. The administration of 20 mg/kg morphine sulfate (but not of loperamide) was accompanied by slight sedative effects, presumably mediated by central opioid receptors. The intensity of the analgesic effect induced by oral morphine sulfate was comparable to that observed after i.v. injection. In contrast, a higher dose of oral loperamide was required in comparison to the i.v. dosage. This could be due to differential metabolism of the two opioids in the liver or to a more restricted ability of loperamide to cross the intestinal barrier. Thus, dose-dependent analgesic effects were induced by oral loperamide alone, which is in line with the *in vitro* results. Here, loperamide crossed the intestinal barrier to a certain degree without an absorption enhancer.

Next, the site of action of loperamide was analyzed using NLXM. This quaternary derivative of naloxone is used to distinguish between central and peripheral sites of action of opioid receptor agonists (Levitskaia et al., 2009; Lewanowitsch and Irvine, 2002). It is a competitive antagonist which binds to mu, delta, and kappa opioid receptors (Zimmerman et al., 1994). Due to the quaternary amine, the opioid receptor antagonist activity is reduced in comparison to standard antagonist naloxone (Bianchetti et al., 1983). It has a greater polarity and reduced lipid solubility, which restricts its passage across the blood brain barrier into the CNS (Brown and Goldberg, 1985; Zimmerman et al., 1994). In the non-inflamed paw neither loperamide nor NLXM had significant effects. In the inflamed paw, the analgesic effect of loperamide was attenuated using 2.5 and 5 mg/kg NLXM. This is in accordance with previous studies showing that the analgesic effect of systemically administered loperamide in models of inflammatory pain (Khalefa et al., 2012), visceral pain (Labuz et al., 2007), or muscle pain (Sánchez et al., 2010) can be antagonized by NLXM. Sánchez et al. and Khalefa et al. have shown that the antinociceptive effect of intraperitoneally (Sánchez et al., 2010) and i.v. (Khalefa et al., 2012) administered loperamide was completely antagonized by NLXM administered systemically before the agonist. In contrast, intracerebroventricular (i.c.v.) and intrathecal (i.t.) NLXM did not abolish the antinociceptive effect of i.v. loperamide (Khalefa et al., 2012). Taken together, these findings support the notion that systemically administered loperamide (at the doses used here) does not cross the blood brain barrier and produces antinociception by activating peripheral opioid receptors in inflamed tissue. However, no effects of NLXM at high doses (10 mg/kg) were observed, which may be explained by a dual (*inverted U-shape curve*) dose-effect relationship (e.g. by ligand-induced conformational changes of opioid receptors). Such phenomena have been observed frequently in various G-protein coupled receptor systems and were extensively reviewed elsewhere (Calabrese, 2009).

The next aim of *in vivo* experiments was to enhance the analgesic effects of orally applied loperamide by chitosan. Although this was found in pilot experiments, replication trials with larger groups of animals did not yield statistically significant effects. All of the previous experiments had shown that the analgesic effect of loperamide alone vanished after 60 min, irrespective whether it was applied i.v. or orally. This was also reported by others (Khalefa et al., 2012). Further experiments are necessary to determine the optimal interval between oral chitosan and opioid administration, the optimal anatomical locus of application (e.g. stomach, duodenum, lower intestine) and other (e.g. hydrophilic) opioid enhancer combinations. Following the "3R" ("Refine, Reduce, Replace") concept to decrease the number of animal

experiments, the *in vitro* setup may help to refine such *in vivo* experiments, e.g. by extrapolating dosages. However, further *in vivo* studies are undoubtedly necessary, since the *in vitro* system is an artificial environment which cannot properly mimic the *in vivo* situation.

In summary, loperamide is applicable as a peripherally acting opioid analgesic in a model of inflammatory pain in rats. The good correlation of intestinal drug permeability between rats and humans (Cao et al., 2006) makes loperamide a promising analgesic drug for clinical application. Absorption enhancers such as chitosan may offer new possibilities for peripherally acting opioids. Chitosan is effective *in vitro*. Epithelial permeability enhancement by chitosan appears to be more effective for hydrophilic opioids (AS006) than for lipophilic ones (loperamide). Future *in vivo* studies should investigate different formulations and application schedules, and address the effects of chitosan on the antinociceptive efficacy of hydrophilic opioids.

9 LITERATURE

Acharya, P., O'Connor, M.P., Polli, J.W., Ayrton, A., Ellens, H., and Bentz, J. (2008). Kinetic identification of membrane transporters that assist P-glycoprotein-mediated transport of digoxin and loperamide through a confluent monolayer of MDCKII-hMDR1 cells. Drug Metab. Dispos. *36*, 452–460.

Agnani, D., Acharya, P., Martinez, E., Tran, T.T., Abraham, F., Tobin, F., Ellens, H., and Bentz, J. (2011). Fitting the elementary rate constants of the P-gp transporter network in the hMDR1-MDCK confluent cell monolayer using a particle swarm algorithm. PLoS ONE *6*, e25086.

Aktories, K., and Barbieri, J.T. (2005). Bacterial cytotoxins: targeting eukaryotic switches. Nature Reviews Microbiology *3*, 397–410.

Alonso, M.J., and Sánchez, A. (2003). The potential of chitosan in ocular drug delivery. J. Pharm. Pharmacol. *55*, 1451–1463.

Amasheh, M., Schlichter, S., Amasheh, S., Mankertz, J., Zeitz, M., Fromm, M., and Schulzke, J.D. (2008). Quercetin enhances epithelial barrier function and increases claudin-4 expression in Caco-2 cells. J. Nutr. *138*, 1067–1073.

Amasheh, M., Luettig, J., Amasheh, S., Zeitz, M., Fromm, M., and Schulzke, J.-D. (2012). Effects of quercetin studied in colonic HT-29/B6 cells and rat intestine in vitro. Annals of the New York Academy of Sciences *1258*, 100–107.

Amasheh, S., Wenzel, U., Boll, M., Dorn, D., Weber, W., Clauss, W., and Daniel, H. (1997). Transport of charged dipeptides by the intestinal H+/peptide symporter PepT1 expressed in Xenopus laevis oocytes. J. Membr. Biol. *155*, 247–256.

Amasheh, S., Schmidt, T., Mahn, M., Florian, P., Mankertz, J., Tavalali, S., Gitter, A.H., Schulzke, J.-D., and Fromm, M. (2005). Contribution of claudin-5 to barrier properties in tight junctions of epithelial cells. Cell Tissue Res *321*, 89–96.

Amasheh, S., Fromm, M., and Günzel, D. (2011). Claudins of intestine and nephron - a correlation of molecular tight junction structure and barrier function. Acta Physiol (Oxf) *201*, 133–140.

Applied Biosystems (2005). 3200 Q TRAP® LC/MS/MS System - DirectIndustry.

Aungst, B.J. (2000). Intestinal permeation enhancers. J Pharm Sci *89*, 429–442.

Aydin, O.N., Ek, R.O., Temoçin, S., Uğur, B., Alaçam, B., and Şen, S. (2012). The antinociceptive effects of systemic administration of tramadol, gabapentin and their combination on mice model of acute pain. Agri *24*, 49–55.

Barber, A., Bartoszyk, G.D., Bender, H.M., Gottschlich, R., Greiner, H.E., Harting, J., Mauler, F., Minck, K.O., Murray, R.D., and Simon, M. (1994). A pharmacological profile of the novel, peripherally-selective kappa-opioid receptor agonist, EMD 61753. Br. J. Pharmacol. *113*, 1317–1327.

Barrot, M. (2012). Tests and models of nociception and pain in rodents. Neuroscience *211*, 39–50.

9 Literature

Le Bars, D., Gozariu, M., and Cadden, S.W. (2001). Animal models of nociception. Pharmacol. Rev. *53*, 597–652.

Bartkowiak, A., and Hunkeler, D. (1999). New microcapsules based on oligoelectrolyte complexation. Ann. N. Y. Acad. Sci *875*, 36–45.

Baselt, R.C. (2004). Disposition of Toxic Drugs and Chemicals in Man, Seventh Edition.

Bernkop-Schnürch, A., and Walker, G. (2001). Multifunctional matrices for oral peptide delivery. Crit Rev Ther Drug Carrier Syst *18*, 459–501.

Bianchetti, A., Nisato, D., Sacilotto, R., Dragonetti, M., Picerno, N., Tarantino, A., Manara, L., Angel, L.M., and Simon, E.J. (1983). Quaternary derivatives of narcotic antagonists: stereochemical requirements at the chiral nitrogen for in vitro and in vivo activity. Life Sci. *33 Suppl 1*, 415–418.

Bileviciute-Ljungar, I., Spetea, M., Guo, Y., Schütz, J., Windisch, P., and Schmidhammer, H. (2006). Peripherally mediated antinociception of the mu-opioid receptor agonist 2-[(4,5alpha-epoxy-3-hydroxy-14beta-methoxy-17-methylmorphinan-6beta-yl)amino]acetic acid (HS-731) after subcutaneous and oral administration in rats with carrageenan-induced hindpaw inflammation. J. Pharmacol. Exp. Ther *317*, 220–227.

Binder, W., and Walker, J.S. (1998). Effect of the peripherally selective κ-opioid agonist, asimadoline, on adjuvant arthritis. Br J Pharmacol *124*, 647–654.

Borchard, G., Lue[beta]en, H.L., de Boer, A.G., Verhoef, J.C., Lehr, C.-M., and Junginger, H.E. (1996). The potential of mucoadhesive polymers in enhancing intestinal peptide drug absorption. III: Effects of chitosan-glutamate and carbomer on epithelial tight junctions in vitro. Journal of Controlled Release *39*, 131–138.

Boxberger, H.J. (2006). Leitfaden für die Zell- und Gewebekultur: Einführung in Grundlagen und Techniken (Wiley-VCH Verlag GmbH).

Brack, A., Labuz, D., Schiltz, A., Rittner, H.L., Machelska, H., Schäfer, M., Reszka, R., and Stein, C. (2004a). Tissue monocytes/macrophages in inflammation: hyperalgesia versus opioid-mediated peripheral antinociception. Anesthesiology *101*, 204–211.

Brack, A., Rittner, H.L., Machelska, H., Leder, K., Mousa, S.A., Schäfer, M., and Stein, C. (2004b). Control of inflammatory pain by chemokine-mediated recruitment of opioid-containing polymorphonuclear cells. Pain *112*, 229–238.

Brown, D.R., and Goldberg, L.I. (1985). The use of quaternary narcotic antagonists in opiate research. Neuropharmacology *24*, 181–191.

Calabrese, E.J. (2009). Getting the dose-response wrong: why hormesis became marginalized and the threshold model accepted. Arch. Toxicol. *83*, 227–247.

Callaghan, R., and Riordan, J.R. (1993). Synthetic and natural opiates interact with P-glycoprotein in multidrug-resistant cells. J. Biol. Chem. *268*, 16059–16064.

Cao, X., Gibbs, S.T., Fang, L., Miller, H.A., Landowski, C.P., Shin, H.-C., Lennernas, H., Zhong, Y., Amidon, G.L., Yu, L.X., et al. (2006). Why is it challenging to predict intestinal

drug absorption and oral bioavailability in human using rat model. Pharm. Res. *23*, 1675–1686.

Caraceni, A., Cherny, N., Fainsinger, R., Kaasa, S., Poulain, P., Radbruch, L., and De Conno, F. (2002). Pain measurement tools and methods in clinical research in palliative care: recommendations of an Expert Working Group of the European Association of Palliative Care. J Pain Symptom Manage *23*, 239–255.

Casettari, L., Vllasaliu, D., Mantovani, G., Howdle, S.M., Stolnik, S., and Illum, L. (2010). Effect of PEGylation on the Toxicity and Permeability Enhancement of Chitosan. Biomacromolecules.

Chaplan, S.R., Bach, F.W., Pogrel, J.W., Chung, J.M., and Yaksh, T.L. (1994). Quantitative assessment of tactile allodynia in the rat paw. J. Neurosci. Methods *53*, 55–63.

Chen, H., Gaul, F., Gou, D., and Maycock, A. (2000). Determination of loperamide in rat plasma and bovine serum albumin by LC. Journal of Pharmaceutical and Biomedical Analysis *22*, 555–561.

Chernushevich, I.V., Loboda, A.V., and Thomson, B.A. (2001). An introduction to quadrupole-time-of-flight mass spectrometry. J Mass Spectrom *36*, 849–865.

Cho, M.H., Kim, K.S., Ahn, H.H., Kim, M.S., Kim, S.H., Khang, G., Lee, B., and Lee, H.B. (2008). Chitosan gel as an in situ-forming scaffold for rat bone marrow mesenchymal stem cells in vivo. Tissue Eng Part A *14*, 1099–1108.

Cho, S.Y., Park, A.R., Yoon, M.H., Lee, H.G., Kim, W.M., and Choi, J.I. (2013). Antinociceptive effect of intrathecal nefopam and interaction with morphine in formalin-induced pain of rats. Korean J Pain *26*, 14–20.

Chopra, S., Mahdi, S., Kaur, J., Iqbal, Z., Talegaonkar, S., and Ahmad, F.J. (2006). Advances and potential applications of chitosan derivatives as mucoadhesive biomaterials in modern drug delivery. J. Pharm. Pharmacol. *58*, 1021–1032.

Crowe, A., and Wong, P. (2003). Potential roles of P-gp and calcium channels in loperamide and diphenoxylate transport. Toxicology and Applied Pharmacology *193*, 127–137.

Dagenais, C., Graff, C.L., and Pollack, G.M. (2004). Variable modulation of opioid brain uptake by P-glycoprotein in mice. Biochem. Pharmacol. *67*, 269–276.

Davis (1999). Delivery of peptide and non-peptide drugs through the respiratory tract. Pharm. Sci. Technol. Today *2*, 450–456.

DeHaven-Hudkins, D.L., and Dolle, R.E. (2004). Peripherally restricted opioid agonists as novel analgesic agents. Curr. Pharm. Des. *10*, 743–757.

DeHaven-Hudkins, D.L., Burgos, L.C., Cassel, J.A., Daubert, J.D., DeHaven, R.N., Mansson, E., Nagasaka, H., Yu, G., and Yaksh, T. (1999). Loperamide (ADL 2-1294), an opioid antihyperalgesic agent with peripheral selectivity. J. Pharmacol. Exp. Ther. *289*, 494–502.

Dennis, S., and Melzack, R. (1983). Perspectives on phylogenetic evolution of pain expression. *Animal Pain: Perception and Alleviation, edited by Kitchell AL, Erickson HH. Bethesda, MD: American Physiological Society*.

9 Literature

Ding, X., Ghobarah, H., Zhang, X., Jaochico, A., Liu, X., Deshmukh, G., Liederer, B.M., Hop, C.E.C.A., and Dean, B. (2013). High-throughput liquid chromatography/mass spectrometry method for the quantitation of small molecules using accurate mass technologies in supporting discovery drug screening. Rapid Commun. Mass Spectrom. *27*, 401–408.

Dingledine, R., and Goldstein, A. (1976). Effect of synaptic transmission blockade on morphine action in the guinea-pig myenteric plexus. J Pharmacol Exp Ther *196*, 97–106.

Dobrila-Dintinjana, R., and Nacinović-Duletić, A. (2011). Placebo in the treatment of pain. Coll Antropol *35 Suppl 2*, 319–323.

Döring, F., Walter, J., Will, J., Föcking, M., Boll, M., Amasheh, S., Clauss, W., and Daniel, H. (1998). Delta-aminolevulinic acid transport by intestinal and renal peptide transporters and its physiological and clinical implications. J. Clin. Invest. *101*, 2761–2767.

Dorkoosh, F.A., Broekhuizen, C.A.N., Borchard, G., Rafiee-Tehrani, M., Verhoef, J.C., and Junginger, H.E. (2004). Transport of octreotide and evaluation of mechanism of opening the paracellular tight junctions using superporous hydrogel polymers in Caco-2 cell monolayers. J Pharm Sci *93*, 743–752.

Elkiweri, I.A., Zhang, Y.L., Christians, U., Ng, K.-Y., Patot, M.C.T. van, and Henthorn, T.K. (2009). Competitive Substrates for P-Glycoprotein and Organic Anion Protein Transporters Differentially Reduce Blood Organ Transport of Fentanyl and Loperamide: Pharmacokinetics and Pharmacodynamics in Sprague-Dawley Rats. Anesth Analg *108*, 149–159.

Endres-Becker, J., Heppenstall, P.A., Mousa, S.A., Labuz, D., Oksche, A., Schäfer, M., Stein, C., and Zöllner, C. (2007). Mu-opioid receptor activation modulates transient receptor potential vanilloid 1 (TRPV1) currents in sensory neurons in a model of inflammatory pain. Mol. Pharmacol. *71*, 12–18.

Escaffit, F., Boudreau, F., and Beaulieu, J.-F. (2005). Differential expression of claudin-2 along the human intestine: Implication of GATA-4 in the maintenance of claudin-2 in differentiating cells. J. Cell. Physiol. *203*, 15–26.

Fasano, A. (1999). Cellular microbiology: can we learn cell physiology from microorganisms? Am. J. Physiol *276*, C765–776.

Fasano, A. (2001). Intestinal zonulin: open sesame! Gut *49*, 159 –162.

Faupel-Badger, J.M., Fuhrman, B.J., Xu, X., Falk, R.T., Keefer, L.K., Veenstra, T.D., Hoover, R.N., and Ziegler, R.G. (2010). Comparison of Liquid Chromatography-Tandem Mass Spectrometry, RIA, and ELISA Methods for Measurement of Urinary Estrogens. Cancer Epidemiology Biomarkers & Prevention *19*, 292 –300.

Fichert, T., Yazdanian, M., and Proudfoot, J.R. (2003). A structure-permeability study of small drug-like molecules. Bioorg. Med. Chem. Lett. *13*, 719–722.

Furuse, M., Hirase, T., Itoh, M., Nagafuchi, A., Yonemura, S., Tsukita, S., and Tsukita, S. (1993). Occludin: a novel integral membrane protein localizing at tight junctions. J. Cell Biol. *123*, 1777–1788.

9 Literature

Furuse, M., Fujita, K., Hiiragi, T., Fujimoto, K., and Tsukita, S. (1998). Claudin-1 and -2: novel integral membrane proteins localizing at tight junctions with no sequence similarity to occludin. J. Cell Biol. *141*, 1539–1550.

Gad, S.C. (2008). Preclinical Development Handbook: ADME and Biopharmaceutical Properties (John Wiley & Sons).

Ganapathy, V., and Miyauchi, S. (2005). Transport systems for opioid peptides in mammalian tissues. AAPS J *7*, E852–856.

Go3R (2012). Go3R. Transinsight GmbH. Dresden.Germany. access date 06. Feb. 2013. http://www.go3r.org>.

González-Mariscal, L., Betanzos, A., Nava, P., and Jaramillo, B.. (2003). Tight junction proteins. Progress in Biophysics and Molecular Biology *81*, 1–44.

Griffiths, W.J., and Wang, Y. (2009). Mass spectrometry: from proteomics to metabolomics and lipidomics. Chem. Soc. Rev. *38*, 1882.

Griffiths, W.J., Jonsson, A.P., Liu, S., Rai, D.K., and Wang, Y. (2001). Electrospray and tandem mass spectrometry in biochemistry. Biochem. J *355*, 545–561.

Grune, B., Fallon, M., Howard, C., Hudson, V., Kulpa-Eddy, J.A., Larson, J., Leary, S., Roi, A., van der Valk, J., Wood, M., et al. (2004). Report and recommendations of the international workshop "Retrieval approaches for information on alternative methods to animal experiments."ALTEX *21*, 115–127.

Gu, J.M., Robinson, J.R., and Leung, S.H. (1988). Binding of acrylic polymers to mucin/epithelial surfaces: structure-property relationships. Crit Rev Ther Drug Carrier Syst *5*, 21–67.

Guan, Y., Johanek, L.M., Hartke, T.V., Shim, B., Tao, Y.-X., Ringkamp, M., Meyer, R.A., and Raja, S.N. (2008). Peripherally acting mu-opioid receptor agonist attenuates neuropathic pain in rats after L5 spinal nerve injury. Pain *138*, 318–329.

Hans, L. (2007). Animal data: The contributions of the Ussing Chamber and perfusion systems to predicting human oral drug delivery in vivo. Advanced Drug Delivery Reviews *59*, 1103–1120.

Hayslett, J.P., Gögelein, H., Kunzelmann, K., and Greger, R. (1987). Characteristics of apical chloride channels in human colon cells (HT29). Pflugers Arch *410*, 487–494.

He, H., Sadeque, A., Erve, J.C., Wood, A.J., and Hachey, D.L. (2000). Quantitation of loperamide and N-demethyl-loperamide in human plasma using electrospray ionization with selected reaction ion monitoring liquid chromatography-mass spectrometry. J. Chromatogr. B Biomed. Sci. Appl. *744*, 323–331.

Hernández-Covarrubias, C., Vilchis-Reyes, M.A., Yépez-Mulia, L., Sánchez-Díaz, R., Navarrete-Vázquez, G., Hernández-Campos, A., Castillo, R., and Hernández-Luis, F. (2012). Exploring the interplay of physicochemical properties, membrane permeability and giardicidal activity of some benzimidazole derivatives. Eur J Med Chem *52*, 193–204.

9 Literature

Hidalgo, I.J., Raub, T.J., and Borchardt, R.T. (1989). Characterization of the human colon carcinoma cell line (Caco-2) as a model system for intestinal epithelial permeability. Gastroenterology *96*, 736–749.

Hirano, S. (1996). Chitin Biotechnology Applications. (Elsevier), pp. 237–258.

Hurst, S., Loi, C.-M., Brodfuehrer, J., and El-Kattan, A. (2007). Impact of physiological, physicochemical and biopharmaceutical factors in absorption and metabolism mechanisms on the drug oral bioavailability of rats and humans. Expert Opin Drug Metab Toxicol *3*, 469–489.

Huwyler, J., Drewe, J., Gutmann, H., Thöle, M., and Fricker, G. (1998). Modulation of morphine-6-glucuronide penetration into the brain by P-glycoprotein. Int J Clin Pharmacol Ther *36*, 69–70.

IASP (1979). Pain terms: a list with definitions and notes on usage. Recommended by the IASP Subcommittee on Taxonomy. Pain *6*, 249.

Ikenouchi, J., Furuse, M., Furuse, K., Sasaki, H., Tsukita, S., and Tsukita, S. (2005). Tricellulin constitutes a novel barrier at tricellular contacts of epithelial cells. J. Cell Biol. *171*, 939–945.

Jian, W., Edom, R.W., Xu, Y., and Weng, N. (2010). Recent advances in application of hydrophilic interaction chromatography for quantitative bioanalysis. Journal of Separation Science *33*, 681–697.

Jonker, J.W., Wagenaar, E., van Deemter, L., Gottschlich, R., Bender, H.M., Dasenbrock, J., and Schinkel, A.H. (1999). Role of blood-brain barrier P-glycoprotein in limiting brain accumulation and sedative side-effects of asimadoline, a peripherally acting analgaesic drug. Br. J. Pharmacol. *127*, 43–50.

Kaldas, M.I., Walle, U.K., and Walle, T. (2003). Resveratrol transport and metabolism by human intestinal Caco-2 cells. J. Pharm. Pharmacol. *55*, 307–312.

Kalvass, J.C., Olson, E.R., Cassidy, M.P., Selley, D.E., and Pollack, G.M. (2007). Pharmacokinetics and pharmacodynamics of seven opioids in P-glycoprotein-competent mice: assessment of unbound brain EC50,u and correlation of in vitro, preclinical, and clinical data. J. Pharmacol. Exp. Ther. *323*, 346–355.

Kataoka, M., Iwai, K., Masaoka, Y., Sakane, T., Sakuma, S., and Yamashita, S. (2011). Scale-up of in vitro permeation assay data to human intestinal permeability using pore theory. Int J Pharm *414*, 69–76.

Keely, S., Rullay, A., Wilson, C., Carmichael, A., Carrington, S., Corfield, A., Haddleton, D.M., and Brayden, D.J. (2005). In vitro and ex vivo intestinal tissue models to measure mucoadhesion of poly (methacrylate) and N-trimethylated chitosan polymers. Pharm. Res. *22*, 38–49.

Khalefa, B.I., Shaqura, M., Al-Khrasani, M., Fürst, S., Mousa, S.A., and Schäfer, M. (2012). Relative contributions of peripheral versus supraspinal or spinal opioid receptors to the antinociception of systemic opioids. Eur J Pain *16*, 690–705.

9 Literature

Khoury, G.F., Stein, C., and Garland, D.E. (1990). Intra-articular morphine for pain after knee arthroscopy. Lancet *336*, 874.

Al-Khrasani, M., Spetea, M., Friedmann, T., Riba, P., Király, K., Schmidhammer, H., and Furst, S. (2007). DAMGO and 6beta-glycine substituted 14-O-methyloxymorphone but not morphine show peripheral, preemptive antinociception after systemic administration in a mouse visceral pain model and high intrinsic efficacy in the isolated rat vas deferens. Brain Res. Bull *74*, 369–375.

Killinger, J.M., Weintraub, H.S., and Fuller, B.L. (1979). Human pharmacokinetics and comparative bioavailability of loperamide hydrochloride. J Clin Pharmacol *19*, 211–218.

King, M., Su, W., Chang, A., Zuckerman, A., and Pasternak, G.W. (2001). Transport of opioids from the brain to the periphery by P-glycoprotein: peripheral actions of central drugs. Nat. Neurosci. *4*, 268–274.

King, R., Bonfiglio, R., Fernandez-Metzler, C., Miller-Stein, C., and Olah, T. (2000). Mechanistic investigation of ionization suppression in electrospray ionization. J. Am. Soc. Mass Spectrom. *11*, 942–950.

Kitteringham, N.R., Jenkins, R.E., Lane, C.S., Elliott, V.L., and Park, B.K. (2009). Multiple reaction monitoring for quantitative biomarker analysis in proteomics and metabolomics. Journal of Chromatography B *877*, 1229–1239.

Ko, Y.K., Youn, A.M., Hong, B.H., Kim, Y.H., Shin, Y.S., Kang, P.-S., Yoon, K.J., and Lee, W.H. (2012). Antinociceptive effect of phenyl N-tert-butylnitrone, a free radical scavenger, on the rat formalin test. Korean J Anesthesiol *62*, 558–564.

Kobayashi, S., Kiyosada, T., and Shoda, S. (1996). Synthesis of Artificial Chitin: Irreversible Catalytic Behavior of a Glycosyl Hydrolase through a Transition State Analogue Substrate. Journal of the American Chemical Society *118*, 13113–13114.

Köhler, C., Grobosch, T., and Binscheck, T. (2011). Rapid quantification of tilidine, nortilidine, and bisnortilidine in urine by automated online SPE-LC-MS/MS. Anal Bioanal Chem *400*, 17–23.

Kondoh, M., Masuyama, A., Takahashi, A., Asano, N., Mizuguchi, H., Koizumi, N., Fujii, M., Hayakawa, T., Horiguchi, Y., and Watanbe, Y. (2005). A novel strategy for the enhancement of drug absorption using a claudin modulator. Mol. Pharmacol. *67*, 749–756.

Kotzé, A.F., Lueßen, H.L., de Leeuw, B.J., de Boer, (A)Bert G, Coos Verhoef, J., and Junginger, H.E. (1998). Comparison of the effect of different chitosan salts and N-trimethyl chitosan chloride on the permeability of intestinal epithelial cells (Caco-2). Journal of Controlled Release *51*, 35–46.

Kotzé, A.F., Lueßen, H.L., de Boer, A.G., Verhoef, J.C., and Junginger, H.E. (1999). Chitosan for enhanced intestinal permeability: Prospects for derivatives soluble in neutral and basic environments. European Journal of Pharmaceutical Sciences *7*, 145–151.

Kowalik, S., Clauss, W., and Zahner, H. (2004). Toxoplasma gondii: changes of transepithelial ion transport in infected HT29/B6 cell monolayers. Parasitol. Res. *92*, 152–158.

9 Literature

Kreusel, K.M., Fromm, M., Schulzke, J.D., and Hegel, U. (1991). Cl- secretion in epithelial monolayers of mucus-forming human colon cells (HT-29/B6). Am. J. Physiol *261*, C574–582.

Krug, S.M., Amasheh, M., Dittmann, I., Christoffel, I., Fromm, M., and Amasheh, S. (2013). Sodium caprate as an enhancer of macromolecule permeation across tricellular tight junctions of intestinal cells. Biomaterials *34*, 275–282.

Kudsiova, L., and Lawrence, M.J. (2008). A comparison of the effect of chitosan and chitosan-coated vesicles on monolayer integrity and permeability across Caco-2 and 16HBE14o-cells. J Pharm Sci *97*, 3998–4010.

Labuz, D., Mousa, S.A., Schäfer, M., Stein, C., and Machelska, H. (2007). Relative contribution of peripheral versus central opioid receptors to antinociception. Brain Res *1160*, 30–38.

Lalatsa, A., Garrett, N.L., Ferrarelli, T., Moger, J., Schätzlein, A.G., and Uchegbu, I.F. (2012a). Delivery of peptides to the blood and brain after oral uptake of quaternary ammonium palmitoyl glycol chitosan nanoparticles. Mol. Pharm. *9*, 1764–1774.

Lalatsa, A., Lee, V., Malkinson, J.P., Zloh, M., Schätzlein, A.G., and Uchegbu, I.F. (2012b). A prodrug nanoparticle approach for the oral delivery of a hydrophilic peptide, leucine(5)-enkephalin, to the brain. Mol. Pharm. *9*, 1665–1680.

Levitskaia, T.G., Creim, J.A., Curry, T.L., Luders, T., Morris, J.E., Sinkov, S.I., Woodstock, A.D., and Thrall, K.D. (2009). Investigation of chitosan for decorporation of 60Co in the rat. Health Phys *97*, 115–124.

Lewanowitsch, T., and Irvine, R.J. (2002). Naloxone methiodide reverses opioid-induced respiratory depression and analgesia without withdrawal. Eur. J. Pharmacol. *445*, 61–67.

Li, H., Sheppard, D.N., and Hug, M.J. (2004). Transepithelial electrical measurements with the Ussing chamber. J. Cyst. Fibros *3 Suppl 2*, 123–126.

Lindmark, T., Söderholm, J.D., Olaison, G., Alván, G., Ocklind, G., and Artursson, P. (1997). Mechanism of absorption enhancement in humans after rectal administration of ampicillin in suppositories containing sodium caprate. Pharm. Res. *14*, 930–935.

Luppi, B., Bigucci, F., Cerchiara, T., and Zecchi, V. (2010). Chitosan-based hydrogels for nasal drug delivery: from inserts to nanoparticles. Expert Opin Drug Deliv *7*, 811–828.

Machelska, H., Pflüger, M., Weber, W., Piranvisseh-Völk, M., Daubert, J.D., Dehaven, R., and Stein, C. (1999). Peripheral effects of the kappa-opioid agonist EMD 61753 on pain and inflammation in rats and humans. J. Pharmacol. Exp. Ther. *290*, 354–361.

Machelska, H., Schopohl, J.K., Mousa, S.A., Labuz, D., Schäfer, M., and Stein, C. (2003). Different mechanisms of intrinsic pain inhibition in early and late inflammation. Journal of Neuroimmunology *141*, 30–39.

MacPherson, R.D. (2002). New directions in pain management. Drugs Today *38*, 135–145.

Majumdar, S., Duvvuri, S., and Mitra, A.K. (2004). Membrane transporter/receptor-targeted prodrug design: strategies for human and veterinary drug development. Adv. Drug Deliv. Rev. *56*, 1437–1452.

9 Literature

Markov, A.G., Veshnyakova, A., Fromm, M., Amasheh, M., and Amasheh, S. (2010). Segmental expression of claudin proteins correlates with tight junction barrier properties in rat intestine. J. Comp. Physiol. B, Biochem. Syst. Environ. Physiol *180*, 591–598.

Martinez, M., Amidon, G., Clarke, L., Jones, W.W., Mitra, A., and Riviere, J. (2002). Applying the biopharmaceutics classification system to veterinary pharmaceutical products. Part II. Physiological considerations. Adv. Drug Deliv. Rev. *54*, 825–850.

Martìn-Padura, I., Lostaglio, S., Schneemann, M., Williams, L., Romano, M., Fruscella, P., Panzeri, C., Stoppacciaro, A., Ruco, L., Villa, A., et al. (1998). Junctional adhesion molecule, a novel member of the immunoglobulin superfamily that distributes at intercellular junctions and modulates monocyte transmigration. J. Cell Biol. *142*, 117–127.

Masuda, A., Goto, Y., Kurosaki, Y., and Aiba, T. (2012). In vivo application of chitosan to facilitate intestinal acyclovir absorption in rats. J Pharm Sci *101*, 2449–2456.

Matsuhisa, K., Kondoh, M., Takahashi, A., and Yagi, K. (2009). Tight junction modulator and drug delivery. Expert Opin Drug Deliv *6*, 509–515.

McDougall, J.J. (2011). Peripheral analgesia: Hitting pain where it hurts. Biochimica et Biophysica Acta (BBA) - Molecular Basis of Disease *1812*, 459–467.

McNicol, E., Strassels, S.A., Goudas, L., Lau, J., and Carr, D.B. (2005). NSAIDS or paracetamol, alone or combined with opioids, for cancer pain. Cochrane Database Syst Rev CD005180.

Meiser, A., and Laubenthal, H. (1997). [Clinical studies on the peripheral effect of opioids following knee surgery. A literature review]. Anaesthesist *46*, 867–879.

Mercer, S.L., and Coop, A. (2011). Opioid Analgesics and P-glycoprotein Efflux Transporters: A Potential Systems-Level Contribution to Analgesic Tolerance. Curr Top Med Chem *11*, 1157–1164.

Merzlikine, A., Rotter, C., Rago, B., Poe, J., Christoffersen, C., Thomas, V.H., Troutman, M., and El-Kattan, A. (2009). Effect of chitosan glutamate, carbomer 974P, and EDTA on the in vitro Caco-2 permeability and oral pharmacokinetic profile of acyclovir in rats. Drug Dev Ind Pharm *35*, 1082–1091.

Messlinger, K. (1997). [What is a nociceptor?]. Anaesthesist *46*, 142–153.

Michiels, M., Hendriks, R., and Heykants, J. (1977). Radioimmunoassay of the antidiarrhoeal loperamide. Life Sci. *21*, 451–459.

Millan, M.J. (1999). The induction of pain: an integrative review. Prog. Neurobiol. *57*, 1–164.

Mizuno, N., Niwa, T., Yotsumoto, Y., and Sugiyama, Y. (2003). Impact of drug transporter studies on drug discovery and development. Pharmacol. Rev. *55*, 425–461.

Moran, G.W., O'Neill, C., and McLaughlin, J.T. (2012). GLP-2 enhances barrier formation and attenuates TNFα-induced changes in a Caco-2 cell model of the intestinal barrier. Regulatory Peptides.

9 Literature

Neitzel, V. Lineare Kalibrationsfunktionen. CLB Chemie in Labor und Biotechnik *53. Jahrgang, Heft 1/2002 9*.

Nicholson, B. (2003). Responsible prescribing of opioids for the management of chronic pain. Drugs *63*, 17–32.

Niemegeers, C.J., McGuire, J.L., Heykants, J.J., and Janssen, P.A. (1979). Dissociation between opiate-like and antidiarrheal activities of antidiarrheal drugs. J. Pharmacol. Exp. Ther. *210*, 327–333.

Niemegeers, C.J.E., Colpaert, F.C., and Awouters, F.H.L. (1981). Pharmacology and antidiarrheal effect of loperamide. Drug Development Research *1*, 1–20.

Niessen, C.M. (2007). Tight junctions/adherens junctions: basic structure and function. J. Invest. Dermatol. *127*, 2525–2532.

Nozaki-Taguchi, N., and Yaksh, T.L. (1999). Characterization of the antihyperalgesic action of a novel peripheral mu-opioid receptor agonist--loperamide. Anesthesiology *90*, 225–234.

Nozaki-Taguchi, N., Shutoh, M., and Shimoyama, N. (2008). Potential utility of peripherally applied loperamide in oral chronic graft-versus-host disease related pain. Jpn. J. Clin. Oncol. *38*, 857–860.

Ooms, L.A., Degryse, A.D., and Janssen, P.A. (1984). Mechanisms of action of loperamide. Scand. J. Gastroenterol. Suppl *96*, 145–155.

Ossipov, M.H., Lai, J., King, T., Vanderah, T.W., Malan, T.P., Jr, Hruby, V.J., and Porreca, F. (2004). Antinociceptive and nociceptive actions of opioids. J. Neurobiol. *61*, 126–148.

Paolicelli, P., de la Fuente, M., Sánchez, A., Seijo, B., and Alonso, M.J. (2009). Chitosan nanoparticles for drug delivery to the eye. Expert Opin Drug Deliv *6*, 239–253.

Pavia, D.L., and Lampman, G.M. (2009). Introduction to spectroscopy (Cengage Learning).

Pert, C.B., and Snyder, S.H. (1973). Opiate receptor: demonstration in nervous tissue. Science *179*, 1011–1014.

Peters, F., Hartung, M., Herbold, M., Schmitt, G., Daldrup, T., and Musshoff, F. (2009). Anhang B zur Richtlinie der GTFCh zur Qualitätssicherung bei forensisch-toxikologischen Untersuchungen - Anforderungen and die Validierung von Analysenmethoden.

Peters, F.T., Drummer, O.H., and Musshoff, F. (2007). Validation of new methods. Forensic Sci. Int *165*, 216–224.

Petersen, S.B., Nolan, G., Maher, S., Rahbek, U.L., Guldbrandt, M., and Brayden, D.J. (2012). Evaluation of alkylmaltosides as intestinal permeation enhancers: Comparison between rat intestinal mucosal sheets and Caco-2 monolayers. European Journal of Pharmaceutical Sciences *47*, 701–712.

Press, B., and Di Grandi, D. (2008). Permeability for intestinal absorption: Caco-2 assay and related issues. Curr. Drug Metab. *9*, 893–900.

Van Rijn, R.M., Whistler, J.L., and Waldhoer, M. (2010). Opioid-receptor-heteromer-specific trafficking and pharmacology. Curr Opin Pharmacol *10*, 73–79.

Ripamonti, C.I. (2012). Pain management. Ann. Oncol. *23 Suppl 10*, x294–x301.

Ripamonti, C.I., Bandieri, E., and Roila, F. (2011). Management of cancer pain: ESMO Clinical Practice Guidelines. Ann. Oncol. *22 Suppl 6*, vi69–77.

Rittner, H.L., and Brack, A. (2007). Leukocytes as mediators of pain and analgesia. Curr Rheumatol Rep *9*, 503–510.

Rosenthal, R., Heydt, M.S., Amasheh, M., Stein, C., Fromm, M., and Amasheh, S. (2012a). Analysis of absorption enhancers in epithelial cell models. Ann. N. Y. Acad. Sci. *1258*, 86–92.

Rosenthal, R., Günzel, D., Finger, C., Krug, S.M., Richter, J.F., Schulzke, J.-D., Fromm, M., and Amasheh, S. (2012b). The effect of chitosan on transcellular and paracellular mechanisms in the intestinal epithelial barrier. Biomaterials *33*, 2791–2800.

Rubelt, M.S., Amasheh, S., Grobosch, T., and Stein, C. (2012). Liquid chromatography-tandem mass spectrometry for analysis of intestinal permeability of loperamide in physiological buffer. PLoS ONE *7*, e48502.

Russell WMS and Burch RL. (1959). The Principles of Humane Experimental Technique.

De Sá, P.G., Nunes, X.P., de Lima, J.T., Filho, J.A., Fontana, A.P., Siqueira, J. de, Quintans-Júnior, L.J., Damasceno, P.K., Branco, C.R., Branco, A., et al. (2012). Antinociceptive effect of ethanolic extract of Selaginella convoluta in mice. BMC Complement Altern Med *12*, 187.

Sadeque, A.J., Wandel, C., He, H., Shah, S., and Wood, A.J. (2000). Increased drug delivery to the brain by P-glycoprotein inhibition. Clin. Pharmacol. Ther *68*, 231–237.

Saika, F., Kiguchi, N., Kobayashi, Y., Fukazawa, Y., and Kishioka, S. (2012). CC-chemokine ligand 4/macrophage inflammatory protein-1β participates in the induction of neuropathic pain after peripheral nerve injury. Eur J Pain *16*, 1271–1280.

Sánchez, E.M., Bagües, A., and Martín, M.I. (2010). Contributions of peripheral and central opioid receptors to antinociception in rat muscle pain models. Pharmacol. Biochem. Behav. *96*, 488–495.

Sandri, G., Bonferoni, M.C., Rossi, S., Ferrari, F., Boselli, C., and Caramella, C. (2010). Insulin-loaded nanoparticles based on N-trimethyl chitosan: in vitro (Caco-2 model) and ex vivo (excised rat jejunum, duodenum, and ileum) evaluation of penetration enhancement properties. AAPS PharmSciTech *11*, 362–371.

Schinkel, A.H., Wagenaar, E., Mol, C.A., and van Deemter, L. (1996a). P-glycoprotein in the blood-brain barrier of mice influences the brain penetration and pharmacological activity of many drugs. J. Clin. Invest. *97*, 2517–2524.

Schinkel, A.H., Wagenaar, E., Mol, C.A., and van Deemter, L. (1996b). P-glycoprotein in the blood-brain barrier of mice influences the brain penetration and pharmacological activity of many drugs. J. Clin. Invest *97*, 2517–2524.

Schipper, N.G., Vârum, K.M., Stenberg, P., Ocklind, G., Lennernäs, H., and Artursson, P. (1999). Chitosans as absorption enhancers of poorly absorbable drugs. 3: Influence of mucus on absorption enhancement. Eur J Pharm Sci *8*, 335–343.

Schütz, J., Brandt, W., Spetea, M., Wurst, K., Wunder, G., and Schmidhammer, H. (2003). Synthesis of 6-Amino Acid Substituted Derivatives of the Highly Potent Analgesic 14-O-Methyloxymorphone. HCA *86*, 2142–2148.

Sevostianova, N., Danysz, W., and Bespalov, A.Y. (2005). Analgesic effects of morphine and loperamide in the rat formalin test: interactions with NMDA receptor antagonists. Eur. J. Pharmacol *525*, 83–90.

Sezer, A.D., and Akbuğa, J. (1999). Release characteristics of chitosan treated alginate beads: II. Sustained release of a low molecular drug from chitosan treated alginate beads. J Microencapsul *16*, 687–696.

Shannon, H.E., and Lutz, E.A. (2002). Comparison of the peripheral and central effects of the opioid agonists loperamide and morphine in the formalin test in rats. Neuropharmacology *42*, 253–261.

Shin, Y., Yoo, D.I., and Min, K. (1999). Antimicrobial finishing of polypropylene nonwoven fabric by treatment with chitosan oligomer. Journal of Applied Polymer Science *74*, 2911–2916.

Shin, Y.G., Dong, T., Chou, B., and Menghrajani, K. (2011). Determination of loperamide in mdr1a/1b knock-out mouse brain tissue using matrix-assisted laser desorption/ionization mass spectrometry and comparison with quantitative electrospray-triple quadrupole mass spectrometry analysis. Arch. Pharm. Res. *34*, 1983–1988.

Shinoda, K., Hruby, V.J., and Porreca, F. (2007). Antihyperalgesic effects of loperamide in a model of rat neuropathic pain are mediated by peripheral δ-opioid receptors. Neurosci Lett *411*, 143–146.

Silva, C.A., Nobre, T.M., Pavinatto, F.J., and Oliveira, O.N., Jr (2012). Interaction of chitosan and mucin in a biomembrane model environment. J Colloid Interface Sci *376*, 289–295.

Silverman, J.A. (1999). Multidrug-resistance transporters. Pharm Biotechnol *12*, 353–386.

Smith, J., Wood, E., and Dornish, M. (2004). Effect of chitosan on epithelial cell tight junctions. Pharm. Res. *21*, 43–49.

Sogias, I.A., Williams, A.C., and Khutoryanskiy, V.V. (2008). Why is chitosan mucoadhesive? Biomacromolecules *9*, 1837–1842.

Sonaje, K., Lin, Y.-H., Juang, J.-H., Wey, S.-P., Chen, C.-T., and Sung, H.-W. (2009). In vivo evaluation of safety and efficacy of self-assembled nanoparticles for oral insulin delivery. Biomaterials *30*, 2329–2339.

Spetea, M., Friedmann, T., Riba, P., Schütz, J., Wunder, G., Langer, T., Schmidhammer, H., and Fürst, S. (2004). In vitro opioid activity profiles of 6-amino acid substituted derivatives of 14-O-methyloxymorphone. Eur. J. Pharmacol. *483*, 301–308.

Stein, C. (1993). Peripheral mechanisms of opioid analgesia. Anesth. Analg *76*, 182–191.

Stein, C., and Machelska, H. (2011). Modulation of Peripheral Sensory Neurons by the Immune System: Implications for Pain Therapy. Pharmacol Rev *63*, 860–881.

Stein, C., and Zöllner, C. (2009). Opioids and sensory nerves. Handb Exp Pharmacol 495–518.

Stein, C., Millan, M.J., Shippenberg, T.S., and Herz, A. (1988a). Peripheral effect of fentanyl upon nociception in inflamed tissue of the rat. Neurosci. Lett. *84*, 225–228.

Stein, C., Millan, M.J., and Herz, A. (1988b). Unilateral inflammation of the hindpaw in rats as a model of prolonged noxious stimulation: alterations in behavior and nociceptive thresholds. Pharmacol. Biochem. Behav. *31*, 445–451.

Stein, C., Gramsch, C., and Herz, A. (1990). Intrinsic mechanisms of antinociception in inflammation: local opioid receptors and beta-endorphin. J. Neurosci. *10*, 1292–1298.

Stein, C., Machelska, H., and Schäfer, M. (2001). Peripheral analgesic and antiinflammatory effects of opioids. Z Rheumatol *60*, 416–424.

Stein, C., Schäfer, M., and Machelska, H. (2003). Attacking pain at its source: new perspectives on opioids. Nat. Med *9*, 1003–1008.

Sun, H., Chow, E.C., Liu, S., Du, Y., and Pang, K.S. (2008). The Caco-2 cell monolayer: usefulness and limitations. Expert Opin Drug Metab Toxicol *4*, 395–411.

Suzuki, T., Mizushima, Y., Umeda, T., and Ohashi, R. (1999). Further biocompatibility testing of silica-chitosan complex membrane in the production of tissue plasminogen activator by epithelial and fibroblast cells. J. Biosci. Bioeng *88*, 194–199.

Taylor, J.R. (1997). An Introduction to Error Analysis: The Study of Uncertainties in Physical Measurements (University Science Books).

Thanou, M., Verhoef, J.C., and Junginger, H.E. (2001a). Chitosan and its derivatives as intestinal absorption enhancers. Adv. Drug Deliv. Rev. *50 Suppl 1*, S91–101.

Thanou, M., Nihot, M.T., Jansen, M., Verhoef, J.C., and Junginger, H.E. (2001b). Mono-N-carboxymethyl chitosan (MCC), a polyampholytic chitosan derivative, enhances the intestinal absorption of low molecular weight heparin across intestinal epithelia in vitro and in vivo. J Pharm Sci *90*, 38–46.

Thiebaut, F., Tsuruo, T., Hamada, H., Gottesman, M.M., Pastan, I., and Willingham, M.C. (1987a). Cellular localization of the multidrug-resistance gene product P-glycoprotein in normal human tissues. Proc. Natl. Acad. Sci. U.S.A. *84*, 7735–7738.

Thiebaut, F., Tsuruo, T., Hamada, H., Gottesman, M.M., Pastan, I., and Willingham, M.C. (1987b). Cellular localization of the multidrug-resistance gene product P-glycoprotein in normal human tissues. Proc. Natl. Acad. Sci. U.S.A. *84*, 7735–7738.

Thomas, V.H., Bhattachar, S., Hitchingham, L., Zocharski, P., Naath, M., Surendran, N., Stoner, C.L., and El-Kattan, A. (2006). The road map to oral bioavailability: an industrial perspective. Expert Opin Drug Metab Toxicol *2*, 591–608.

Tonini, M., Waterman, S.A., Candura, S.M., Coccini, T., and Costa, M. (1992). Sites of action of morphine on the ascending excitatory reflex in the guinea-pig small intestine. Neurosci. Lett. *144*, 195–198.

Tseong, L.F. (1995). Pharmacology of Opioid Peptides (Taylor & Francis).

Valenta, C., and Auner, B.G. (2004). The use of polymers for dermal and transdermal delivery. Eur J Pharm Biopharm *58*, 279–289.

Vandenbossche, J., Huisman, M., Xu, Y., Sanderson-Bongiovanni, D., and Soons, P. (2010). Loperamide and P-glycoprotein inhibition: assessment of the clinical relevance. J. Pharm. Pharmacol. *62*, 401–412.

Vann, R.E., Wise, L.E., Varvel, S.A., Philibin, S.D., Walentiny, D.M., and Porter, J.H. (2009). Route of administration influences substitution patterns in rats trained to discriminate methadone vs. vehicle. Drug Alcohol Depend *103*, 124–130.

Vllasaliu, D., Exposito-Harris, R., Heras, A., Casettari, L., Garnett, M., Illum, L., and Stolnik, S. (2010). Tight junction modulation by chitosan nanoparticles: comparison with chitosan solution. Int J Pharm *400*, 183–193.

Wade, L.G. (2002). Organic Chemistry (Prentice Hall).

Wadhwa, S., Paliwal, R., Paliwal, S.R., and Vyas, S.P. (2009). Chitosan and its role in ocular therapeutics. Mini Rev Med Chem *9*, 1639–1647.

Wandel, C., Kim, R., Wood, M., and Wood, A. (2002). Interaction of morphine, fentanyl, sufentanil, alfentanil, and loperamide with the efflux drug transporter P-glycoprotein. Anesthesiology *96*, 913–920.

Wang, J. (2009). Analysis of macrolide antibiotics, using liquid chromatography-mass spectrometry, in food, biological and environmental matrices. Mass Spectrom Rev *28*, 50–92.

Wang, B.C., Li, D., Budzilovich, G., Hiller, J.M., Rosenberg, C., Hillman, D.E., and Turndorf, H. (1994). Antinociception without motor blockade after subarachnoid administration of S-(+)-ibuprofen in rats. Life Sci. *54*, 715–720.

Watts, T.L., and Fasano, A. (2000). Modulation of intestinal permeability: a novel and innovative approach for the oral delivery of drugs, macromolecules and antigens. Biotechnol. Genet. Eng. Rev. *17*, 433–453.

WHO (1996). WHO GUIDELINES FOR CANCER PAIN AND PALLIATIVE CARE REACH HEALTH WORKERS IN 31 LANGUAGES | Cancer Pain Release.

Wiese, M., and Pajeva, I.K. (2001). Structure-activity relationships of multidrug resistance reversers. Curr. Med. Chem *8*, 685–713.

Yaksh, T.L., and Rudy, T.A. (1978). Narcotic analgestics: CNS sites and mechanisms of action as revealed by intracerebral injection techniques. Pain *4*, 299–359.

Yamashita, S., Konishi, K., Yamazaki, Y., Taki, Y., Sakane, T., Sezaki, H., and Furuyama, Y. (2002). New and better protocols for a short-term Caco-2 cell culture system. Journal of Pharmaceutical Sciences *91*, 669–679.

Yang, F., Wang, H., Zhao, Q., Chen, X., Jiang, J., and Hu, P. (2012). Simultaneous determination of a novel anxiolytic agent buagafuran and one metabolite in human plasma by ultra-performance liquid chromatography-tandem mass spectrometry. J Pharm Biomed Anal *76C*, 59–64.

Yeh, T.-H., Hsu, L.-W., Tseng, M.T., Lee, P.-L., Sonjae, K., Ho, Y.-C., and Sung, H.-W. (2011). Mechanism and consequence of chitosan-mediated reversible epithelial tight junction opening. Biomaterials *32*, 6164–6173.

Youdim, K.A., and Saunders, K.C. (2010). A review of LC-MS techniques and high-throughput approaches used to investigate drug metabolism by cytochrome P450s. J. Chromatogr. B Analyt. Technol. Biomed. Life Sci. *878*, 1326–1336.

Zimmerman, D.M., Gidda, J.S., Cantrell, B.E., Schoepp, D.D., Johnson, B.G., and Leander, J.D. (1994). Discovery of a potent, peripherally selective trans-3,4-dimethyl-4-(3-hydroxyphenyl)piperidine opioid antagonist for the treatment of gastrointestinal motility disorders. J. Med. Chem. *37*, 2262–2265.

Zimmermann, M. (1983). Ethical guidelines for investigations of experimental pain in conscious animals. Pain *16*, 109–110.

Zöllner, C., and Stein, C. (2007). Opioids. Handb Exp Pharmacol 31–63.

10 Figure legends

10 FIGURE LEGENDS

10 Figure legends

10 Figure legends

11 Table legend

11 TABLE LEGEND

12 List of abbreviations

12 LIST OF ABBREVIATIONS

µg	microgram
aa	acetic acid
ac	alternate current
ANOVA	analysis of variance
ATP	adenosine triphosphate
AUC	area under the curve
BL	base line
cAMP	cyclic adenosine monophosphate
CFA	complete Freund's adjuvant
CNS	central nervous system
conc.	concentration
cps	counts per second
dc	direct current
ddH_2O	double-distilled water
DMSO	Dimethyl sulfoxide
EDTA	Ethylenediaminetetraacetic acid
EIS	turbo electrospray ion source
ESI+	positive ionization mode
FBS	fetal bovine serum
Fig.	figure
GDP	guanosine diphosphate
GTP	guanosine triphosphate

12 List of abbreviations

HEPES	4-(2-hydroxyethyl)-1-piperazineethanesulfonic acid
HPLC	high performance liquid chromatography
i.c.v.	intracerebroventricular
i.p.	intraperitoneal
i.pl.	intraplantar
i.t.	intrathecal
i.v.	intravenous
IASP	International Association for the Study of Pain
IS	internal standard
JAM	junctional adhesion molecules
kg	kilogram
LC-MS/MS	liquid chromatography coupled with tandem mass spectrometry
LLOQ	lower limit of quantification
LOP	loperamide
m/z	mass-to-charge ratio
MAGI	membrane-associated guanylate kinase
MALDI	matrix-assisted laser desorption/ionization
mg	milligram
min	minute
mL	milliliter
MRM	multiple reaction mode

12 List of abbreviations

MS	mass spectrometry
MS/MS	tandem mass spectrometry
MUPP1	multi-PDZ domain protein 1
ng	nanogram
NLXM	naloxone methiodide
NSAIDs	non-steroidal anti-inflammatory drugs
PBS	phosphate buffered saline
PepT1	intestinal oligopeptide transporter
PFP	pentafluorophenyl
P-gp	p-glycoprotein
pH	"power of hydrogen"
pk_a	acid dissociation constant
PKC α	protein kinase C α
PNS	peripheral nervous system
PPT	paw-pressure threshold
Q1	quantifier ion
Q2	qualifier ion
QC	quality control
R^{para}	paracellular restistance
RPMI	Roswell Park Memorial Institute medium
RSD	relative standard deviation
R^{trans}	transcellular resistance
s.c.	subcutaneous

12 List of abbreviations

SEM	standard error of mean
TER	transepithelial resistance
TJ	tight junction
TJs	tight junctions
ULOQ	upper limit of quantification
WHO	World Health Organization
ZO1, ZO2	zona occludens (1, 2)

13 Acknowledgement

13 ACKNOWLEDGEMENT

First of all, I would like to thank my research guide, Prof. Dr. med. Christoph Stein, for giving me the great opportunity to conduct my doctoral thesis in his lab on such an inspiring research topic. He always supported me with his great knowledge in pain research with his helpful suggestions and comments. I would also like to thank my advisor, Prof. Hans-Dieter Volk, for providing me with the opportunity to complete my doctoral thesis at the Humboldt University of Berlin. I wish to express my sincere appreciation to PD Dr. Salah Amasheh, I am extremely grateful and indebted to him for his encouragement, sincerity, expertise and valuable guidance. Thank you also to Prof. Dr. Michael Fromm for giving me the opportunity to conduct an important part of my work in his research lab. I would like to thank Dr. Thomas Grobosch for providing me with the necessary facilities and helpful support during the LC-MS/MS method development. He has brought me closer to the world of analytical chemistry. Furthermore, I would like to thank my colleagues of the anesthesiology and clinical physiology lab for their help and encouragement. I especially wish to express my sincere gratitude to Dr. Melanie Busch-Dienstfertig for her help and encouragement. I loved our inspiring discussions in order to get the best out of me. I would like to thank Dr. Marian Brackmann, Ph.D. Sara González, Lena John and Dr. Dominika Labuz for the great atmosphere at the laboratory which always made my workdays enjoyable. I thank my family for their continuous encouragement and support, my husband Florian for his immeasurable support during this phase of my life. I appreciate his patience and enthusiasm for science, which helped me to become the scientist I always wanted to be. Last but not least, I am grateful for my gorgeous son Tim, who fulfills me with pleasure every day.

14 Eigenständigkeitserklärung

14 EIGENSTÄNDIGKEITSERKLÄRUNG

Hiermit erkläre ich, die Dissertation selbständig und nur unter Verwendung der angegebenen Hilfen und Hilfsmittel angefertigt zu haben.

Ich habe mich anderwärts nicht um einen Doktorgrad beworben und besitze einen entsprechenden Doktorgrad nicht.

Ich erkläre die Kenntnisnahme der dem Verfahren zugrunde liegenden Promotionsordnung der Mathematisch-Naturwissenschaftlichen Fakultät I der Humboldt-Universität zu Berlin vom 01. September 2005.

Ort/Datum Unterschrift (Miriam Rubelt)

15 Curriculum vitae

15 CURRICULUM VITAE

16 CONFERENCES AND POSTERS

09.–11. December 2009 Brain Days, Berlin, Germany

Chair: Prof. Dr. Helmut Kettenmann

Poster: *„New sensitive LC-MS/MS method for quantification of a novel pain relieving drug: analyzes of intestinal transport mediated by absorption enhancers"*

M. Heydt, S. Amasheh, T. Grobosch, C. Stein

07.-12. March 2010 Drug Delivery Foundation, Lake Tahoe, Nevada, USA

Organizers: Gordon L. Amidon (Ann Arbor, Michigan, USA); Peter Langguth (Mainz, Germany); Hans Lennernäs (Uppsala, Sweden); James Polli (Baltimore, MD, USA); Shinji Yamashita (Osaka, Japan)

Poster: *"Paracellular transport of AS006 - a novel pain relieving drug - is augmented by the absorption enhancer chitosan"*

M. Heydt [1], S. Amasheh [2], T. Grobosch [3], L. Lang [1], C. Stein [1]

[1] Dep. of Anesthesiology and [2] Clinical Physiology, Charité Campus Benjamin Franklin, [3] Institute of Toxicology - Clinical Toxicology and Berlin Poison Information Centre, Berlin, Germany

10.-11. June 2010 Berlin Neuroscience Forum (BNF), Liebenwalde, Brandenburg, Germany

Program Committee: Ingolf Blasig, Michael Brecht, Ulrich Dirnagl, Gabriel Curio, Karl Einhäupl, Matthias Endres, Uwe Heinemann, Andreas Herz, Isabella Heuser, Helmut Kettenmann, Gary Lewin, Randolf Menzel, Jochen Pflüger, Constance Scharff, Dietmar Schmitz, Werner Sommer, Christoph Stein, Bertram Wiedenmann

Poster: *"Paracellular transport of AS006 - a novel pain relieving drug - is augmented by the absorption enhancer chitosan"*

M. Heydt [1], S. Amasheh [2], T. Grobosch [3], L. Lang [1], C. Stein [1]

[1] Dep. of Anesthesiology and [2] Clinical Physiology, Charité Campus Benjamin Franklin, [3] Institute of Toxicology - Clinical Toxicology and Berlin Poison Information Centre, Berlin, Germany

16 Conferences and posters

26.-29. March 2011 Deutsche Physiologische Gesellschaft Regensburg, University of Regensburg, Germany

Acta Physiologica 2011; Volume 201, Supplement 682
The 90th Annual Meeting of The German Physiological Society
26/03/2011-29/03/2011
Regensburg, Germany

Poster: *"Paracellular transport of a hydrophilic opioid receptor agonist is increased by chitosan"*

M. Heydt [1], S. Amasheh [2], T. Grobosch [3], L. Lang [1], C. Stein [1]

[1] Dep. of Anesthesiology and [2] Clinical Physiology, Charité Campus Benjamin Franklin, [3] Institute of Toxicology - Clinical Toxicology and Berlin Poison Information Centre, Berlin, Germany

17 PUBLICATION LIST

Rosenthal, R., **Heydt, M.S.,** Amasheh, M., Stein, C., Fromm, M., and Amasheh, S. (2012a). Analysis of absorption enhancers in epithelial cell models. Ann. N. Y. Acad. Sci. *1258*, 86–92.

Rubelt, M.S., Amasheh, S., Grobosch, T., and Stein, C. (2012). Liquid chromatography-tandem mass spectrometry for analysis of intestinal permeability of loperamide in physiological buffer. PLoS ONE *7*, e48502.